DEGRADATION OF AND ENERGY TRANSFER IN OXIDE-BASED MICROSCALE AND NANOSCALE PHOSPHORS DOPED WITH RARE-EARTH ELEMENTS

by

Odireleng Martin Ntwaeaborwa
(MSc)

A thesis submitted in fulfilment of the requirements for the degree

PHILOSOPHIAE DOCTOR

in the

Faculty of Natural and Agricultural Sciences
Department of Physics

at the

University of the Free State

Promoter: Prof. H.C. Swart
Co-promoter: Dr. R.E. Kroon

August 2006

Dedicated to the memory of the late
Gabobidiwe Anne Lekwene

ACKNOWLEDGEMENTS

- I thank *God* for giving me strength and courage (Philippians 4:13) to complete this study.
- I am indebted to my promoter, *Prof. Hendrik C. Swart* for his professional guidance and support. Above all, I thank him for allowing me freedom to pursue my ideas.
- I am grateful to my co-promoter *Dr. R.E. (Ted) Kroon* for his fruitful discussions and advice. Most importantly, I thank him for his suggestions in organization of chapters and ideas.
- I thank all *staff members of the Department of Physics* (UFS) and post graduate students (*Simon Dhlamini, Lisa Coetsee and Roy Chen*) for their assistance and support.
- I am thankful to *Dr. Thembela K. Hillie* for introducing me to degradation of phosphors and pulsed laser deposition technique and for his continued support for the duration of this study.
- I thank *Prof. Paul H. Holloway* for introducing me to luminescent nanoparticle phosphors, and for his fruitful discussions and guidance in all the papers published from this study. I also thank Mrs Ludie Harmon and Mrs Bette Holloway for their support during my stay in Gainesville (Florida, USA).
- I am grateful to *Heesun Yang, Jung-Sik Bang, Kwanhoon Kim, Hyeok-Jin Lee, Soo Yeon Seo and Theiry Dubroca* (Dept. of Materials Science and Engineering, University of Florida) who helped me with preparation and PL measurements of nanoparticle phosphors.
- I owe my special words of gratitude to my wife *Molly* and our son *Tlotlang, my parents, brothers* and *sisters* for their moral support.
- I thank *Prof. Ntate D. Kgwadi* (North West University) and the late *Mrs Gabobidiwe A. Lekwene* for their inspiration and encouragement.
- I am grateful for the financial support from the *South African National Research Foundation, University of the Free State* and the *University of Florida.*

ABSTRACT

This study was aimed at investigating degradation of and energy transfer in oxide based phosphors for application in low voltage field emission displays. Cathodoluminescence degradation of commercial Y_2O_3:Eu powder, Y_2O_3:Eu thin film and sol-gel SiO_2:Ce,Tb nanoparticle powder phosphors was studied by Auger electron spectroscopy (AES) and cathodoluminescence (CL) spectroscopy. Energy transfer from ZnO nanoparticles to Eu^{3+} and Ce^{3+} was demonstrated by exciting ZnO-SiO_2:Eu and ZnO-SiO_2:Ce powder phosphors with a 325 nm HeCd laser beam. Energy transfer was also demonstrated between Ce^{3+} - Eu^{3+} and Ce^{3+}- Tb^{3+} ion pairs co-doped in SiO_2.

The Y_2O_3:Eu powder, Y_2O_3:Eu thin film and sol-gel SiO_2:Ce,Tb nanoparticle powder phosphors were irradiated with an electron beam of energy 2 keV in a vacuum chamber maintained at 1×10^{-6}, 1×10^{-7} or 1×10^{-8} Torr O_2. The effect of surface coating on the surface and CL intensity degradation was also investigated by coating some of the films with a thin layer of Ta_2O_5. Degradation of CL intensity of Y_2O_3:Eu thin film and SiO_2:Ce,Tb nanoparticle powder phosphors occurred simultaneously with desorption of oxygen from the surface. In the case of Y_2O_3:Eu powder phosphors, there was no desorption of atomic species during electron beam irradiation. Possible mechanisms for the degradation of CL intensity and desorption of atomic species are discussed.

Energy transfer from ZnO nanoparticles to Eu^{3+} and Ce^{3+} occurred when ZnO-SiO_2:Eu and ZnO-SiO_2:Ce powders were irradiated with a 325 nm HeCd laser beam at room temperature. Embedding of ZnO nanoparticles in SiO_2:Eu and SiO_2:Ce resulted in complete suppression of green photoluminescence of the ZnO nanoparticles and a subsequent enhancement of red and blue photoluminescence of Eu^{3+} and Ce^{3+} respectively. The blue photoluminescence was enhanced slightly more than the red photoluminescence. Possible mechanisms of energy transfer from ZnO nanoparticles to Ce^{3+} and Eu^{3+} ions are discussed.

Furthermore, it was demonstrated that for different concentrations of Ce^{3+} and Eu^{3+} in SiO_2:Ce,Eu, blue photoluminescence of Ce^{3+} was enhanced by an energy transfer from Eu^{3+}. The enhancement was largest when 0.5 mol% Ce^{3+} was co-doped with 0.5 mol% Eu^{3+}. In the case of different concentrations of Ce^{3+} and Tb^{3+} in SiO_2:Ce,Tb, green photoluminescence of Tb^{3+} was enhanced by an energy transfer from Ce^{3+}. The enhancement was largest when 0.5 mol% Ce^{3+} was co-doped with 1 mol % Tb^{3+}. Possible mechanisms of energy transfer from Eu^{3+} to Ce^{3+}, and from Ce^{3+} to Tb^{3+} are discussed.

KEY WORDS

Cathodoluminescence, degradation, photoluminescence, energy transfer

ACRONYMS

- AES – Auger electron spectroscopy
- APPHs – Auger peak-to-peak heights
- CL – Cathodoluminescence
- EtOH - Ethanol
- FTIR – Fourier transform infrared spectroscopy
- PL – Photoluminescence
- PLD – Pulsed laser deposition
- RGA - Residual gas analyser
- TEM – Transmission electron microscopy
- XPS – X-ray photoelectron spectroscopy
- XRD – X-ray diffraction

TABLE OF CONTENTS

Title page..... i

Dedication..... ii

Acknowledgement..... iii

Abstract..... iv

Key words..... v

Acronyms..... v

List of figures..... x

Chapter 1: Introduction

1.1. Overview..... 1

1.2. Statement of the problem..... 3

1.3. Research Objectives..... 4

1.4. Thesis Layout..... 5

References..... 6

Chapter 2: Background Information

2.1. Emissive Displays..... 7

2.1.1. Cathode ray tubes..... 7

2.1.2. Flat panel displays..... 8

2.1.3. Field emission displays..... 8

2.1.4. Comparison between a CRT and a FED..... 9

2.2. Fundamentals of phosphors..... 10

2.3. Vocabulary of luminescence..... 11

2.3.1. Cathodoluminescence..... 12

2.3.2. Photoluminescence..... 17

2.3.3 Applications of cathodoluminescence and photoluminescence..... 18

2.4. Cathodoluminescence degradation..... 18
2.5. Pfahnl's law and an electron stimulated surface chemical reaction..... 20
2.6. Thin film phosphors and surface coatings..... 24
2.7. Energy transfer in phosphors..... 25
References..... 28

Chapter 3: An overview of research techniques

3.1. Introduction..... 31
3.2. Auger electron spectroscopy..... 31
3.3. X-ray photoelectron spectroscopy..... 33
3.4. Pulsed laser deposition..... 35
3.5. X-ray diffraction..... 37
3.6. Fourier transform infrared spectroscopy..... 38
3.7. Scanning electron microscopy..... 39
References..... 41

Chapter 4: Degradation of Y_2O_3:Eu powder phosphors

4.1. Introduction..... 42
4.2. Experimental..... 42
4.3. Results and discussion..... 43
4.4. Conclusion..... 49
References..... 50

Chapter 5: Degradation of pulsed laser deposited Y_2O_3:Eu thin film phosphors

5.1. Introduction..... 51
5.2. Experimental..... 51
5.3. Results and discussion..... 52
4.4. Conclusion..... 56
References..... 57

Chapter 6: Degradation of SiO_2:Ce,Tb powder phosphors

6.1. Introduction..... 58
6.2. Experimental..... 58
6.3. Results and discussion..... 58
6.4. Conclusion..... 66
References..... 67

Chapter 7: Preparation of ZnO and rare-earths-doped SiO_2 nanoparticle phosphors by a sol-gel process

7.1. Introduction..... 68
7.2. Sol-gel..... 68
7.3. Experimental..... 69
7.3.1. Preparation of ZnO nanoparticles..... 69
7.3.2. Preparation of SiO_2:Eu and SiO_2:Eu with adsorbed ZnO nanoparticles..... 71
7.3.3. Preparation of SiO_2 nanoparticle phosphors co-doped different concentrations of Ce^{3+}-Eu^{3+}, Ce^{3+}-Tb^{3+} and Eu^{3+}-Tb^{3+} ion pairs..... 72
7.4. Results and discussions..... 72
7.5. Conclusion..... 77
References..... 78

Chapter 8: Enhanced photoluminescence of SiO_2:Eu and SiO_2:Ce induced by an energy transfer from embedded ZnO nanoparticles

8.1. Introduction..... 79
8.2. Results and discussions..... 79
8.3. Conclusion..... 86
References..... 87

Chapter 9: Energy transfer between Ce^{3+}, Eu^{3+} and Tb^{3+} in SiO_2 matrices

9.1. Introduction..... 88
9.2. Results and discussions..... 88
9.3. Conclusion..... 94
References..... 95

Chapter 10: Summary and Conclusion..... 96

Future prospects..... 98
Publications..... 99
International conferences..... 100
National conferences..... 102
Biography..... 104

LIST OF FIGURES

Figure 2.1. The basic components of a CRT tube.....8

Figure 2.2. A cross-sectional view of a field emission display.....9

Figure 2.3. A comparison between a CRT and a FED having similar screen dimensions.....10

Figure 2.4. Total number of electrons leaving a surface as a function of primary electron energy.....13

Figure 2.5. CL process in a phosphor grain.....14

Figure 2.6. Models of cathodoluminescent transitions.....15

Figure 2.7. Intra-atomic luminescent transitions in Eu^{3+}.....16

Figure 2.8. Configurational coordinate model of a luminescent centre.....19

Figure 2.9. (a) Two centres D and A separated by a distance R, (b) energy transfer between D and A (an illustration of equation 2.13), and (c) the overlap between D emission and A absorption spectra.....26

Figure 3.1. Three basic steps of the AES: (1) removal of the K electron (2) filling of the vacancy by the L_1 electron and (3) emission of the Auger electron.....32

Figure 3.2. The PHI model 549 Auger electron spectrometer.....33

Figure 3.3. Schematic diagram of the XPS process in copper.....34

Figure 3.4. Quantum 2000 scanning x-ray photoelectron spectrometer.....35

Figure 3.5. A picture of laser plume during ablation.....36

Figure 3.6. The PLD system for growing thin solid films.....37

Figure 3.7. Philips APD 3720 x-ray diffractometer.....38

Figure 3.8. Simplified layout of a FTIR spectrometer 39

Figure 3.9. Nicolet model 20 SXB FTIR spectrometer.....39

Figure 3.10. Leo-field secondary electron microscope.....40

Figure 4.1. Schematic diagram of the AES system and the S2000 optical spectrometer.....43

Figure 4.2. RGA spectra taken (a) before degradation at base pressure of 2.9×10^{-9} and (b) after degradation at 1×10^{-7} Torr O_2.....44

Figure 4.3. Auger spectra of Y_2O_3:Eu powders (a) before and (b) after degradation at 1×10^{-7} Torr O_2.....45
Figure 4.4. CL spectra of Y_2O_3:Eu before and after degradation at 1×10^{-7} Torr O_2.....46
Figure 4.5. CL intensity of Y_2O_3:Eu powders and the APPHs of O, Y, and C as a function of electron dose during degradation at (a) 1×10^{-8} Torr O_2 and (b) 1×10^{-7} Torr O_2.....47
Figure 4.6. Normalised CL intensity of Y_2O_3:Eu powder phosphor during degradation at 1×10^{-8} Torr O_2 and 1×10^{-7} Torr O_2.....48
Figure 4.7. APPH ratios of O/Y as a function of electron dose during degradation at (a) 1×10^{-7} Torr O_2 and (b) 1×10^{-8} Torr O_2.....49
Figure 5.1. Schematic diagram of the PLD system.....52
Figure 5.2. XPS spectra of Ta_2O_5-coated Y_2O_3:Eu thin film grown on a Si (100) substrate.....53
Figure 5.3. Auger spectra of Ta_2O_5-coated Y_2O_3:Eu thin film (a) before and (b) after degradation at 1×10^{-6} Torr O_2.....54
Figure 5.4. Normalised Auger peak heights of O as a function of electron dose for (a) uncoated and (b) Ta_2O_5-coated Y_2O_3:Eu thin films.....55
Figure 5.5. Normalised CL intensity of (a) uncoated and (b) Ta_2O_5-coated Y_2O_3:Eu thin films as a function of electron dose.....56
Figure 6.1. CL emission spectra of SiO_2:Ce,Tb powder phosphors before and after degradation 1×10^{-7} Torr O_2.....59
Figure 6.2. AES spectra (1) before and (2) after degradation 1×10^{-7} Torr O_2.....60
Figure 6.3. APPHs of O, Si and C as a function of electron dose at (a) 1×10^{-8} Torr O_2 and (b) 1×10^{-7} Torr O_2.....61
Figure 6.4. Normalised CL intensity of SiO_2:Ce,Tb powder phosphors as a function of electron dose of 2 keV electrons at (1) 1×10^{-8} Torr O_2 and (2) 1×10^{-7} Torr O_2.....62
Figure 6.5. Normalised APPHs of O as a function of electron dose of 2 keV electrons at (1) 1×10^{-7} Torr O_2 and (2) 1×10^{-8} Torr O_2.....63

Figure 6.6. XPS survey spectra of (1) degraded and (2) undegraded SiO_2:Ce,Tb powder phosphors 64
Figure 6.7. XPS high resolution peaks of SiO_2 from (1) degraded and (2) undegraded SiO_2:Ce,Tb powder phosphors 65
Figure 7.1. A flow diagram for the sol-gel preparation of ZnO nanoparticles.....70
Figure 7.2. A flow diagram for the sol-gel preparation of SiO_2:Eu, with adsorbed ZnO nanoparticles.....71
Figure 7.3. XRD patterns from (a) calcined ZnO-SiO_2 nanoparticle, (b) dried ZnO nanoparticle and (c) standard ZnO microparticle powders.....73
Figure 7.4. The SEM photograph of dried and powdered ZnO nanoparticles.....74
Figure 7.5 The SEM photograph of calcined SiO_2:Eu powder phosphor.....74
Figure 7.6. Schematic diagram showing the primary and secondary particles.....75
Figure 7.7. FTIR spectra from (1) ZnO nanoparticles, (2) ZnO microparticles, (3) ZnO-SiO_2:Eu and (4) SiO_2.....76
Figure 7.8. XPS survey spectrum of ZnO-SiO_2:Eu (ZnO = 5 mol% and Eu = 1 mol%).....77
Figure 8.1. Photoluminescence emission spectra from (1) dried ZnO nanoparticles, (2) ZnO nanoparticles suspended in EtOH and (3) standard ZnO microparticle powders.....80
Figure 8.2. UV emission spectra from (1) ZnO nanoparticles suspended in EtOH (2) dried ZnO nanoparticles and (3) standard ZnO microparticle powders.....81
Figure 8.3. Photoluminescence emission spectra from (1) ZnO-SiO_2:Eu and (2) SiO_2:Eu.....82
Figure 8.4. Photoluminescence emission spectra from (1) ZnO-SiO_2:Ce and (2) SiO_2:Ce.....82
Figure 8.5. Excitation of ZnO nanoparticles and energy transfer to Eu^{3+} ions in SiO_2.....83
Figure 8.6. Possible transitions in ZnO and Eu^{3+} ions and proposed mechanism of energy transfer from ZnO to Eu^{3+} ions.....84

Figure 8.7. Possible transitions in ZnO and Eu^{3+} ions and proposed mechanism of energy transfer from ZnO to Ce^{3+} ions.....85
Figure 9.1. PL emission spectra of SiO_2:Ce,Eu nanoparticle powder phosphors with concentrations of Ce^{3+} and Eu^{3+} ions varied between 0 and 1 mol %.....89
Figure 9.2. Possible transitions in Ce^{3+} and Eu^{3+} ions, and proposed mechanism of energy transfer from Eu^{3+} ions to Ce^{3+} ions.....90
Figure 9.3. PL emission spectra of SiO_2:Ce (5 mol%) and SiO_2:Eu (5 mol%) nanoparticle powder phosphors.....91
Figure 9.4. PL emission spectra of SiO_2:Ce,Eu with different concentrations of Ce^{3+} and Tb^{3+} ions.....92
Figure 9.5. Possible transitions in Ce^{3+} and Tb^{3+} ions that result in an energy transfer from Ce^{3+} ions to Ce^{3+} ions.....93

CHAPTER 1: INTRODUCTION

1.1. OVERVIEW

Initially, only sulphide powder phosphors (e.g. ZnS:Cu,Au,Al, ZnS:Ag,Cl and Y_2O_2S:Eu) were used in electronic displays such as cathode ray tubes (CRTs) and field emission displays (FEDs) [1]. However, it has been established that cathodoluminescence (CL) intensity of these phosphors degrades rapidly under prolonged electron beam exposure by releasing volatile sulphur compounds (SO_x) which may contaminate the emitter tips of FED devices [2]. At high temperatures and poor vacuum pressures, these phosphors have been found to be chemically unstable, resulting in the degradation of the surface layer and a detrimental effect on the CL efficiency [3]. The CL efficiency of sulphide phosphors can also be affected by high current densities and low voltages required for FEDs [3].

Oxide phosphors have been reported to be more chemically and thermodynamically stable under high current densities and at elevated temperatures [4,5,6]. Unlike sulphide phosphors, oxide phosphors do not release volatile compounds detrimental to emitter tips of FEDs during electron beam exposure [5,6]. Oxide phosphors have therefore been considered to replace sulphide phosphors in low-voltage FEDs.

In order to solve technological problems associated with the CL degradation of powder phosphors more effort has been directed to the development of thin films of oxide phosphors for application in FEDs. Compared to powders, thin film phosphors offer advantages such as good adhesion to the substrate, better thermal stability, less outgassing, uniform properties across the covered areas and they also offer higher resolution with less material [6,7]. The rate of CL intensity degradation can be reduced by coating the film surface with a thin material that has good optical properties and is transparent to light resulting from excitation by low energy electrons [8].

The realization that micro-sized materials and nanomaterials (nanoparticles) have different electronic and optical properties has resulted in increased research activities on luminescent properties of nanoparticles over the past ten years. The differences in electronic and optical properties have been ascribed to the quantum confinement effect of charge carriers (electrons and holes) in the restricted volume of nanoparticles. Quantum confinement can lead to effects such as increased spacing of energy levels and increased bandgap, resulting in spectral shifts [9,10]. Based on the difference in electronic and optical properties, it has been speculated that CL intensity of nanoscale phosphors (nanophosphors) may be superior to that of micro-sized phosphors under low-voltage excitation [9]. Luminescent properties of nanophosphors (oxide and sulphide) are also being evaluated for application in low-voltage FEDs.

There has been a rapid increase in synthesis and characterization of nanophosphors over the past ten years due to the realization that a nanoparticle can transfer energy to another nanoparticle non-radiatively via electronic interaction (i.e. long range resonance transfer) [11,12]. This suggests that energy transfer processes could be used to enhance cathodoluminescence and photoluminescence intensity of nanophosphors. Nongami *et al.* [12], Hayakawa *et al.* [13] and Bang *et al.* [11] have reported an energy transfer from CdS, SnO_2 and ZnO nanoparticles, respectively, to Eu^{3+} ions embedded in SiO_2 matrices. This transfer of energy resulted in considerable enhancement of red photoluminescence of the Eu^{3+} ions.

Energy transfer in micro-sized powder phosphors has also been reported between rare-earth elements such as Tb^{3+}, Ce^{3+}, Eu^{3+}, Sm^{3+} etc. co-doped with different concentrations in different host matrices. For example, Lin and Su [14] observed energy transfer from Ce^{3+} to Tb^{3+} ions in $Mg_2Y_8(SiO_4)_4O_2$. Nazarov *et al.* [15] reported energy transfer between Tb^{3+} and Eu^{3+} co-doped in $CaWO_4$. In general, the probability of energy transfer between co-doped rare-earth activator elements has been found to depend on the host matrix and the concentration of the activators [15]. This finding has inspired many researchers to explore energy transfer between rare-earth elements co-doped with different concentrations in different host matrices.

A variety of methods have been used to synthesize nanoscale phosphors that could be used in low-voltage FEDs. These include chemical vapour deposition, hydrothermal, sol-gel, high-temperature organometallic and microwave-assisted methods. The sol-gel method has been widely used [11,12,13] to prepare a variety of luminescent nanoparticle materials for use in flat panel displays. This method was also used in this study to synthesize nanoscale phosphors, which were characterized for application in low-voltage FEDs.

1.2. STATEMENT OF THE PROBLEM

A lot of research has been devoted to cathodoluminescence degradation of micro-sized sulphide phosphors since they are used in many display applications including CRTs and FEDs. A mechanism that shows the relationship between their CL degradation and surface chemical reactions has been established. Since these phosphors are not very efficient at low voltages required for FEDs, micro-sized and nanoparticle oxide phosphors are being investigated to replace them.

Investigation of oxide phosphors has mainly been limited to luminescent properties of thin films of europium-doped yttrium oxide (Y_2O_3:Eu) phosphor. A proper way to evaluate these phosphors for application in low-voltage FEDs would be to study their luminescent properties including CL and surface degradation during prolonged electron beam exposure. It is important to determine the mechanism that shows the correlation between their CL degradation and changes on the surface chemical composition during electron beam exposure. Williams [4] studied the CL degradation of micro-sized oxide thin film and powder phosphors but could not determine the mechanism that correlates the CL degradation with changes on the surface chemical composition during electron beam exposure.

In the case of oxide nanophosphors, the focus has mainly been on enhancement of photoluminescence by an energy transfer from embedded nanoparticles to luminescent centres. Energy transfer in nanophosphors could also be evaluated between pairs of

activator ions co-doped in different host matrices. Considering the fact that oxide nanophosphors have potential for application in low-voltage FEDs, it is imperative to study their degradation and determine the mechanism that shows the relationship between their CL degradation and changes that occur on the surface during electron beam exposure.

1.3. RESEARCH OBJECTIVES

To investigate:

(i) the CL degradation of micro-sized Y_2O_3:Eu powder and thin film phosphors.

(ii) the effect of surface coating on luminescent intensity of thin films of Y_2O_3:Eu phosphor.

(iii) the CL degradation of SiO_2:Ce,Tb nanoparticle powder phosphors.

(iv) non-radiative energy transfer from ZnO nanoparticles to Eu^{3+} and Ce^{3+} ions embedded in SiO_2 .

(v) non-radiative energy transfer between Ce^{3+}-Tb^{3+}, Ce^{3+}-Eu^{3+} and Eu^{3+}-Tb^{3+} ion pairs confined in SiO_2 with different concentrations.

1.4. THESIS LAYOUT

Chapter 2 provides background information on electronic displays (cathode ray tubes and field emission display), fundamentals of phosphors and luminescence processes such as cathodoluminescence and photoluminescence. Detailed information on energy transfer in phosphors and of cathodoluminescence degradation of sulphide phosphors is also provided.

A summary of surface analysis techniques used in this study is provided in *chapter 3*. This includes a brief description on how each of these techniques works.

Chapters 4, 5, and *6* deal with cathodoluminescence degradation of Y_2O_3:Eu powder, pulsed laser deposited Y_2O_3:Eu thin film and sol-gel SiO_2:Ce,Tb powder phosphors respectively. Possible mechanisms that relate changes on the surface chemical composition to the decrease of CL intensity are discussed.

Preparation and encapsulation of ZnO nanoparticles into SiO_2:Eu and SiO_2:Ce and co-doping of Ce^{3+}-Eu^{3+}, Ce^{3+}-Tb^{3+} and Eu^{3+}-Tb^{3+} ion pairs in SiO_2 matrices by a sol-gel process is discussed in *chapter 7*.

Energy transfer between ZnO nanoparticles and Ce^{3+} and Eu^{3+} embedded in SiO_2 is discussed in *chapter 8* and energy transfer between Ce^{3+}-Eu^{3+}, Ce^{3+}-Tb^{3+} and Eu^{3+}-Tb^{3+} ions pairs co-doped with different concentrations in SiO_2 is discussed in *chapter 9*. Possible mechanisms for energy transfer from one luminescent centre to another are discussed.

A summary of the thesis, conclusion and suggestions for possible future studies are discussed in *chapter 10*.

REFERENCES

[1] Pham-Thi M. and Morel A., *J. Electrochem. Soc.* **138** (4) (1999) 1100

[2] Trottier T.A., *Ph.D. dissertation*, University of Florida, Florida, (1998)

[3] Coopeland T.S., Lee B., Qi J. and Elrod A.K., *J. Lumin.* **97** (2002) 168

[4] Williams L.C., *Ph.D. dissertation*, University of Florida, Florida (2004)

[5] Cho K.G., Kumar D., Holloway P.H. and Singh R.K., *Appl. Phys. Lett.* **73**(21) (1998) 3058

[6] Lee R.Y., Zhang F.L., Penczek J. and Wagner B.K., *J. Vac. Sci. Technol. B* **16** (2) (1998) 855

[7] Hirata G.A., McKittrick J., Avalos-Borja M., Siqueros J.M. and Devlin D., *Applied Surface Science* **113/114** (1997) 509

[8] Fitz-Gerald J.M., Trottier T.A., Singh R.K. and Holloway P.H., *Appl. Phys. Lett.* **72**(15) (1998) 1838

[9] Wong E.M., Bonevich J.E. and Searson P.C., *J. Phy Chem B* 102 (1998) 7770

[10] Kagan C.R., Murray C.B. and Bawendi M.G., *Phys. Rev. B* **54** (12) (1996) 8633

[11] Bang J., Yang H. and Holloway P.H., *J. Chem. Phys.* **123** (2005) 1

[12] Nogami M., Enomoto T. and Hayakawa T., *J. Lumin.* 97 (2002) 147.

[13] Hayakawa T., Selvan T. and Nogami M., *J. Sol. Sci. Tech.* 19 (2000) 779.

[14] Lin J. and Su Q., *J. Mat. Chem.* **5**(8) (1995) 1151

[15] Nazarov M.V., Jeon D.Y. , Kang J.H., Popovici E-J., Muresan L-E., Zamoryanskaya M.V. and Tsukerblat B.S., *Sol. State Comm.* **131** (2004) 307

CHAPTER 2: BACKGROUND INFORMATION

2.1. EMISSIVE DISPLAYS

Emissive displays are electronic devices that involve the conversion of electrical energy to luminous energy as a function of the real image signal [1]. They are divided into three categories, namely projection, off-screen and direct-view. A projection display is an electronic device that utilizes a viewing screen separate from the optical source. An off-screen display is a device where the image is not viewed on a screen. A direct-view display is a device where the image is generated in the immediate proximity of the viewing screen. Direct-view displays are classified into cathode ray tubes (CRTs) and flat panel displays (FPDs).

2.1.1. CATHODE RAY TUBES

A CRT is a vacuum tube in which an electron beam is accelerated with high voltage (20 kV or more) and projected toward a phosphor (material that emits light when struck with a beam of electrons) deposited on a screen that forms the front face of the tube [2]. The electron beam is produced by an assembly called an "electron gun"(cathode) located at the rear of the tube as illustrated in figure 2.1. To form an image on the screen, the beam is deflected in the vertical and horizontal directions either by the electrostatic effect of electrodes within the tube or by magnetic fields produced by coils located around the neck of the tube [2]. When the electron beam strikes the phosphor-coated screen, a tiny bright visible spot is produced on the screen. The image is formed when the beam is rastered across the screen. CRTs are commonly used to obtain visual display of electronic information in oscilloscopes, radar systems, television receivers and computer monitors. Typical values of cathode to anode distance (**D**) (see figure 2.1) range from 25 to 100 cm.

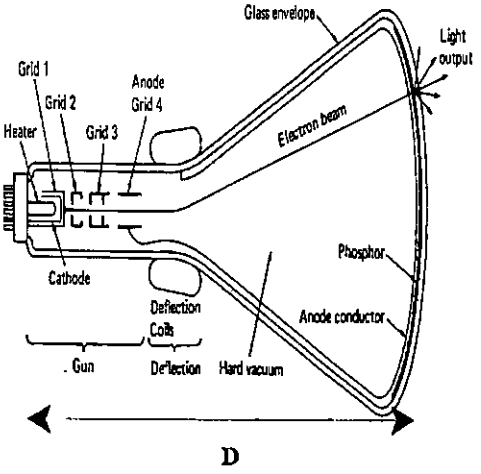

Figure 2.1. The basic components of a CRT tube [2].

2.1.2. FLAT PANEL DISPLAYS

FPDs are flat and light and do not require a great deal of power to accelerate electrons from the cathode to the anode. They are often defined as ideal displays that are thin, have low volume, an even surface, a high resolution, high contrast, sunlight readability and are solid state and lightweight [2]. Some examples of FPDs are plasma display panel (PDP), vacuum fluorescent display (VFD), liquid crystal display (LCD) and field emission display (FED). Since the FED is promising to give a better performance compared to other FPDs [2], many industrial groups are investing in its development. It is in line with this that this study is aimed at investigating phosphors for application in low voltage FEDs.

2.1.3. FIELD EMISSION DISPLAYS

A FED is an emissive vacuum electron device in which electron emitters (arranged in a grid) are individually controlled by "cold" cathodes to generate light. It shares many common features with the VFD and the CRT. The image is formed by impinging electrons from a cathode onto a phosphor-coated screen that is typically kept at a potential of 5 kV or less [3]. A cross sectional view of the FED is shown in figure 2.2. The electron source in the FED consists of a matrix-addressed array of millions of cold

emitters. This array of field emitters is placed in close proximity (0.1 – 3 mm) [4] with a phosphor faceplate and is aligned such that each pixel has its own set of field emitters.

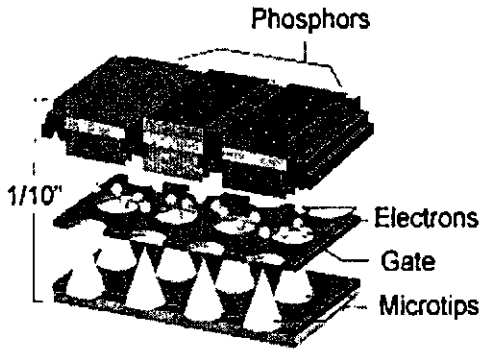

Figure 2.2. A cross-sectional view of a field emission display [5].

2.1.4. COMPARISON BETWEEN A CRT AND A FED

CRT and FED share many common features, including a glass vacuum envelope, a phosphor coated anode and a cathode electron source. They both generate light by cathodoluminescence (CL) process, i.e. electrons from the cathode are accelerated across a vacuum gap to bombard the phosphor screen (anode) and produce light. The major difference between these two displays is the source of electrons. In the CRT, three electron guns are used to raster a beam of electrons across the screen that is typically kept at a potential of 20 kV or more, whereas the FED employs an array of field emitters to accelerate electrons to the screen usually kept at 5 kV or less [3,6]. The basic design of the CRT is such that a certain distance (usually 25 – 100 cm) is required between the cathode and the anode to ensure a proper focus and raster capability. In the FED, the distance between the cathode and the anode ranges from 0.1 to 3 mm [4]. Figure 2.3 compares a CRT and a FED, having similar screen dimensions. In view of common features between the CRT and the FED, the FED manufacturers have adopted the standard CRT phosphors [7].

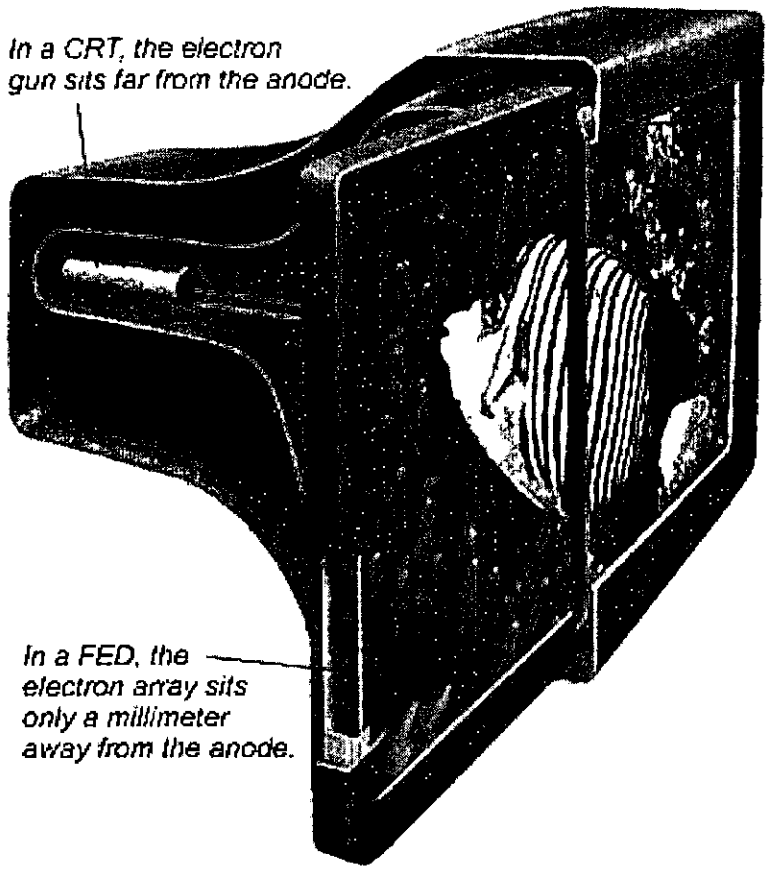

Figure 2.3. A comparison between a CRT and a FED having similar screen dimensions [8].

2.2. FUNDAMENTALS OF PHOSPHORS

A phosphor is any sensitive material that emits visible light when exposed to photons or a beam of electrons [7]. The amount of light emitted depends on the amount of energy used for excitation. Phosphors are usually in the form of powders, but in some cases they may be in the form of thin solid films. They are synthesised by intentionally introducing an impurity with a relatively low concentration into an inorganic crystalline material [7]. The impurity that activates the crystal to luminesce is referred to as an activator or a dopant, while the crystal itself is referred to as the host matrix [7,9]. A phosphor is usually identified by its chemical formula, e.g. ZnS:Cu, where ZnS is the host matrix and Cu is the activator. If more than one activator is used, commas are used to separate them (e.g. ZnS:Cu,Au,Al), and these additional activators (Au and Al) are called co-

activators. The host materials of activators should have wide bandgaps and be transparent enough to enable the transfer of visible light to the surface. A phosphor should also be chemically stable in the presence of water since it is usually suspended in an aqueous solution during the screen deposition process [7]. In addition, it should be thermally stable since the CRT (or FED) glass envelope must be outgassed in vacuum by baking at temperatures ranging from 250 – 350 °C [7].

Phosphors are usually unique to particular applications since their characteristics are tailored to the type of stimulus and the wavelength of the output radiation. In both the CRT and FED, phosphors are excited by a beam of electrons accelerated from the cathode to the anode. In plasma monitors, phosphors are excited by UV light produced by electromagnetically charged plasma. The operating conditions of a FED place a number of critical requirements on a phosphor. These include good chromaticity, high luminance, high efficiency, low saturation and good aging properties at low voltage and high current densities [10]. All these requirements must be considered when preparing phosphors for FEDs.

2.3. VOCABULARY OF LUMINESCENCE

Luminescence is the phenomenon of emission of light from various phosphor materials [9]. It may be divided into two kinds, namely phosphorescence and fluorescence. Phosphorescence is a slow process in which emission continues for a few seconds, minutes or even hours after removing excitation [11], whereas fluorescence is a fast process in which emission stops abruptly after turning off the excitation [9,11]. Each type of luminescence may be referred to by a name according to the method of excitation. For example: photofluorescence (photophosphorescence) is an excitation caused by photons, cathodofluorescence (cathodophosphorescence) is an excitation caused by high energy electrons and electrofluorescence (electrophosphorescence) refers to excitation caused by the passage of an electric current through the specimen. For some manifestation of luminescence, it is not necessary to attempt their classification into either fluorescence or phosphorescence and the terms photoluminescence,

cathodoluminescence and electroluminescence are currently being used. In this study, only cathodoluminescence and photoluminescence processes are discussed.

2.5. CATHODOLUMINESCENCE

Cathodoluminescence (CL) is defined as luminescence stimulated by a collision between an energetic beam of electrons (primary electrons) and a solid material (phosphor) resulting in an emission of visible light. The most common example is the CL process taking place on the screen of a television set: CRT or FED. Two types of collisions are possible, namely elastic and inelastic collisions. An elastic collision occurs between primary electrons and atoms of target material. This collision type produces back-scattered electrons, which suffer virtually no loss of energy. Inelastic collisions involve electron-electron and electron-plasmon interactions. In these cases, a single primary electron undergoes rapid inelastic collision within a phosphor. Each collision can produce secondary electrons (secondaries). The secondaries whose energies exceed the work function of the phosphor will escape into vacuum; otherwise they will be trapped within the lattice. Figure 2.4 depicts the number of electrons, N(e), emitted as a function of energy (E) during collision between primary electrons and target material. The peak on the right is due to those electrons, which have undergone purely elastic collision without losing energy. All the electrons whose energy is below this peak have undergone inelastic collision. The large peak on the left is due to those secondaries that escape to the vacuum [12] and they are referred to as "true secondaries". The "true secondaries" are not responsible for the CL process, it is rather those secondaries trapped within the phosphor that are pertinent to CL since they can generate electron-hole pairs when they couple.

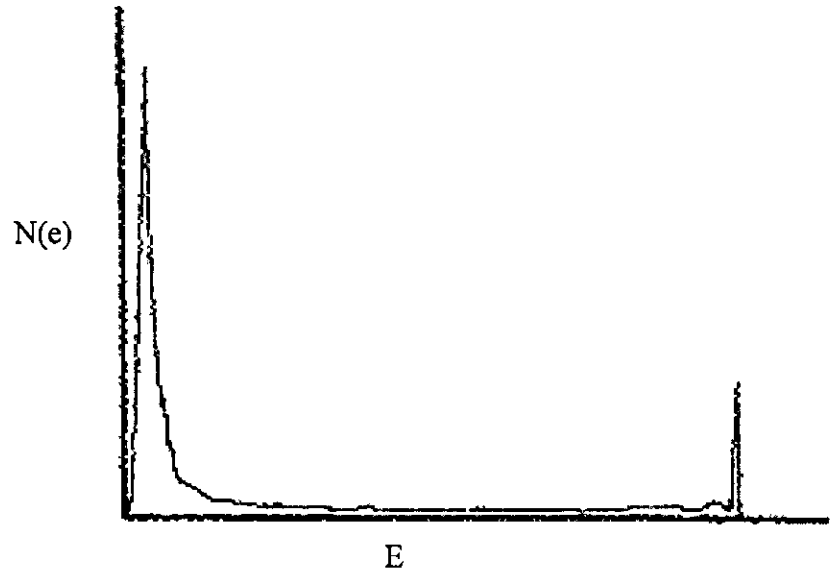

Figure 2.4 Total number of electrons leaving a surface as a function of energy [12].

2.5.1. EMISSION OF LIGHT IN A PHOSPHORS BY A CL PROCESS

When an energetic electron is incident on a phosphor, a number of physical processes occur. These include emission of secondary electrons, Auger electrons and back-scaterred electrons. Hundreds of free electrons and free holes are produced along the path of the incident electron (primary electron). As illustrated in Figure 2.5, the free electrons and holes may couple and produce electron-hole (e-h) pairs.

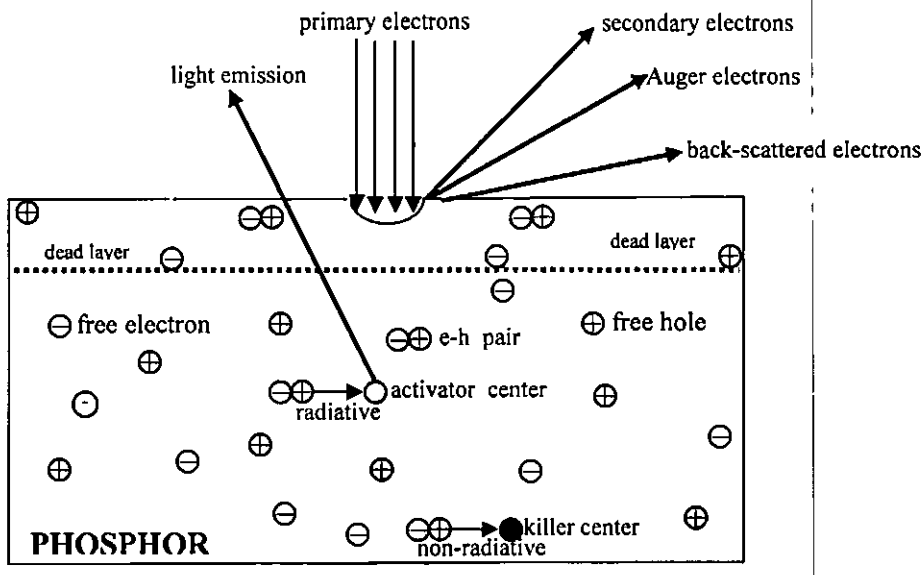

Figure 2.5. CL process in a phosphor grain.

The e-h pairs can diffuse through the phosphor and transfer their energy to activator ions and subsequently emit light [13,14]. This process is referred to as radiative recombination. Unwanted process in which the e-h pairs recombine non-radiatively by transferring their energy to killer centres (incidental impurities and inherent lattice defects) is also possible. The e-h pair can also diffuse to the surface of the phosphor and recombine non-radiatively [13]. A thin "dead" (non-luminescent) layer may be formed on the surface.

2.5.1. MODELS OF CATHODOLUMINESCENCE TRANSITIONS

FED or CRT phosphors may be classified into two groups according to transitions that occur when they are bombarded with an energetic electron (2 – 10 keV). One group includes phosphors where cathodoluminescent transitions occur in the bandgap and the other group includes phosphors where transitions are localized in luminescent centres such as rare-earth elements. These are referred to as bandgap and intra-atomic transitions respectively.

2.3.1.2.1. BANDGAP TRANSITION PHOSPHORS

Figure 2.6 shows models of bandgap transitions in a phosphor. During bombardment of a phosphor by an energetic electron (2 – 10 keV), free electrons and free holes are generated in the conduction and valence bands respectively [7]. If the crystal is perfect, i.e. free from impurities and lattice defects, the free electrons and holes may recombine directly and subsequently emit photons. The energy of each photon is equal to the bandgap between the valence and conduction bands [7]. This direct recombination process is represented by model (a) in Figure 2.6. However, this intrinsic emission due to band-to-band transition is rarely found in CRT/FED phosphors except in the ultraviolet emission band of ZnO phosphor [15]. The presence of activator impurities, incidental impurities and lattice defects usually distort the crystal and create localized energy levels (impurity levels) in the bandgap. This provides effective recombination paths for the free electrons and holes as represented by (b), (c) and (d) in Figure 2.6. The photon energy of these transitions is smaller than the bandgap in accordance with the impurity level.

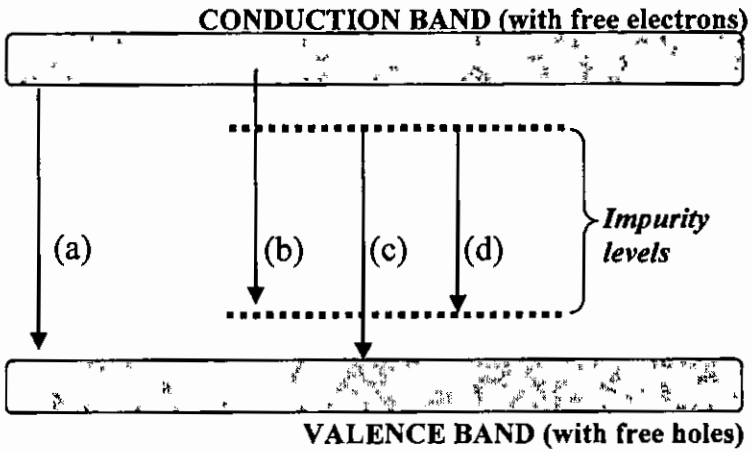

Figure 2.6. Models of cathodoluminescent transitions.

Model (b) in figure 2.6, i.e. transition between a free electron in the conduction and a hole trapped by an acceptor level was first proposed for the blue and green luminescence

of Ag and Cu activators in ZnS, respectively [16]. Model (c) represents a transition between a deep donor level and the valence band (a free hole). However, both (b) and (c) rarely occur in CRT/FED phosphors. Model (d), i.e. transition between a donor and an acceptor, was later accepted for CRT/FED phosphors. It has been speculated that cathodoluminescent process in ZnS:Cu,Al,Au (green) and ZnS:Ag,Cl (blue) occur according to model (d) in which Cu and Ag produce deep acceptor levels and Al and Cl produced shallow donor levels [7].

2.3.1.2.2. INTRA-ATOMIC TRANSITION PHOSPHORS

In many rare-earth-doped phosphors such as Y_2O_2S:Eu and Y_2O_3:Eu, light emission does not involve a transition between an activator ion (Eu^{3+}) and a host matrix (Y_2O_2S or Y_2O_3). It results from transitions localized within luminescent centres (Eu^{3+} ions). This has been attributed to a shielding effect of the $4f$ electrons by the $5s$ and $5p$ electron shells of the Eu^{3+} [17,18]. Figure 2.7 shows an energy level diagram of luminescent transitions within Eu^{3+}. The diagram shows that absorbed excitation (high energy electrons) induces transitions to higher f levels whereupon non-radiative transitions to the ^5D_J (J = 0,1,2,3) states occur. This is followed by radiative transitions to the ground state.

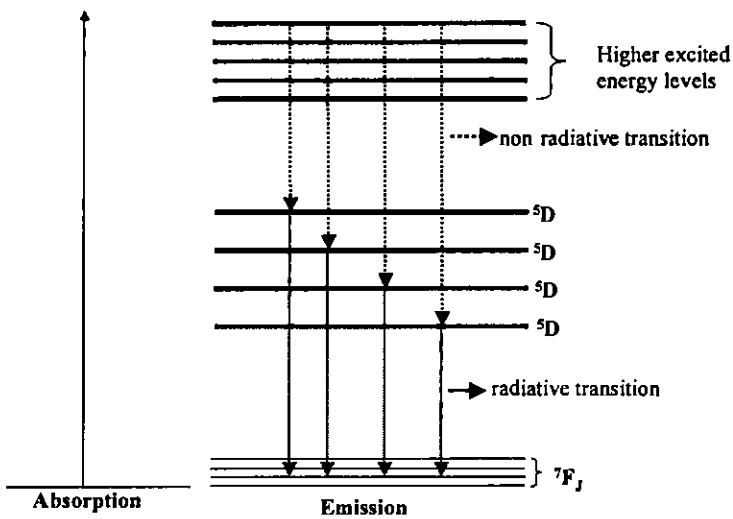

Figure 2.7. Intra-atomic luminescent transitions in Eu^{3+} ion.

2.5. PHOTOLUMINESCENCE

Photoluminescence refers to luminescence stimulated by the interaction of a photon (visible, ultraviolet or infrared) with a solid material (phosphor). It is divided into two major types, namely intrinsic photoluminescence and extrinsic photoluminescence [19]. Intrinsic photoluminescence is displayed by materials, which contain no impurity atoms. Extrinsic photoluminescence results from intentionally incorporated impurities, in most cases metallic impurities or intrinsic defects [19].

2.5.1. INTRINSIC PHOTOLUMINESCENCE

There are three kinds of intrinsic photoluminescence, namely band-to-band, exciton and cross-luminescence. Band-to-band photoluminescence occurs when an electron in the conduction band recombines with a hole in the valence band. This process can only be observed in materials of high purity and high lattice quality. An exciton is a composite particle resulting from the coupling of an electron and a hole [20]. It then travels in a crystal and produces luminescence by releasing its energy at luminescent centres [20]. Cross-luminescence is produced by the recombination of an electron in the valence band with a hole in the outermost core band [19].

2.5.1. EXTRINSIC PHOTOLUMINESCENCE

Extrinsic photoluminescence is produced by intentionally incorporated impurities. In most cases this is produced by metallic impurities and defects [19]. Extrinsic luminescence is divided into two types, namely localized and delocalized luminescence. In a delocalized luminescence the excited electrons and holes of the host lattice participate in luminescence process [19]. ZnS:Cu,Al,Au is an example of a phosphor where delocalized luminescence occur. In localized luminescence, the host lattice does not contribute to luminescence process. The luminescence process is confined to activators such as Eu^{3+} ions in Y_2O_3:Eu phosphor .

2.5. APPLICATIONS OF CATHODOLUMINESCENCE AND PHOTOLUMINESCENCE

Cathodoluminescence and photoluminescence have many applications in light- emitting devices such as CRTs, FEDs, fluorescent lamps, solid state lasers, optical wave guides and fiber amplifier. In CRTs and FEDs light emission is produced by cathodoluminescence process in which the electrons, from the cathode, interact with phosphor material deposited on the screen of the device. Photoluminescence can be used to determine the bandgap of new semiconductor compounds, to identify specific defects, to understand the physics underlying the recombination mechanisms in semiconductors and also to determine the quality of materials by quantifying the amount of radiative recombination produced [19].

2.5. CATHODOLUMINESCENCE DEGRADATION

Cathodoluminescence intensity of CRT/FED phosphor is known to degrade drastically due to prolonged exposure to a beam of electrons. Degradation of the CL intensity of phosphors has been a subject of interest since the 1960s. It is defined as a reduction (quenching) of luminescence efficiency of phosphors during electron beam or photon exposure [7]. There are two kinds of effects that contribute to the CL degradation. These are (1) the presence of a killer (incidental impurities or lattice defects) and (2) thermal quenching (an increase in temperature) [7].

2.5.1. KILLERS

Killers are defects caused by incidental impurities (adsorbed atoms or molecules) as well as defects that are inherent to the lattice. The impurities adsorbed at the surface may quench cathodoluminescence by producing a non-luminescent surface layer [7] when they react with ambient vacuum species. There are two ways in which killers can quench luminescence of phosphors. First, bypassing killers are capable of capturing free carriers in competition with luminescent centres during diffusion of the free carriers produced by

excitation, allowing them to recombine non-radiatively. Second, ionization of impurity atoms may quench luminescence when competing with intra-ionic radiative transitions during resonant energy transfer processes [21].

2.4.2. THERMAL QUENCHING

Thermal quenching refers to reduction in luminescence of a luminescent centre due to an increase in temperature. It occurs at high temperatures when thermal vibrations of atoms surrounding the luminescent centre transfer energy away from the centre resulting in a non-radiative recombination, and a subsequent depletion of the excess energy as phonons in the lattice [22]. Thermal quenching process can be described in terms of configurational coordinate model of a luminescent centre shown in figure 2.8.

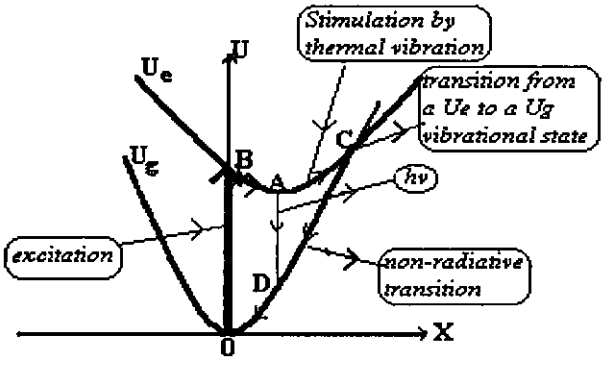

Figure 2.8. Configurational coordinate model of a luminescent centre [23].

The U_g and U_e in figure 2.8 represent the energies of luminescent centres in the ground state and in the excited state, respectively. If the centre is optically excited, the system undergoes a vertical transition from the stable ground state (point 0 on the U_g) to the excited state (point B on the U_e). This transition causes the system to adapt to the new equilibrium situation by changing its atomic configuration from B to the new equilibrium (A) along the curve U_e, with excess energy dissipated as heat. In a short while, the system undergoes a vertical jump, a radiative transition, from A to D, emitting the energy difference between the two states as radiation. This transition is then followed by the

slower rearrangement of the atomic configuration from A to 0 along U_g, with excess energy dissipated as heat. If the system temperature is too high, the luminescent centre can be stimulated from A to C along U_e. The centre may transit, at the crossing point C, from the vibration state of the excited state to a different vibration state of the ground state 0, with the vibration energy dissipated into the host lattice. Thus, the non-radiative relaxation from A competes at high temperatures with a radiative transition from A to D, causing thermal quenching of emission [7].

2.5. PFANHL'S LAW AND AN ELECTRON STIMULTED SURFACE CHEMICAL REACTION

Extensive research performed on the CL degradation of phosphors over the past four decades has resulted in the proposal of Pfanhl's law that describes the rate of degradation of CL intensity, and in the development of a model called an electron stimulated surface chemical reaction (ESSCR), which predicts that the CL degradation is depended upon the type of gas in the vacuum, gas pressure, beam voltage and electron (coulombic) dose [24].

2.5.1. PFANHL'S LAW

Pfanhl's law was proposed by A. Pfahnl [25] in the 1960s after investigating the CL degradation in a large number of phosphors. He attributed the CL degradation in non-activated phosphors such as ZnO and $CaWO_4$ phosphors to the creation of new non-radiative recombination sites, whereas in many Ce^{3+} activated phosphors he attributed the CL degradation to both increasing non-radiative recombination and de-activation of luminescent sites by charge compensation (i.e. $Ce^{3+} \rightarrow Ce^{2+}$). The expression (Pfanhl's law) that describes the rate of CL intensity of phosphors is given by [25]:

$$I(N) = \frac{I_0}{(1 + CN)}, \tag{2.1}$$

where I is the aged CL intensity, I_0 is the initial CL intensity, N is the number of electrons per unit area and C is the burn parameter which is equal to the inverse of the number of electrons per unit area required to reduce the intensity to half its original value [25].

2.5.2. ELECTRON STIMULATED SURFACE CHEMICAL REACTION

A mathematical model of an ESSCR developed by Holloway *et al* [24] shows the correlation between degradation of CL intensity and the depletion of sulphur (S) from the surface of ZnS:Cu,Al,Au and ZnS:Ag,Cl powder phosphors. According to this model, the concentration of S on the surface, C_S, can be represented by a standard chemical rate equation:

$$\frac{dC_S}{dt} = -kC_S C_{as}^n, \tag{2.2}$$

where k is a chemical rate constant, C_{as}^n is the concentration of the adsorbed atomic species that will react with ZnS, n is the order of the surface reaction; and the first order surface reactions are assumed [25]. Assuming that the reaction takes place on the surface, C_{as} can be expressed as:

$$C_{as} = Z\phi_{ma} C_m J \tau_{as}, \tag{2.3}$$

where Z is the number of reactive atomic species produced from the parent molecule, ϕ_{ma} is the dissociation cross section of the molecule to atoms, C_m is the surface concentration of the molecular species, J is the current density causing the dissociation, and τ_{as} is the lifetime of a reactive atomic species [25]. C_m controls the rate of production of C_{as} and can be expressed as:

$$C_m = \sigma(\tau_o \, e^{Q/kT})\left(\frac{P_m}{\sqrt{2\pi mkT}}\right), \tag{2.4}$$

where σ is the molecular sticking coefficient and the first term in brackets is the molecular mean stay time on the surface, while the second term in brackets is the

molecular flux onto the surface. τ_o is the mean time between attempts by the adsorbed molecule to escape from the surface, Q is the energy required to desorb from the surface, k is Boltzman's constant, T is absolute temperature, and P_m is the partial pressure of the molecular gas in the vacuum. Substituting equations (2.3) and (2.4) into (2.2) gives:

$$\frac{dC_s}{dt} = -k\sigma C_s Z\phi_{ma} J\tau_{as}(\tau_o e^{Q/kT})(\frac{P_m}{\sqrt{2\pi mkT}}). \tag{2.5}$$

Equation (2.5) may be written as

$$\frac{dC_s}{C_s} = -K'JP_m dt, \tag{2.6}$$

where K' is defined by

$$K' = k\sigma Z\phi_{ma}\tau_{as}(\tau_o e^{Q/kT})(\sqrt{2\pi mkT}). \tag{2.7}$$

Integrating equation (2.7) with respect to time yields

$$C_s = C_s^0 e^{-K'P_m Jt}, \tag{2.8}$$

where the boundary conditions of $C_s = C_s^0$ at time equal to zero were applied. Jt is equal to coulomb per unit area or the electron dose, also known as the coulombic dose [24]. This model predicts that the concentration of S will decrease exponentially with coulombic dose, and the rate of loss will be larger at higher gas pressures. Since the C_S and the CL intensity are correlated, equation (2.8) can be written in terms of the CL intensity, I_{CL}, as

$$I_{CL} = I_{CL}^0 e^{-K'P_m Jt} \tag{2.9}$$

The study of degradation of sulphide phosphors such as ZnS:Cu,Al,Au, ZnS:Ag,Cl and Y_2O_2S:Eu showed a direct correlation between the decrease of CL intensity and changes

in the surface chemistry during prolonged exposure to a beam of electrons. These changes suggest that electron beam stimulated surface chemical reactions are occurring.

In the case of ZnS phosphors, it has been widely accepted that ZnS can combine with reactive atomic species from electron-beam-dissociated ambient vacuum gases such O_2 and H_2O to form a non-luminescent layer of either ZnO or $ZnSO_4$ [26,27]. The formation of these layers can be expressed by the following chemical reactions:

$$ZnS + 2O_2 \rightleftharpoons ZnSO_4 \tag{2.10}$$

$$2ZnS + 3O_2 \rightleftharpoons 2ZnO + 2SO_2 \tag{2.11}$$

$$ZnS + H_2O \rightleftharpoons ZnO + H_2S(\uparrow) \tag{2.12}$$

Itoh *et al.* [27] reported that a $ZnSO_4$ layer was formed on the surface when ZnS:Cu,Al,Au was degraded in an H_2O, which is not in agreement with equations (2.10) and (2.12). Swart *et al.* [26] used XPS to confirm that a ZnO layer was formed on the surface of the ZnS:Cu,Al,Au phosphor according to reaction (2.11). Sebastian *et al.* [28] proposed the formation of ZnO layer according to reaction (2.12). Chen *et al.* [29] degraded ZnS:Cu,Al,Au powder phosphors in different mixture of gases and concluded that $ZnSO_4$ layer was formed when degrading in the dry O_2 ambient and ZnO layer was formed when degrading in an H_2O ambient. Along with the formation of ZnO layer, Sebastian *et al.* [28] demonstrated that subsurface point defects of isoelectronic oxygen, which led to an increased probability of non-radiative recombination, were also created. In the case of Y_2O_2S:Eu, the ESSCR led to the formation of less luminescent Y_2O_3:Eu layer [25], which decreased the CL intensity significantly.

2.6. THIN FILM PHOSPHORS AND SURFACE COATINGS

Physical and luminescent properties of Y_2O_3:Eu thin films grown by either pulsed laser deposition or metalorganic techniques have been investigated by various researchers [30-34]. It has been reported that post-deposition annealing at temperatures ranging from 800°C to 1200°C improved luminescent intensity of thin film phosphors considerably [16,30-33]. However, the study of luminescent properties of Y_2O_2S:Eu thin films demonstrated that Eu^{3+} ions substituted Y^{3+} ions in the lattice and formed luminescent centres even without post-deposition annealing [35].

Singh *et al.* [33] investigated the effects of optical properties of different substrates and of surface roughness on the brightness of Y_2O_3:Eu thin films grown by the PLD technique. The films were grown on quartz, lanthanum-aluminum oxide (LAO), sapphire and silicon substrates. The films grown on quartz exhibited the highest CL brightness followed by those on sapphire, LAO and silicon substrates, respectively [33]. The results show that both the optical properties and the surface roughness play a major role in controlling the CL brightness of thin films, i.e. films grown on substrates with good optical properties like quartz have a better light output and rough surfaces also increase light output by suppressing total internal reflection.

Thin film phosphors are generally less bright than powder phosphors because an estimated 80% to 90% of the light generated within the film is lost due to internal reflection [31]. However, the effects of total internal reflection can be reduced by tailoring the surface using various methodologies including variation in processing conditions, modifying the surface and adding a buffer layer between the film and the substrate [33].

Coating thin film phosphors with materials that delay the onset of degradation can reduce the rate of degradation of CL intensity. Fitz-Gerald *et al.* [36] coated Y_2O_2S:Eu phosphor with $TaSi_2$ and they observed a significant reduction in the rate of loss of CL intensity, and the coating did not affect the integrity of the phosphor. Hillie and Swart [34] coated

ZnS:Cu,Au,Al thin film phosphor with CdO and established that CdO coating delayed the formation of a non-luminescent ZnO layer on the surface thereby reducing the rate of loss of CL intensity considerably. Trottier [37] established that some coatings such as SiO_2 and Ag increased the rate of degradation of Y_2O_2S:Eu thin film phosphors. It is therefore important to use coating materials with selected optical properties, which are not detrimental to the handling qualities, brightness and chromaticity of phosphors and they must be thin enough to be transparent to light resulting from excitation by low energy electrons [36].

2.7. ENERGY TRANSFER IN PHOSPHORS

The process of energy transfer in phosphors involves interaction between two luminescent centres referred to as the sensitizer (energy donor) and the activator (energy acceptor). The interaction can be an exchange interaction (e.g. spectral or wave function overlap) or an electric or a magnetic multipolar interaction [20]. Energy transfer can occur between a pair of identical luminescent centres (e.g. two identical rare-earth ions) or between two non-identical centres. Energy transfer between two identical centres, especially two identical rare-earth ions, has been an issue of research for the past two decades. In this study, energy transfer was evaluated between non-identical centres.

The process of energy transfer between two non-identical centres, a sensitizer/energy donar (D) and an energy acceptor (A) separated by a distance R in a phosphor, is illustrated in figure 2.9.

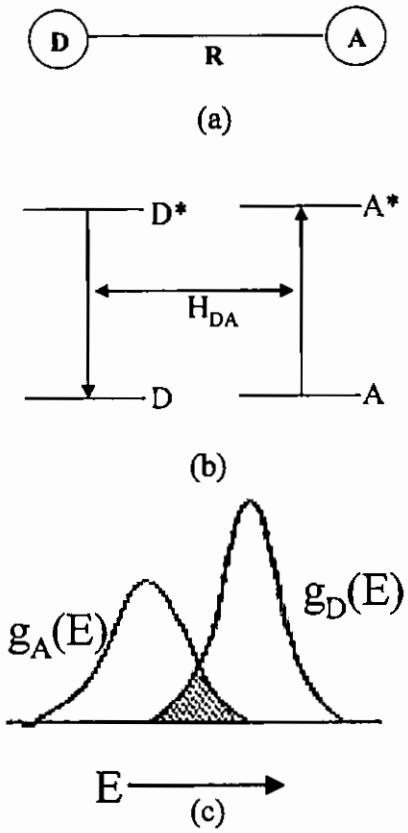

Figure 2.9. (a) Two centers D and A separated by a distance R, (b) energy transfer between D and A, and (c) the overlap between *D* emission and *A* absorption spectra [20].

Energy transfer can only occur if the energy differences between the ground states and the excited states of D and A are equal and if a suitable interaction (e.g. spectral or wavefunction overlap) exists between the centres [20]. The rate of energy transfer (P_{DA}) between D and A is given by [20]:

$$P_{DA} = \frac{2\pi}{\hbar}\left|< D, A^* \left| H_{DA} \right| D^*, A >\right|^2 \cdot \int g_D(E).g_A(E)dE, \qquad (2.13)$$

where the matrix element represents the interaction between the initial state $\left|D^*, A>\right.$ and the final state $<D, A^*\left|\right.$. H_{AD} is the interaction Hamiltonian and D^* and A^* are the excited states of D and A. The integral represents the spectral overlap between D emission and A

absorption where $g_x(E)$ is the normalized optical line function of center x ($x = D$ or A). D^* can decay to the ground state non-radiatively by transferring energy to A with a rate P_{DA} (transfer rate) or radiatively with a rate P_D (radiative rate). The critical distance (R_c) for energy transfer is defined as the distance for which P_{DA} equals P_D. For $R > R_c$, radiative emission from D prevails, and energy transfer from D to A dominates for $R < R_c$ [20].

REFERENCES

[1] Ziegler J.P. and Howard B.M., *Electrochemical Society Interface*, (Summer 1994) 27

[2] Tannas L.E., *Flat Panel Display and CRTs*, Van Nostrand Reinhold, 1985

[3] Lowe A.C. and Plesko P., SID 92 Digest (1992)

[4] Abrams B. L., Thomes W.J., Bang J-S. and Holloway P.H., *Rev. Adv. Mater. Sci,* **5** (2003) 139.

[5] Sasaki K.Y. and Talbot J.B., *Adv. Mat.*, **11**(12) (1999) 91

[6] Talin A.A., Dean K.A. and Jaskie J.E., *Solid-State Electronics*, (2001) 964

[7] Hase T., Kano T., Nakazawa E. and Yamamoto H., *Advances in Electronics and Electrophysics*, **79** (1990) 271

[8] Candescent Technology Corporation, Technology Primer, December 1999 (http://www.candescent.com/Candescent/techprim.htm)

[9] Greenwich University, October 2000, pp 1-2 (http://www.phosphors.co.uk/phosphors.htm)

[10] Zhang F.L., Yang S., Stoffers C., Penczek J., Yocom P.N. and Zaremba D., *App. Phys. Lett.* **72** (18) (1998) 2226

[11] Streetman B.G., *Solid state electronic devices 3/ed*, Prentice Hall, London, 1990

[12] Hudson J.B., *Surface Science: An Introduction*, Butterworths-Heineman, Boston, 1992

[13] Stoffers C., Yang S., Jacobsen S. M. and Summers C.J., *Saturation of phosphor under low voltage excitation*, Proceedings for the First International Conference on the Science and Technology of Display Phosphors, San Diego, Nov. 1995

[14] Raue R., Vink A.T. and Welker T., *Phillips Tech. Rev*, **44** (12) (1989) 335

[15] Miyanto S., *Japanese J. Appl. Phy.* **17** (1978) 1129

[16] Curie D., *Luminescence in crystals,* John Wiley and Sons, New York (1963)

[17] McKittrick J., Bacalski C.F. and Hirata G.A., *J. Am. Ceram. Soc.* **85** (5) (2000)1241

[18] Jones S.L., Kumar D., Singh R.K. and Holloway P.H., *Appl. Phys. Lett.* **71**(3) (1996) 404

[19] Inventors, February 2005, pp 1-3
http://inventors.about.com/library/inventors/blphotoluminescence.htm

[20] Blasse G. and Grabmaier B.C., Luminescent Material, Springer-Verlag, Berlin, 1994.

[21] Godlewski M. and Skowronski M., *Phys. Rev.* **B 32** (1985), 4007

[22] Park W., Wagner B.K., Russell G., Yasuda K. and Summers C.J, *J. Mater. Res.* **15**(11) (2000), 2288

[23] Hillie K.T., *PhD Thesis,* University of the Free State, South Africa (2001)

[24] Holloway P.H., Trottier T.A., Sebastian J., Jones S., Zhang X-M., Bang J-S., Abrams B., Thomes W.J and Kim T-J., *J. Appl. Phys.* **88**(2000) 1.

[25] Pfahnl A., in *Advances in electron tube techniques,* Pergamon, New York, (1961) 204

[26] Swart H.C., Oosthuizen L., Holloway P.H. and Berning G.L.P., *Surf. Interface Anal.* **26** (1998) 339

[27] Itoh S., Kimizuka T. and Tonegwa T., *J. Electrochem. Soc.* 136 (1989) 1819

[28] Sebastian J.S., Swart H.C., Trottier T.A., Jones S.L. and Holloway P.H., *J. Vac. Technol.* **A 15(4)** (1997) 2352.

[29] Chen S.H., Greeff A.P. and Swart H.C., *J. Lumin.* **109** (2004) 93

[30] Cho K.G., Kumar D., Holloway P.H. and Singh R.K., *Appl. Phys. Lett.* **73**(21) (1998) 3058.

[31] Jones S.L., Kumar D. , Cho K.G., Singh R.K. and Holloway P.H., *Displays* **19** (1999) 151

[32] Gu G., Ong P.P., Chen C. and Roth S., *J. Phys. D: Appl. Phys.* **33**(2000),p 1263

[33] Singh R.K., Chen Z., Kumar D., Cho K. and Ollinger M., *Appl. Surf. Sci.* **197-198** (2002) 321

[34] Hillie K.T. and Swart H.C., *Appl. Surf. Sci.***177(1-2)** (2001) 73

[35] Daud A., Futaki H., Ohmi K., Tanaka S. and Kobahashi H. (1995), Proceedings of the first international conference on the science and technology of phosphors, 41.

[36] Fitz-Gerald J.M., Trottier T.A., Singh R.K. and Holloway P.H., *Appl. Phys. Lett.* **72**(15) (1998) 1838.

[37] Trottier T.A., *Ph.D. dissertation*, University of Florida, Florida, (1998)

CHAPTER 3: AN OVERVIEW OF RESEARCH TECHNIQUES

3.1. INTRODUCTION

A wide variety of surface analysis techniques were used to study degradation, morphology and crystallinity of oxide-based powder and thin film phosphors. These include Auger electron spectroscopy (AES), x-ray photoelectron spectroscopy (XPS), x-ray diffraction (XRD), Fourier transform infrared spectroscopy (FTIR) and scanning electron microscopy (SEM). In addition, the pulsed laser deposition (PLD) technique was used to grow and coat thin luminescent films. The AES and the XPS were used to monitor the elemental composition on the surfaces of powder and thin film phosphors during electron or x-ray bombardment, respectively. The SEM was used to obtain information about morphology of powder phosphors. The XRD was used to identify crystalline phases of powder samples and the FTIR was used to identify and/or verify compounds synthesized by a sol-gel process. This chapter provides an introductory overview of some of the techniques used in this study.

3.2. AUGER ELECTRON SPECTROSCOPY

Auger electron spectroscopy (AES) was developed in the late 1960s and it derives its name from Pierre Auger, a French physicist who discovered the Auger effect in the mid 1920s [1]. The basic Auger process involves three steps. First, an electron from the core level (K level) of an isolated atom is removed by an incident primary electron with sufficient energy (typically in the range of 2-10 keV). Second, the resulting vacancy in the K level is immediately filled out by an electron from the L_1 level and the energy released in this transition is simultaneously transferred to a second electron in the L_2 level. Third, this electron is ejected from the atom as an Auger electron. The Auger electrons are detected and analyzed with an electron spectrometer. In the Auger process illustrated in figure 3.1, the final state is a doubly-ionized atom with core holes in L_1 and L_2 shells.

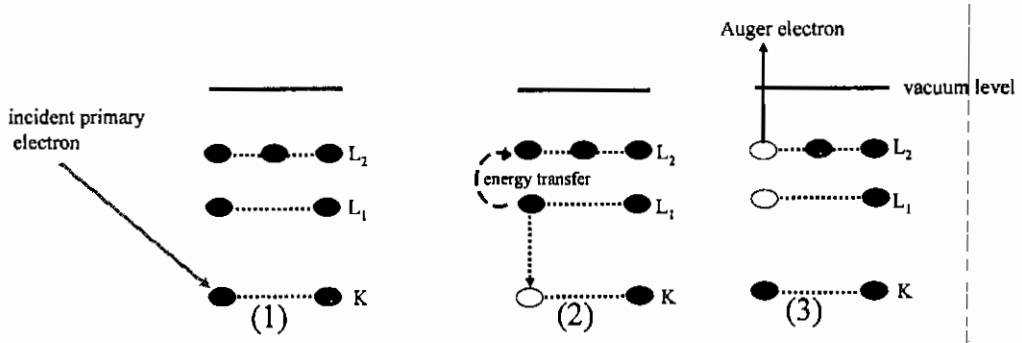

Figure 3.1. Three basics steps of the AES: (1) removal of the K electron (2) filling of the vacancy by the L_1 electron and (3) emission of the Auger electron from the L_2 level.

The emitted Auger electron is referred to as a KLL electron [2]. It should be noted that Hydrogen and Helium atoms cannot be detected by AES because they have no electrons occupying the L level [1,2]. The energy of the Auger electron (E_{KLL}) can be estimated from the binding energies of the levels involved in the Auger process by the expression:

$$E_{KLL} = E_K - E_{L_1} - E_{L_2}, \tag{3.1}$$

where E_K, E_{L_1}, E_{L_2} are the energies associated with levels K, L_1 and L_2 respectively. The energy of Auger electrons is usually between 20 and 2000 eV [2]. This energy is characteristic of the atom from which it was emitted and the number of electrons is dependent on the concentration of that element in the sample [2], i.e. it is independent of the energy of the primary electron. The essential components of an AES spectrometer are ultra high vacuum (UHV) chamber, electron gun, electron energy analyzer and electron detector [1]. Figure 3.2 shows the PHI model 549 Auger spectrometer used in this study.

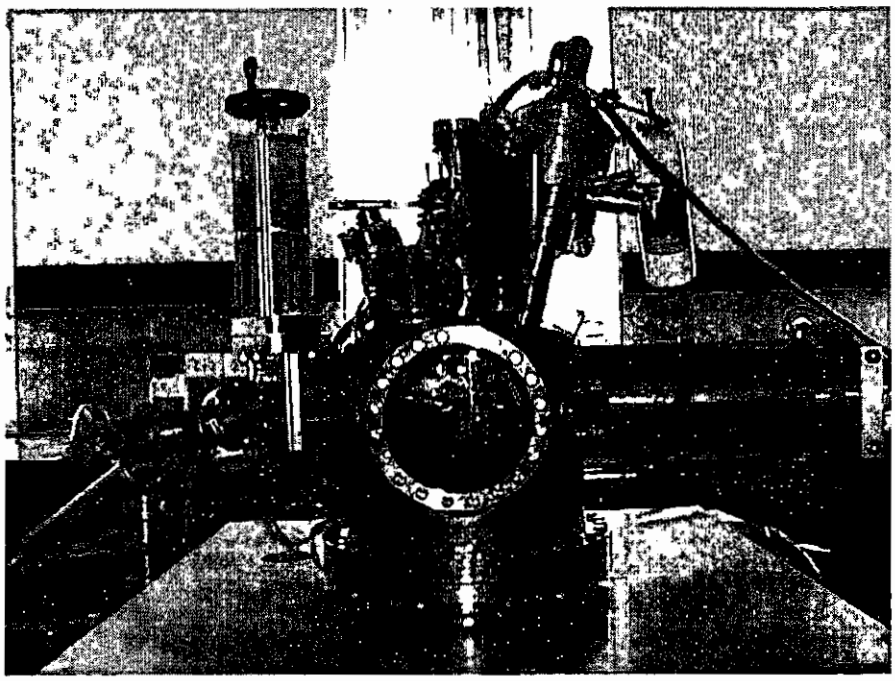

Figure 3.2. The PHI model 549 Auger spectrometer.

3.3. X-RAY PHOTOELECTRON SPECTROSCOPY

X-ray photoelectron spectroscopy (XPS), also known as electron spectroscopy for chemical analysis (ESCA), is a widely used surface technique to obtain chemical information at surfaces of various materials. The XPS process involves the ejection of an electron (photoelectron) in vacuum from the K level of an atom by an energetic incident x-ray photon [3]. Photoelectrons are collected and analyzed to produce a spectrum of emission intensity versus electron binding energy. In general, the binding energies of the photoelectrons are characteristic of the element from which they are emitted [4]. The schematic of the XPS process is shown in figure 3.3.

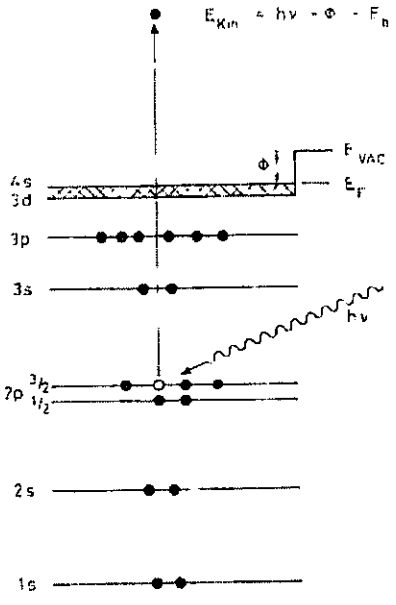

Figure 3.3. Schematic diagram of the XPS process in copper [5].

The kinetic energy (E_K) of the ejected photoelectron is dependent on the energy of the incident photon ($h\nu$) according to the following equation [5]:

$$E_K = h\nu - \Phi - E_b, \tag{3.2}$$

where $h\nu$ is the x-ray photon energy, E_b is the binding energy of the photoelectron in the parent atom and Φ is the work function of the target material. The low kinetic energy (0 - 1500 eV) of emitted photoelectrons limit the depth from which it can emerge and this means that the XPS is a very surface-sensitive technique [4]. The basic components of a XPS spectrometer are an x-ray source, electron energy analyzer for the photoelectrons, and an electron detector. The XPS spectrometer used in this study was the Quantum model 2000, shown in figure 3.4, from the South African Council for Scientific and Industrial Research (CSIR).

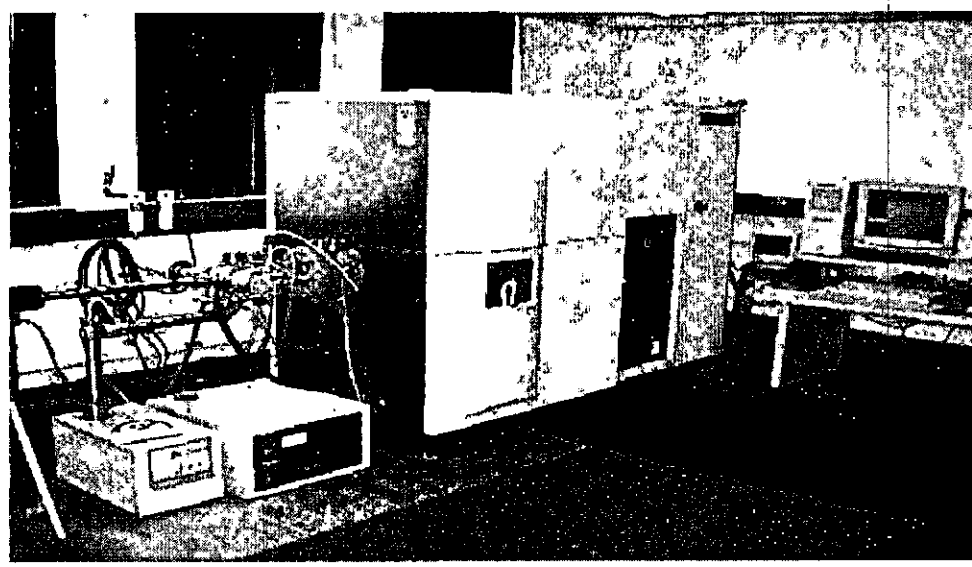

Figure 3.4 Quantum 2000 scanning x-ray photoelectron spectrometer.

3.4. PULSED LASER DEPOSITION

The pulsed laser deposition (PLD) technique for growing thin films involves ablation of a solid target in a high vacuum chamber – either in vacuum or in the presence of some background gas by means of laser pulses [6]. In this technique, a laser beam (usually an excimer laser) is directed at a solid target and its interaction with the target produces a plume of the target material that is ablated on a heated substrate placed directly in the line of the plume. An example of a laser plume during ablation is shown in figure 3.5.

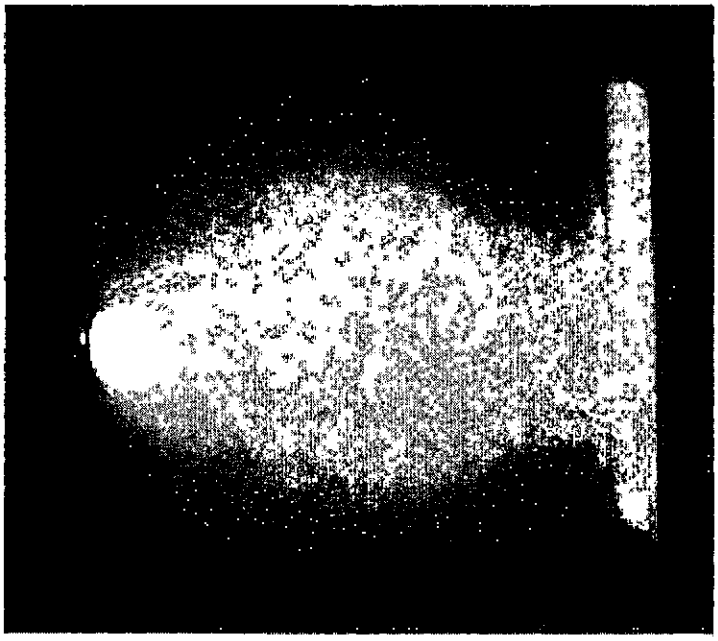

Figure 3.5. A picture of laser plume during ablation [7].

Multiple targets can be loaded inside the chamber on a rotating holder and be sequentially exposed to the laser beam, thereby enabling the in-situ growth of heterostructures and superlattices with relatively clean interfaces [6]. The PLD technique has a number of advantages over conventional thin-film deposition techniques (e.g. spray pyrolysis and MOCVD), including cost-effectiveness, stoichiometric transfer, and inherent simplicity for the growth of multilayered structures [6]. The PLD system used in this study (see figure 3.6) was from the Laser Institute at the University of Stellenbosch.

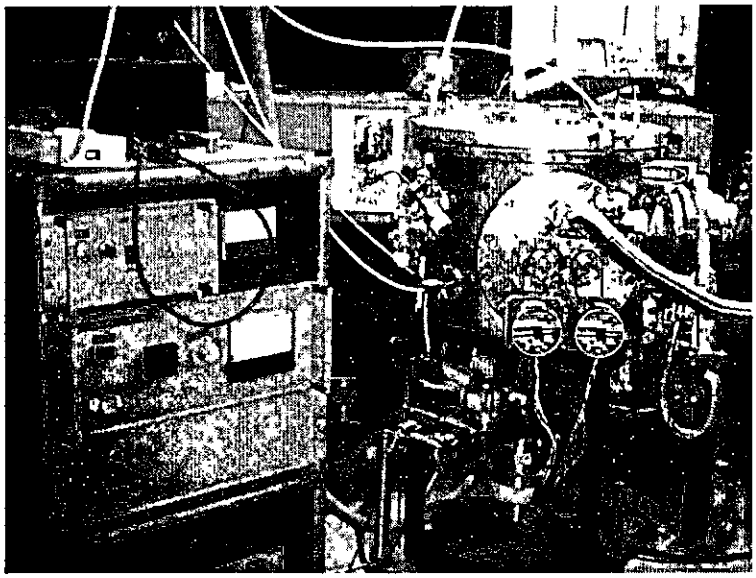

Figure 3.6. The PLD system for growing thin solid films.

3.5. X-RAY DIFFRACTION

X-ray Diffraction (XRD) is a powerful non-destructive technique used to investigate structural properties of crystalline materials. It can be used in applications such as phase identification, determination of grain size, composition of solid solution, lattice constants, and degree of crystallinity in a mixture of amorphous and crystalline substances [4]. A diffraction pattern is produced when a material is irradiated with a collimated beam of x-rays. The x-ray diffractometer used in this study was Philips APD model 3720, shown in figure 3.7, from the Major Analytical Instrumentation Center (MAIC) at the University of Florida (USA).

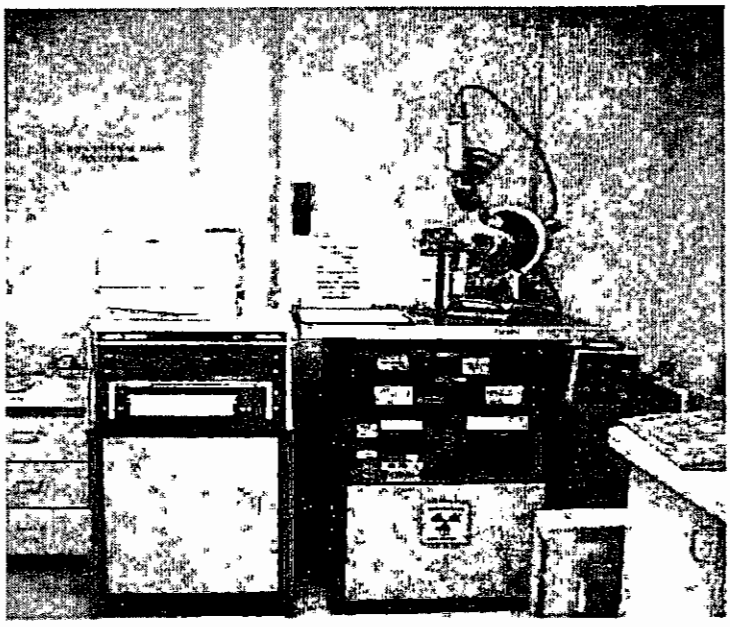

Figure 3.7. Philips APD 3720 x-ray diffractometer.

3.6. FOURIER TRANSFORM INFRARED SPECTROSCOPY

Infrared (IR) spectroscopy is a non-destructive analytical technique used to identify organic and inorganic compounds. IR spectra are obtained by detecting changes in absorption (transmittance) intensity as a function of frequency. If an unknown compound is subjected to IR radiation of a specific frequency (usually between 300 and 4000 cm^{-1}), it will absorb the energy allowed by vibration of the bonded atoms [8]. The compound will be identified by fingerprinting, i.e. by matching the spectrum obtained with the reference spectrum. Most commercial instruments measure IR radiation using Fourier transform spectrometers, hence the technique is popularly known as Fourier transform infrared (FTIR) spectroscopy. The three basic components of the FTIR system are a radiation source, an interferometer, and a detector [1]. A simplified layout of a typical FTIR spectrometer is shown in figure 3.8. The FTIR spectrometer used in this study was a Nicolet Model 20 SXB, shown in figure 3.9 from Particle Engineering Research Centre (PERC) at the University of Florida.

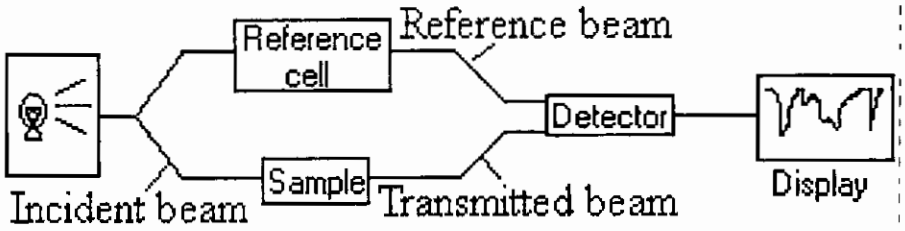

Figure 3.8. Simplified layout of a FTIR spectrometer [5].

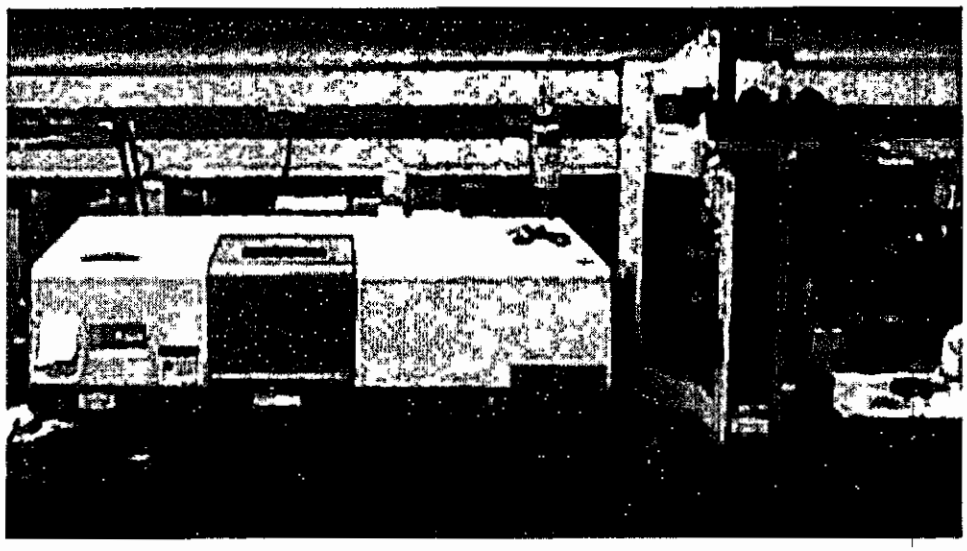

Figure 3.9. Nicolet Model 20 SXB FTIR spectrometer.

3.7. SCANNING ELECTRON MICROSCOPY

Scanning electron microscopy (SEM) is a technique in which a beam of finely focused electrons is used to examine materials on a nanometer to micrometer scale. The examination can yield information about topography, morphology, composition and crystallography of materials [9]. When a beam of primary electrons impinges the surface of a sample, it generates low energy secondary electrons. The intensity of these secondary electrons is governed by the surface topography of the sample. An image of the sample surface is therefore constructed by measuring secondary electron intensity as a function of the position of the scanning primary electron beam [4]. In this study, the

SEM images of powder and thin film samples were obtained using Leo-Field Emission Scanning Electron Microscope model 1525 (see figure 3.10) from the CSIR.

Figure 3.10. Leo-Field Scanning Electron Microscope.

REFERENCES

[1] Settle A (ed)., Handbook of Instrumental Techniques for Analytical Chemistry, Prentice Hall, New Jersey, 1997

[2] Semicon FarEast: www.SemiconfarEast.com, 2001

[3] Briggs D. and Seah M.P., *Handbook of X-ray Photoelectron Spectroscopy,* Perkin-Elmer Cooperation: Physical Electronic Division, Nowalk, 1979

[4] Hong Kong Baptist University: www.hkpu.edu.hk/~csar/fesem.html

[5] Smith G.C., Surface Analysis by Electron Spectroscopy, Plenum Press, New York, 1994

[6] Cheung J.T., in Pulsed laser deposition of thin films, edited by Chrisey D.B. and Hubler G.K. (Wiley, New York) (1994)

[7] Williams L.C., *PhD dissertation,* University of Florida, USA, 2004

[8] Bio-Log Forum: www.forumsci.co.il/HPLC/FTIR_page.html

[9] University of Nebrsaka-Lincon: www.unl.edu/CMRAcfem/semoptic.html

CHAPTER 4: DEGRADATION OF Y_2O_3:Eu POWDER PHOSPHORS

4.1. INTRODUCTION

In this chapter, degradation of the CL intensity and the corresponding surface changes on the chemical composition of commercial Y_2O_3:Eu powder phosphor are discussed. The standard Y_2O_3:Eu powder phosphor was obtained from Phosphor Technology in the United Kingdom. Y_2O_3:Eu is a well-known red-emitting photoluminescence and cathodoluminescence phosphor used in high resolution and projection television screens, and fluorescent lighting. It has replaced the traditional red-emitting yttrium oxysulphide (Y_2O_2S:Eu) phosphor because of its efficiency at high temperatures and stability in poor vacuum pressure [1]. It has a quantum efficiency that approaches 100% and it fulfils all the requirements for a good red-emitting phosphor [2]. It is considered one of the most promising oxide-based phosphors to be used in low voltage FEDs.

4.2. EXPERIMENTAL

Auger electron spectroscopy (AES) and Cathodoluminescence (CL) spectroscopy were used to monitor changes on the surface and the corresponding decrease of the CL intensity, respectively, during electron beam bombardment. The AES measurements were taken in an ultrahigh vacuum (UHV) chamber using a PHI Model 549 Auger spectrometer. The chamber was first evacuated to 2.9×10^{-9} Torr before backfilling to 1×10^{-7} or 1×10^{-8} Torr O_2. The CL data was collected with an S2000 miniature fiber optics spectrometer. Figure 4.1 shows the schematic diagram of the PHI Model 549 Auger spectrometer with a quartz view port of the S2000 spectrometer mounted approximately 60° to the incident electron beam.

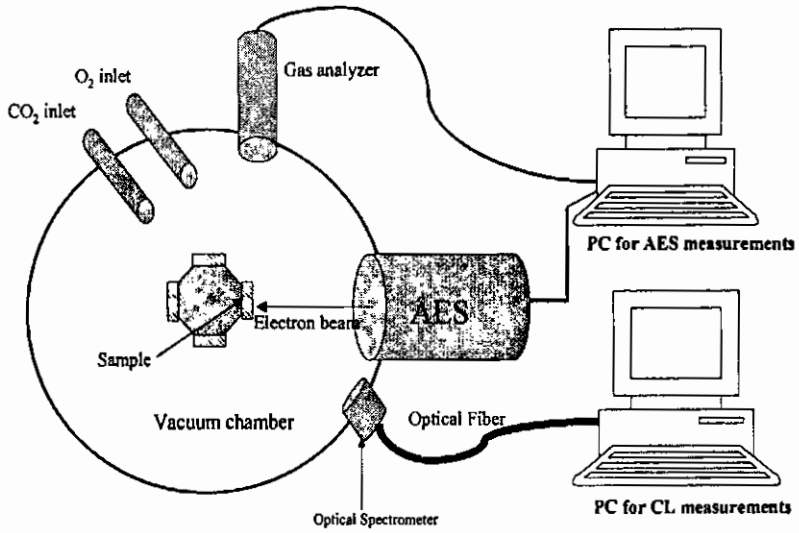

Figure 4.1. The schematic diagram of the AES system and the S2000 Optical Spectrometer.

Both the Auger and the CL measurements were taken simultaneously with the same electron beam of energy 2 keV and the beam current of 10 μA. The diameter of the electron beam was 120 μm, which was determined by measuring the beam current as a function of distance while moving the edge of the Faraday cup perpendicular to the electron beam (see ref. [5]). The current density was calculated by dividing the beam current with the beam area and its value was 88.5 mA/cm^2. Residual gas mass analyses (RGA) were performed using an Anavac-2 mass analyzer. The RGA spectra were collected before and after bombarding the Y_2O_3:Eu powder phosphors with 2 keV electrons.

4.3. RESULTS AND DISCUSSIONS

Figure 4.2 shows the RGA spectra taken at base pressure of (a) 2.9×10^{-9} Torr O_2 when the electron beam was off and after 10 hours of degradation at (b) 1×10^{-7} Torr O_2. Residual gases such as water vapour (H_2O), methane (CH_4), carbon monoxide (CO) Argon (Ar) and (CO_2) were present at base pressure before O_2 was leaked into the system. After degradation, all other gases except H_2, CO and Ar were removed from the vacuum chamber. The removal of these gases is attributed to electron beam induced

surface chemical reactions. The RGA data shows that there was no O_2 in the system before backfilling to 1×10^{-7} Torr O_2.

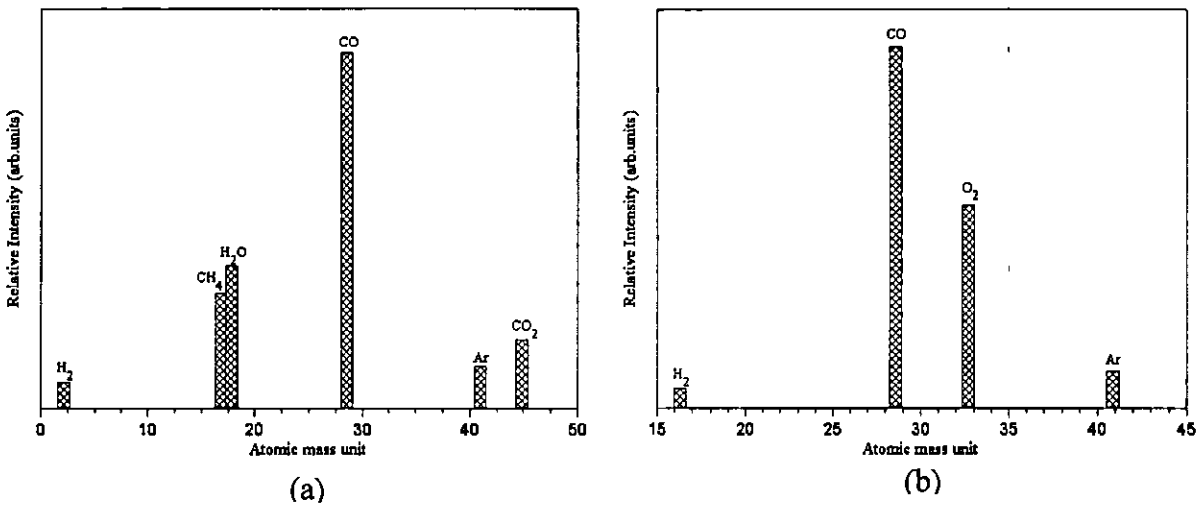

Figure 4.2. RGA spectra taken (a) before degradation at base pressure of 2.9×10^{-9} Torr and (b) after degradation at 1×10^{-7} Torr O_2.

Figure 4.3 shows the Auger spectra taken before and after degradation with a 2 keV electron beam at 1×10^{-7} Torr O_2. The elements present on the surface were yttrium (Y), adventitious carbon (C) and oxygen (O). The intensity of the Auger peak of Y and O increased slightly after degradation suggesting that there was an increase in the atomic concentration of each of these elements. The absence of C Auger peak after degradation is attributed to a reaction between C and O to form volatile CO_x species.

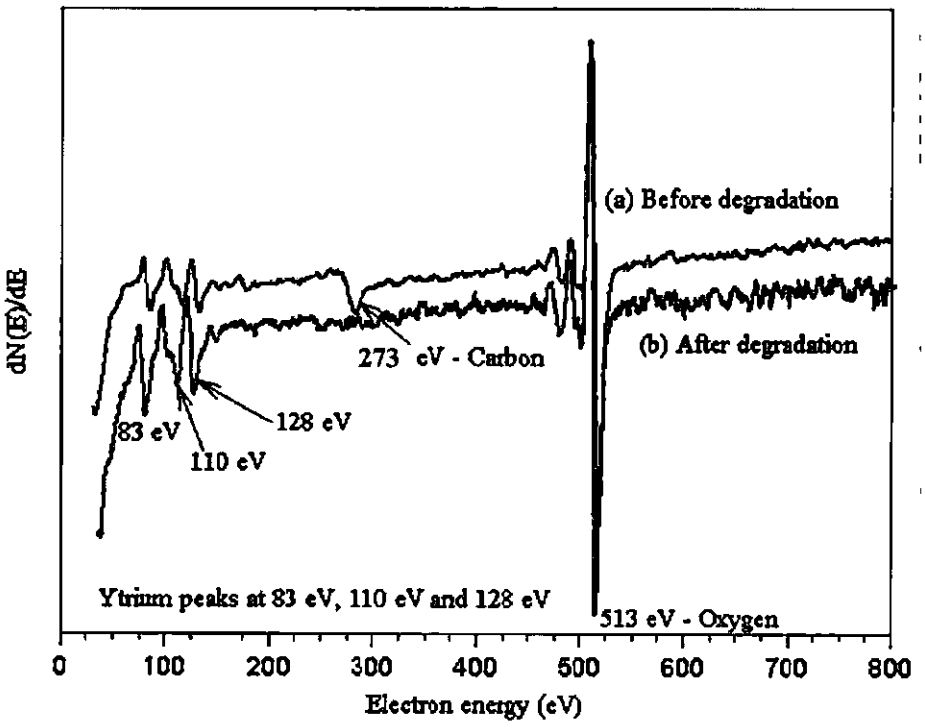

Figure 4.3. Auger spectra of Y_2O_3:Eu powders (a) before and (b) after degradation at 1×10^{-7} Torr O_2.

The CL emission spectra of Y_2O_3:Eu powders (a) before and (b) after 10 hours of degradation are shown in figure 4.4. Due to a shielding effect of the 4*f* electrons by the 5*s* and 5*p* electron shells of the Eu^{3+} ion, light emission in Y_2O_3:Eu does not involve a transition between an activator (Eu^{3+}) and a solid state band (Y_2O_3) [3,4]. It results from $f\rightarrow f$ electronic transitions in the Eu^{3+} ion (see figure 2.7). The main emission peak due to a $^5D_0 - {}^7F_2$ transition is at a wavelength of 611 nm. Less intense emission peaks at 535 nm, 590 nm, 628 nm and 711 nm due to $^5D_0\rightarrow{}^7F_J$ (J = 0,1,2,3,...) transitions are also visible. The fact that the main emission peak at 611 nm did not shift from its original position during degradation suggests that exposure to electron beam did not change the radiative relaxation process for Eu^{3+}. After degradation, the main emission peak is only 20% of the initial intensity, showing a significant reduction in the CL intensity.

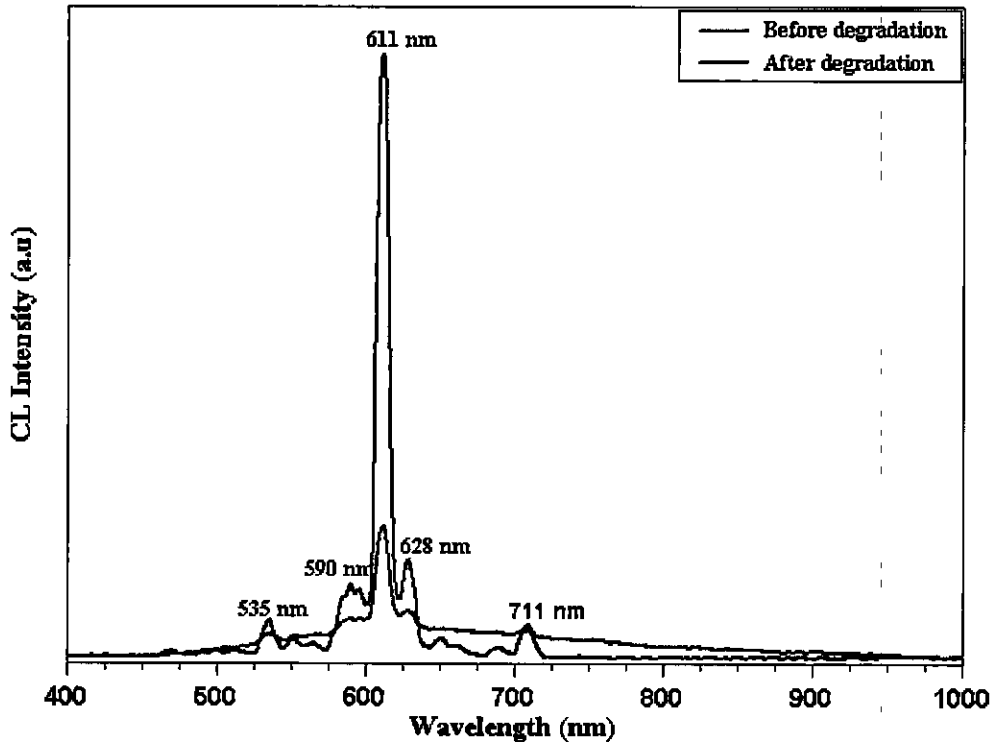

Figure 4.4. CL spectra of Y_2O_3:Eu before and after degradation at 1×10^{-7} Torr O_2.

Figures 4.5 (a) and (b) show the Auger peak-to-peak heights (APPHs) of O, Y and C and the CL intensity as a function of electron dose during degradation at 1×10^{-8} and 1×10^{-7} Torr O_2, respectively.

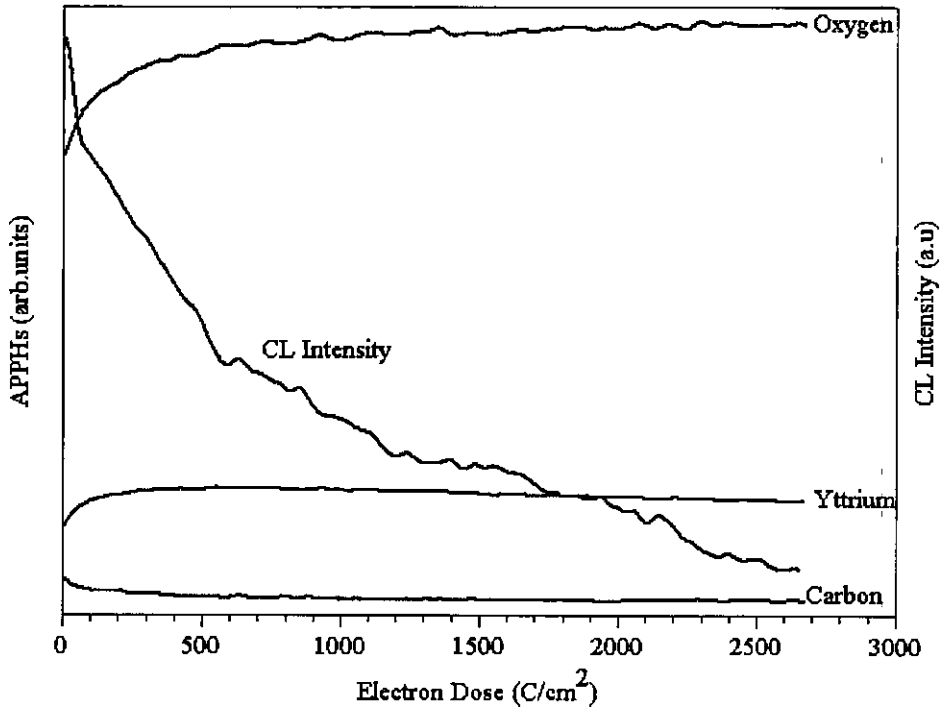

(a)

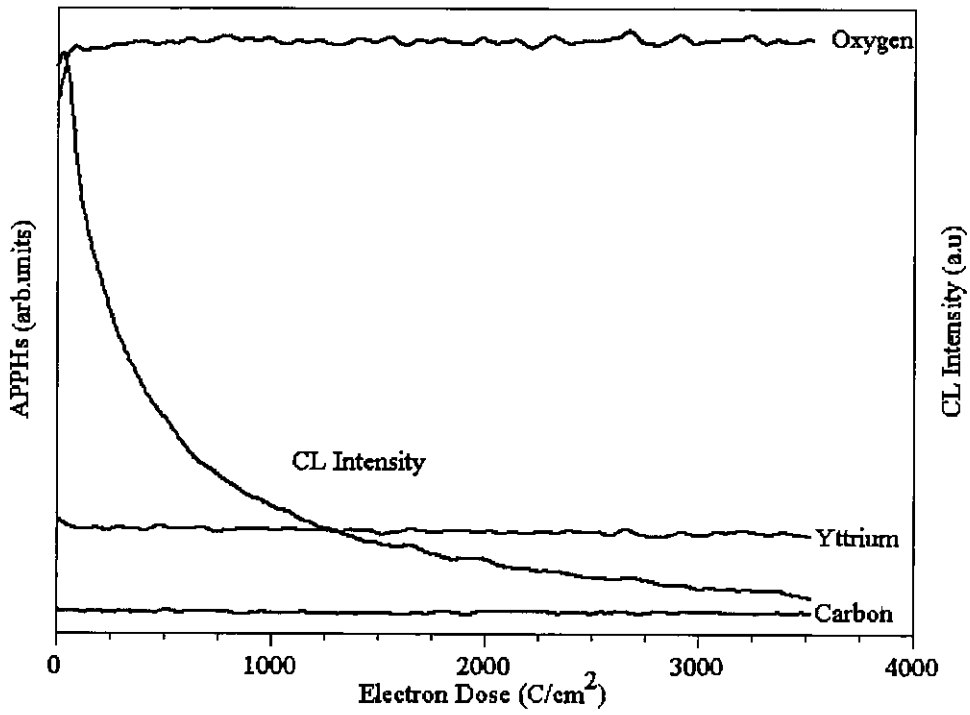

(b)

Figure 4.5. The CL intensity of Y_2O_3:Eu powders and the APPHs of O,Y, and C as a function of electron dose during degradation at (a) 1×10^{-8} Torr O_2 and (b) 1×10^{-7} Torr O_2.

Initially, the Auger peaks of Y and O increased marginally before stabilizing for the duration of the experiment. The increase is probably due to removal of C from the surface according to the ESSCR model discussed in chapter 2 (sec 2.3.5). The CL intensity from both graphs decreased continuously with exposure time. Figure 4.6 shows the normalized CL intensity curves during degradation at 1×10^{-8} and 1×10^{-7} Torr O_2. Consistent with the results of Swart *et al.* [5] and Itoh *et al.* [6], the decrease of degradation of CL intensity was faster at higher oxygen pressure (i.e. at 1×10^{-7} Torr).

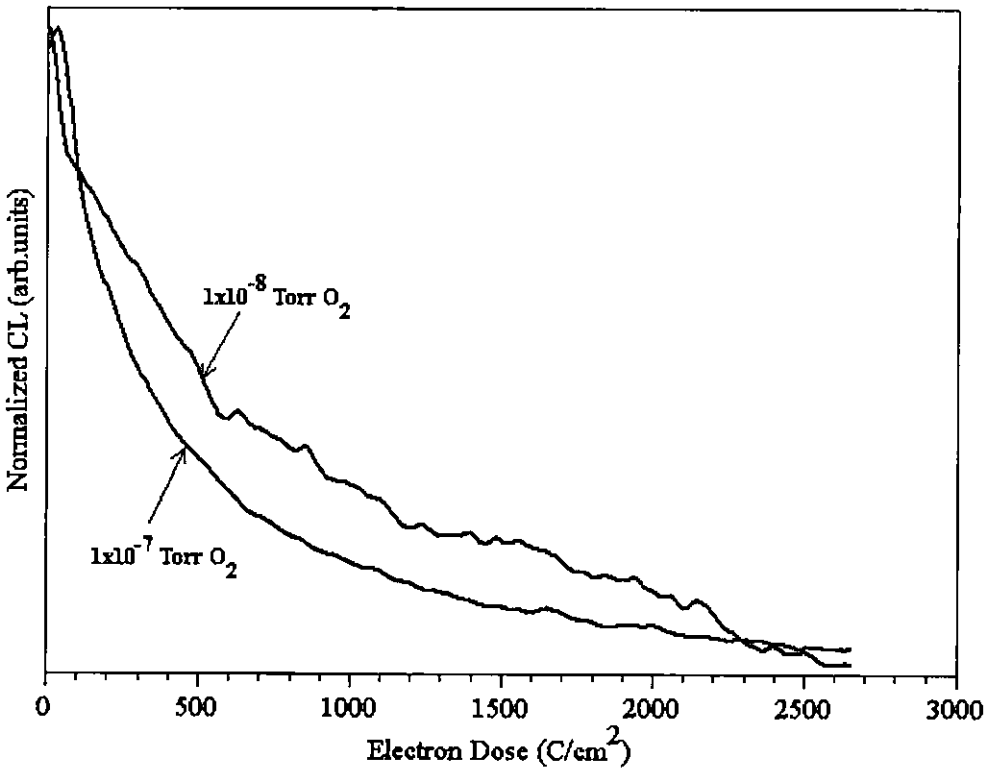

Figure 4.6. Normalised CL intensity of Y_2O_3:Eu powder phosphor during degradation at 1×10^{-8} Torr O_2 and 1×10^{-7} Torr O_2.

The ESSCR model proposed for the degradation of ZnS phosphors could be applicable to Y_2O_3:Eu powder phosphors. It should be recalled that the dissociation of Zn-S bonds by electron beam bombardment is followed by desorption of S and the increase of Zn and O Auger peaks due to the formation of a dead layer of ZnO. In the case of Y_2O_3:Eu powders, no desorption of atomic species was observed from the surface during

degradation. In stead there was a relative increase in the Auger peak from O at (a) 1×10^{-7} and (b) 1×10^{-8} Torr O_2 as shown by the peak ratios of O/Y as a function of the electron dose in figure 4.7. The data suggest that a less efficient oxygen-rich Y_2O_{3+x} ($x > 0$) layer was formed on the surface according to the ESSCR model. This layer could be responsible for the degradation of CL intensity.

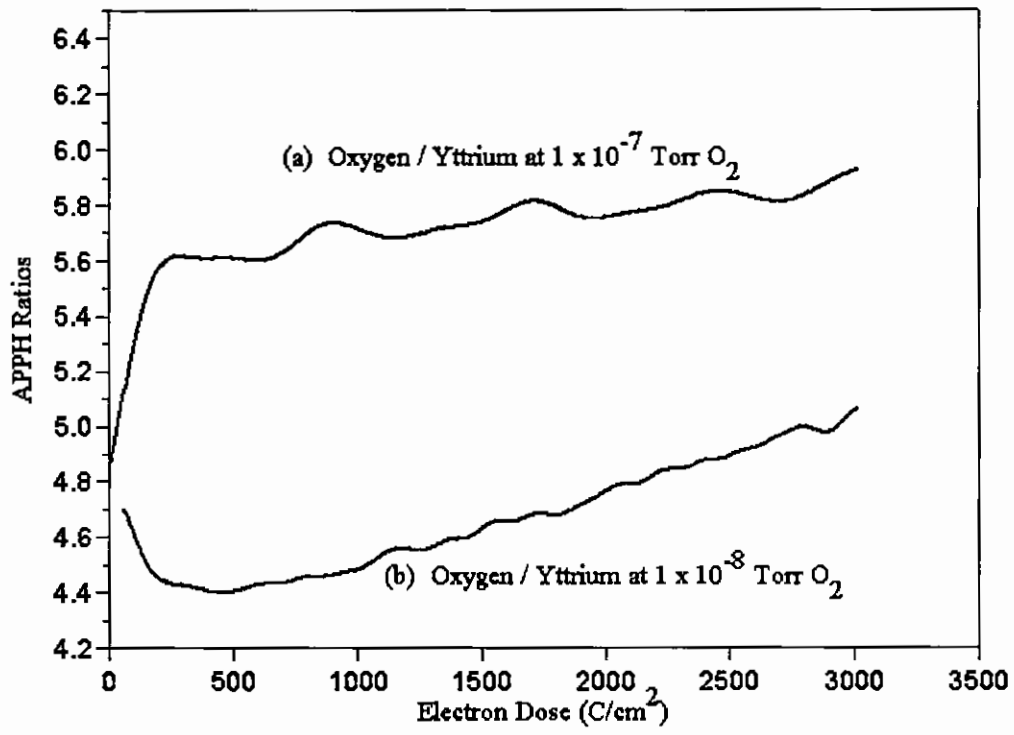

Figure 4.7. APPH ratios of O/Y as a function of electron dose during degradation at (a) 1 x 10^{-7} Torr O_2 and (b) 1 x 10^{-8} Torr O_2.

4.4. CONCLUSION

Degradation of CL intensity of Y_2O_3:Eu phosphor powder was investigated by AES and CL spectroscopy. The degradation was attributed to the formation of a less luminescent oxygen-rich layer of Y_2O_{3+x} on the surface. The rate of decrease of CL intensity was higher at 1×10^{-7} compared to 1×10^{-8} Torr O_2. The electron beam irradiation could also cause incorporation of O isoeletronic traps in the near surface region [7] resulting in an increased non-radiative recombination.

REFERENCES

[1] Hase T., Kano T., Nakazawa E. and Yamamoto H., *Advances in electronics and electron physics*, **79** (1990) 271

[2] Blasse G. and Grabmaier B.C., Luminescent Material, Springer-Verlag, Berlin, 1994.

[3] McKittrick J., Bacalski C.F. and Hirata G.A., *J. Am. Ceram. Soc.* **85** (5) (2000) 1241

[4] Jones S.L., Kumar D., Singh R..K. and Holloway P.H,. *Appl. Phys. Lett.* **71**(3) (1996) 404

[5] Swart H.C., Oosthuizen L., Holloway P.H. and Berning G.L.P., *Surf. Interface Anal.* **26** (1998) 339

[6] Itoh S., Kimizuka T. and Tonegwa T. , *J. Electrochem. Soc.* **136** (1989) 1819

[7] Sebastian J.S., Swart H.C., Trottier T.A., Jones S.L. and Holloway P.H., *J. Vac. Sci. Technol.* (A) **15** (4) (1997) 2349

CHAPTER 5: DEGRADATION OF PULSED LASER DEPOSITED Y_2O_3:Eu THIN FILM PHOSPHORS

5.1. INTRODUCTION

The PLD technique was used to grow thin luminescent films of Y_2O_3:Eu phosphor on silicon (Si) (100) substrates. A protective surface layer of tantalum pentioxide (Ta_2O_5) was ablated on some of the films in order to decrease the rate of degradation of CL intensity. In addition to its good optical properties, Ta_2O_5 was chosen because it is known to be absorption-free over the wavelengths ranging from 390 nm to 1000 nm [1]. This makes it an excellent coating material for all materials emitting within the visible region of the electromagnetic spectrum.

5.2. EXPERIMENTAL

A commercial Y_2O_3:Eu powder phosphor obtained from Phosphor Technology (UK) was first ground using a mortar and a pestle, annealed at 800°C in laboratory air for 24 hours, and then pressed without binders into pellets to make solid targets for laser ablation. Si (100) substrates were first ultrasonically degreased for 5 minutes in acetone, methanol and isopropanol sequentially; and then blown-dry with nitrogen gas. The pressed Y_2O_3:Eu and commercial Ta_2O_5 targets were mounted on a rotating holder and a Si (100) substrate was mounted on a heater (perpendicular to targets' holders). The distance between the targets and the substrate was 4.2 cm. The schematic diagram of the PLD system is shown in figure 5.1. The ablation process was carried out at 0.3 Torr O_2 backfilled from a base pressure of 5.1×10^{-5} Torr, and a substrate temperature of 700 °C using a Lambda-physik EMG 308 nm XeCl excimer laser. The laser beam was operated at a repetition rate of 10 Hz, an energy density of 6.2 J/cm^2 and pulse duration of 25 ns. Ablation of Y_2O_3:Eu was achieved with 900 laser pulses and only 50 pulses were used to ablate Ta_2O_5.

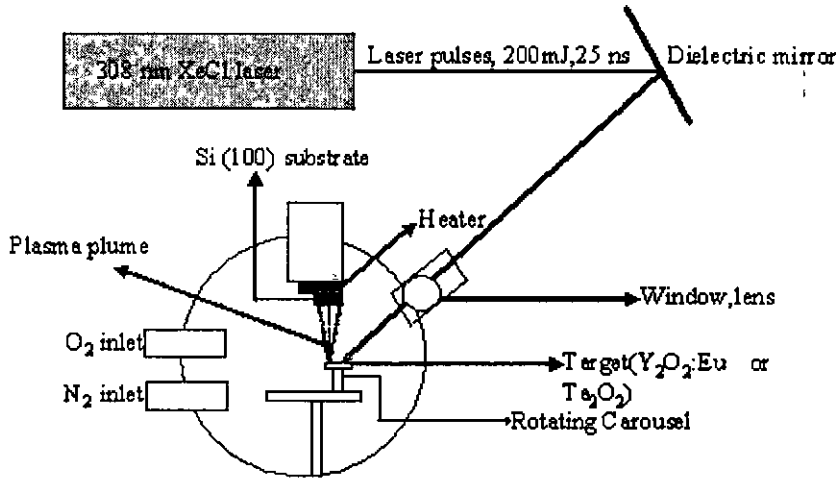

Figure 5.1 Schematic diagram of the PLD system.

XPS was used to determine the chemical composition of the major chemical elements, AES was used to examine the changes on surface chemical composition and CL spectroscopy was used to monitor the decrease in the CL intensity during degradation.

5.3. RESULTS AND DISCUSSIONS

Figure 5.2 shows the XPS spectrum of Ta_2O_5-coated Y_2O_3:Eu thin film. The presence of Y,O and Ta on the surface suggests that Y_2O_3:Eu and Ta_2O_5 were ablated on the Si (100) substrate. Eu^{3+} ions could not be detected by the XPS probably due to their relatively low concentration in Y_2O_3 matrix.

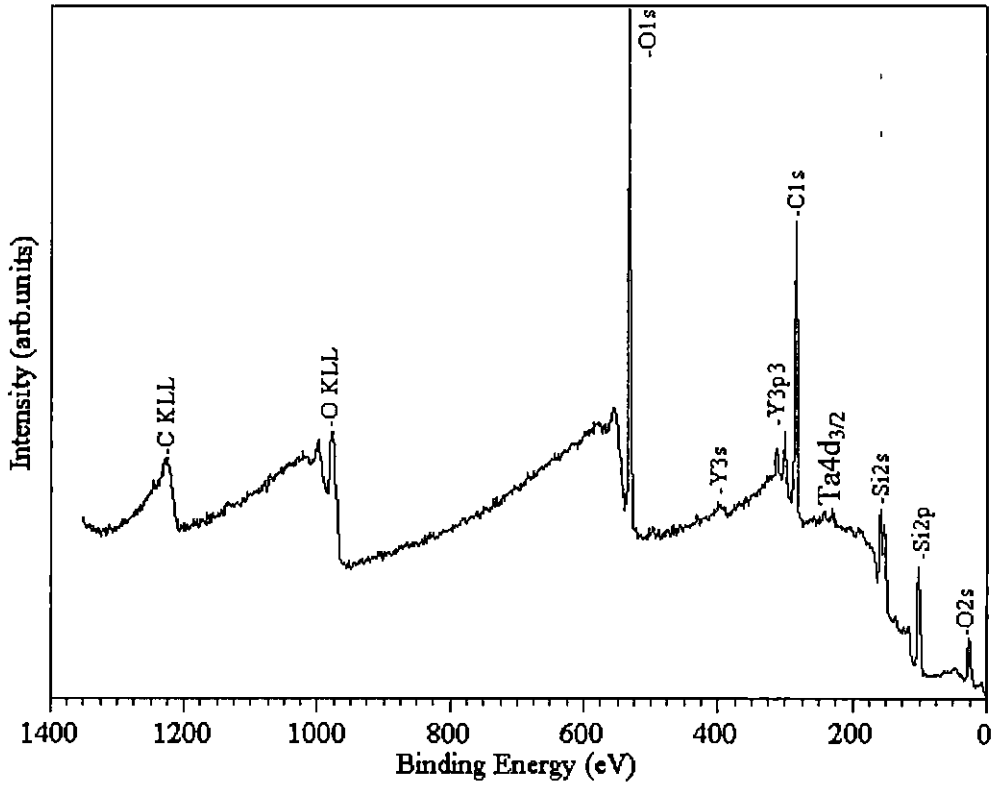

Figure 5.2. XPS spectrum of Ta_2O_5-coated Y_2O_3:Eu thin film grown on a Si (100) substrate.

The Auger and the CL data were collected in a 1×10^{-6} Torr O_2 vacuum backfilled from a base pressure of 3×10^{-9} Torr. Both the uncoated Y_2O_3:Eu and Ta_2O_5-coated thin films were irradiated for 10 hours with a 2 keV, 88.5 mA/cm^2 beam of electrons.

The AES spectra of Ta_2O_5-coated Y_2O_3:Eu thin films (a) before and after 10 hours of (b) degradation at 1×10^{-6} Torr O_2 are shown in figure 5.3. The fact that the AES could not detect even the most intense Auger peak of Y at 127 eV [2] and Ta suggests that the ablated Y_2O_3:Eu and Ta_2O_5 films were too thin. It is therefore reasonable to tentatively assign the peak at 83 eV to Si (from the substrate) rather than Y. It should be noted that the Auger peak from elemental Si is at 92 eV [2] and the peak at 83 eV is associated with Si in the SiO_x ($x > 0$) compound (see chapter 6). It is therefore most likely that the interfacial SiO_x layer was formed during pulsed laser ablation. Choi *et al.* [3], Bardal *et al.* [4] and Sharma *et al.* [5] reported that the SiO_x layer was formed at the interface

during epitaxial growth of Y_2O_3 films on the Si (100) substrates. The intensity of O Auger peak from the degraded sample is less than that of the O peak from undegraded sample, showing that O desorbed from the surface during degradation. The absence of C after degradation suggests that C reacted with O to form volatile CO_x species.

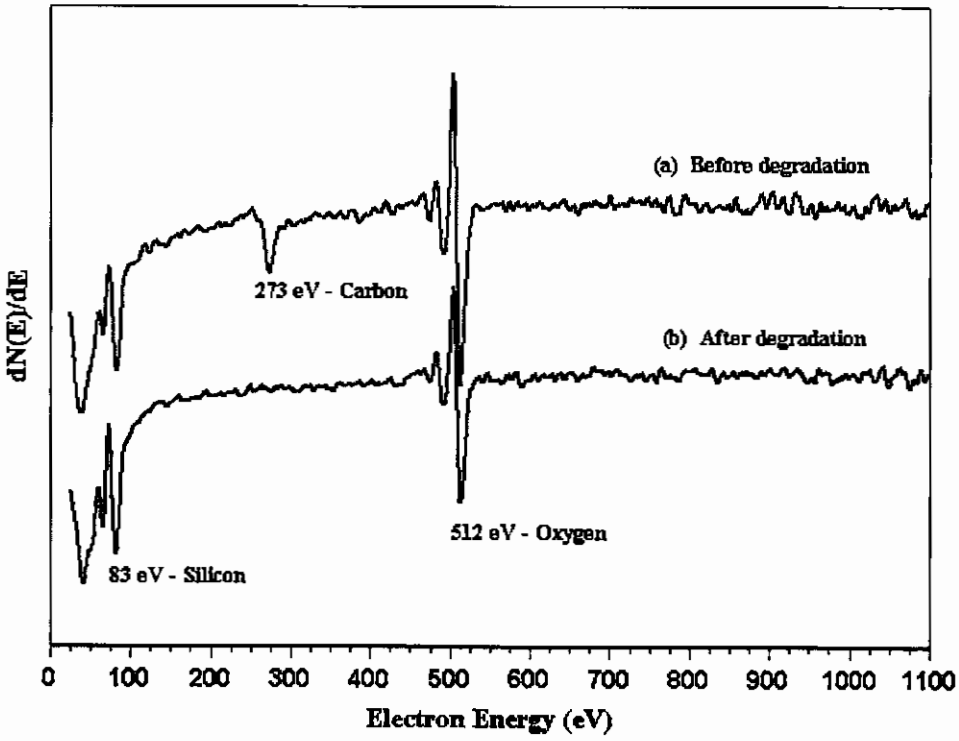

Figure 5.3. Auger spectra of Ta_2O_5-coated Y_2O_3:Eu thin film (a) before and (b) after degradation at 1×10^{-6} Torr O_2.

Figures 5.4 and 5.5 shows respectively the normalised APPHs of O and CL intensity as a function of the electron dose for uncoated and Ta_2O_5-coated Y_2O_3:Eu thin films. The Auger peak from O was decreasing with the CL intensity in both the uncoated and Ta_2O_5-coated films, showing that there is a correlation between desorption of O and the decrease of CL intensity. In ambient laboratory light, the red light emitted from the uncoated film was more intense than that of the Ta_2O_5-coated film. The low intensity from the Ta_2O_5-coated film could be attributed to light trapping by total internal reflection at the substrate-phosphor and Ta_2O_5-phosphor interfaces due to smooth surfaces. Jones *et al.*

[6] and Singh *et al.* [7] pointed out that smooth surfaces are responsible for light trapping at interfaces. Although the CL intensity of Ta_2O_5-coated film was less than that of the uncoated film, it is clear that the Ta_2O_5 layer reduced both the CL degradation and desorption of O significantly. If light trapping can be overcome by making the surface rougher, by inserting a buffer layer between the substrate and the ablated material or by post-ablation annealing at elevated temperatures (~1000°C) as reported by Jones *et al.* [6] and Singh *et al.* [7], then Ta_2O_5 would make a good protective layer in reducing the rate of CL degradation and desorption of atomic species from phosphor surfaces. Desorption of O from the surface suggest that a less-luminescent, oxygen-deficient Y_2O_{3-x} ($0<x<3$) surface layer was formed. This layer could be responsible for the degradation of the CL intensity.

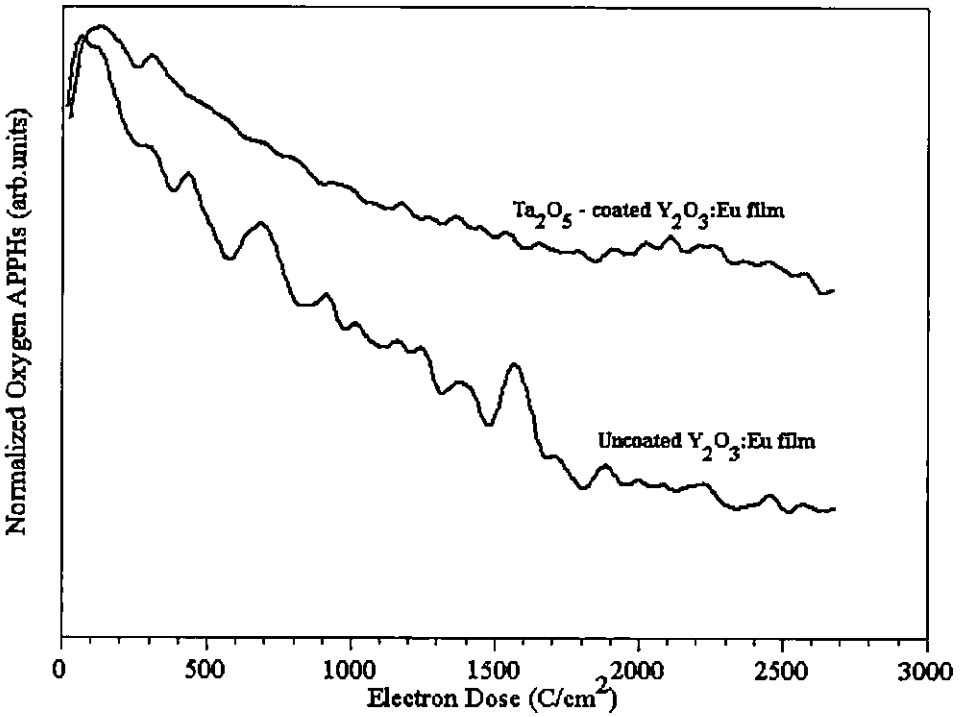

Figure 5.4. Normalised Auger peak heights of O as a function of electron dose for (a) uncoated and (b) Ta_2O_5-coated Y_2O_3:Eu thin films.

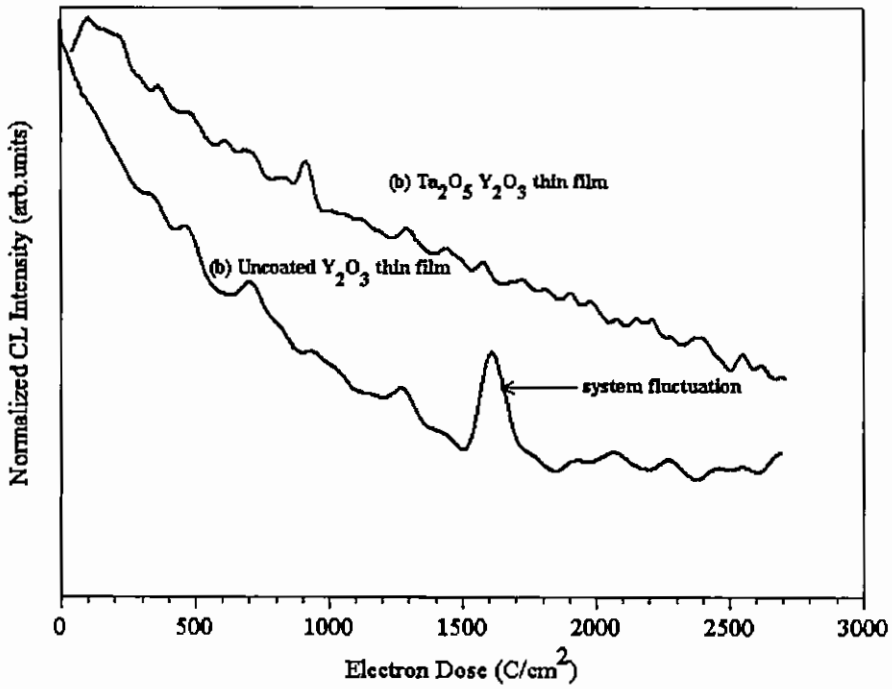

Figure 5.5. Normalised CL intensity of (a) uncoated and (b) Ta_2O_5-coated Y_2O_3:Eu thin films as a function of electron dose.

It is clear that Y_2O_3:Eu powders (chapter 4) and thin films display different behaviour of degradation when exposed to a beam of 2 keV electrons. In the case of powders, the decrease of CL intensity was faster and there was a slight increase in the concentration of O on the surface relative to that of Y. In the case of thin films, the decrease of CL intensity was relatively slow and O was desorbed from the surface. The reason for the differences is not yet known at this stage.

5.4. CONCLUSION

Uncoated and Ta_2O_5-coated Y_2O_3:Eu thin films were successfully grown on Si (100) substrates using the PLD technique. The changes on the surface chemical composition and degradation of CL intensity of the films were investigated with the AES and the CL spectroscopy, respectively. The degradation of CL intensity occurred simultaneously with desorption of oxygen. A Ta_2O_5 layer reduced the rate of degradation of CL intensity and of desorption of oxygen from the surface of the films. The fact that thin films were less bright than powders suggests that total internal reflection occurred at smooth interfaces.

REFERENCES

[1] Boughaba S., Sproule G.I., McCaffrey J.P., Islam M. and Graham M.J., *Thin Solid Films.* **358** (2000) 104

[2] Handbook of Auger electron spectroscopy (Physical electronics, Minnesota, 1976)

[3] Choi S.C., Cho M.H., Wangbo S.W. and Whang C.N., *Appl. Phys. Lett.* **71** (7) (1997) 903

[4] Bardal A., Eibl O., Matthee T., Friedl G. and Wecker J., *J Mater. Res.* **8** (1993) 2112

[5] Sharma R.N. and Rastogi A.C., *J. Appl. Phys.* **76** (1994) 4215

[6] Jones S.L., Kumar D., Cho K.G., Singh R.K. and Holloway P.H., *Displays* **19** (1999) 151

[7] Singh R.K., Chen Z, Kumar D., Cho K. and Ollinger M., *Appl. Surf. Sci.* **197-198** (2002) 321

CHAPTER 6: DEGRADATION OF SiO_2:Ce,Tb POWDER PHOSPHORS

6.1. INTRODUCTION

In this chapter, cathodoluminescence degradation of SiO_2:Ce,Tb (0.5 mol%Ce^{3+} and 1 mol% Tb^{3+}) nanoparticle powder phosphors prepared by a sol-gel process is discussed. Information on the synthesis of SiO_2:Ce,Tb by the sol-gel process is provided in chapter 7 (section 7.2.3). SiO_2:Ce,Tb powder samples were characterized with AES, CL spectroscopy and XPS.

6.2. EXPERIMENTAL

The AES data was collected with a PHI model 549 Auger spectrometer. The samples were irradiated for 10 hours with a 2 keV and 54 mA/cm^2 beam of electrons incident at ~ 90° to the sample in an ultra high vacuum chamber containing either 1×10^{-8} or 1×10^{-7} Torr O_2. The CL data was collected simultaneously with the AES data using an Ocean Optics S2000 spectrometer, which was mounted at ~60° to the incident beam of electrons.

The XPS data was collected with a Quantum 2000 spectrometer using Al K_α x-rays of energy 1486.6 eV. Survey scans were collected from 0 to 1400 eV with a beam diameter of 100 μm and a pass energy of 188 eV. High resolution scans were collected with a pass energy of 29 eV.

6.3. RESULTS AND DISCUSSION

The CL spectra before and after degradation are shown in figure 6.1. The strongest emission peak due to the $^5D_4 \rightarrow {}^7F_5$ transition in Tb^{3+} ions was only 50% of the initial intensity after degradation, showing a significant decrease of the CL intensity during 10 hours exposure to 2 keV electrons.

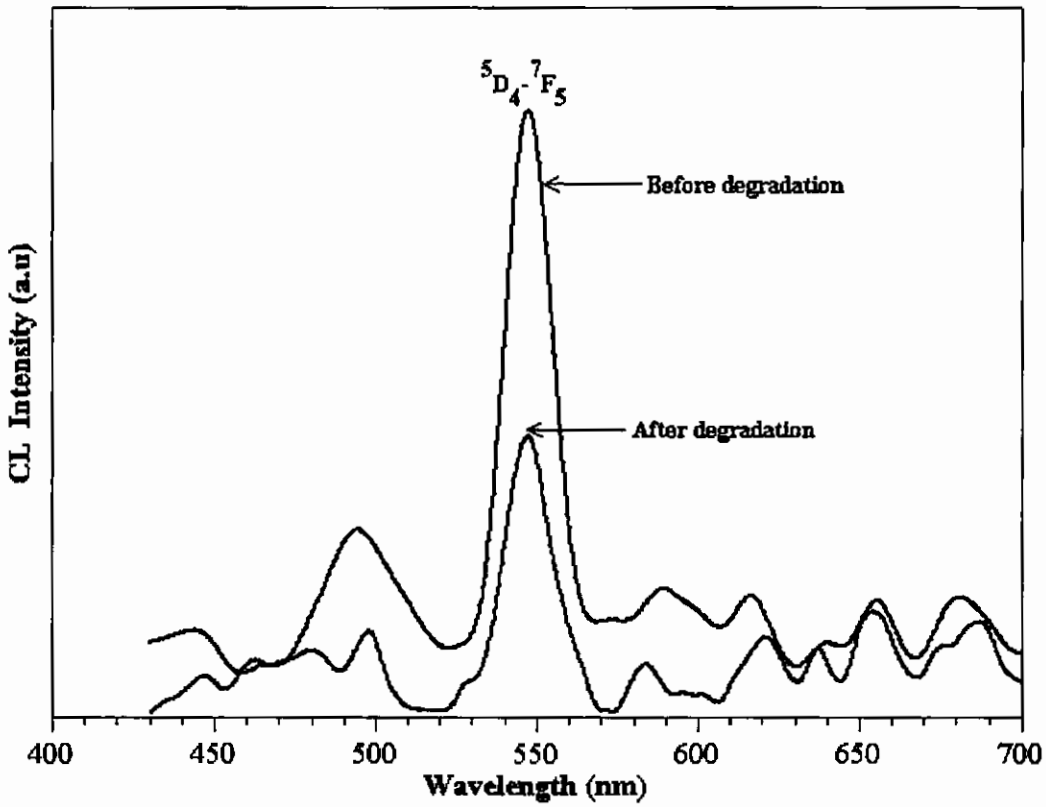

Figure 6.1. CL emission spectra of SiO_2:Ce,Tb powder phosphors before and after degradation at 1×10^{-7} Torr O_2.

The AES spectra (1) before and (2) after degradation at 1×10^{-7} Torr O_2 are shown in figure 6.2. The absence of C (usually at 273 eV) suggests that there was less contamination from hydrocarbons in the UHV chamber. Before degradation, the Si Auger peak associated with SiO_2 [1,2] was at 76.5 eV (spectrum 1). After degradation, this peak was at 83.5 eV as shown in spectrum (2). The shift from low energy to higher energy has been attributed to the change in the density of state in the valence band and relaxation effects [1,2]. It has been reported that prolonged electron beam exposure reduces the peak intensity of Si peak in SiO_2 at ~70 – 80 eV due to development of the new peak at ~92 eV, which is associated with elemental Si [1,2,3,4]. In this study, no Si peak was observed at ~92 eV. Instead, the Si peak at 76.5 eV has shifted (by 7 eV) to 83.5 eV and the peak intensity has been slightly reduced.

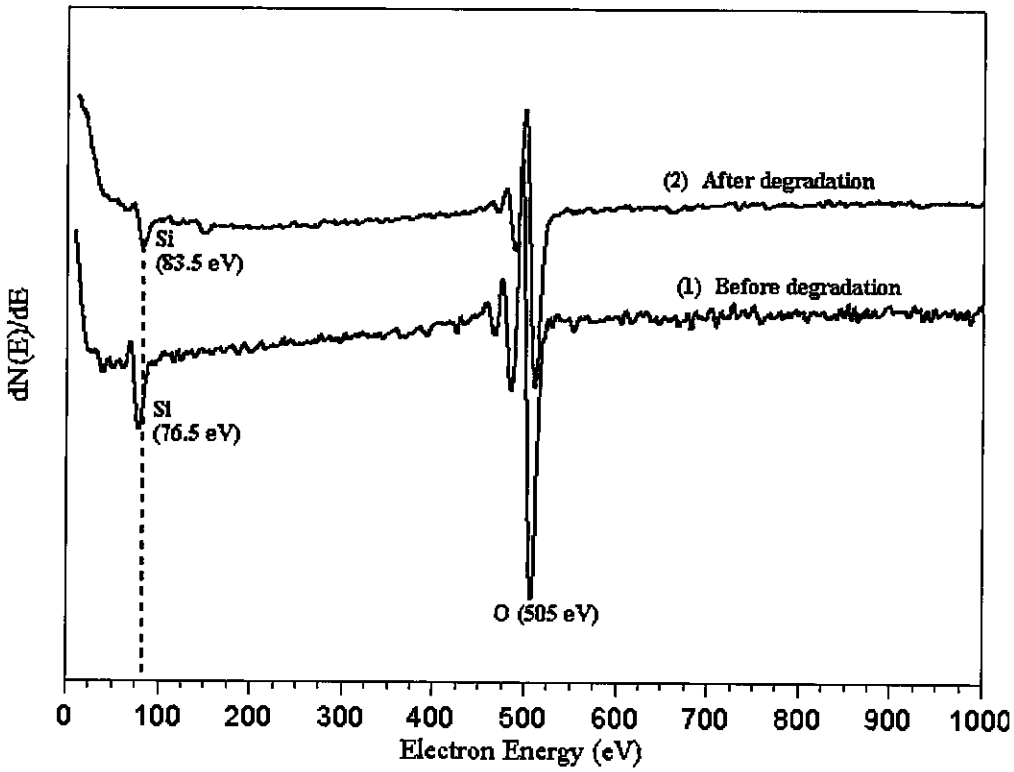

Figure 6.2. AES spectra (1) before and (2) after degradation.

The CL intensity of SiO_2:Ce,Tb and Auger electron peak-to-peak heights (APPHs) from O, Si and adventitious carbon (C) at (1) 1×10^{-7} and (2) 1×10^{-8} Torr O_2 are shown in figure 6.3 as a function of electron dose. The concentration of C on the surface was relatively low. It is clear that as the CL intensity decreased, the Auger peak intensity from O also decreased while the peaks from Si and C remained constant.

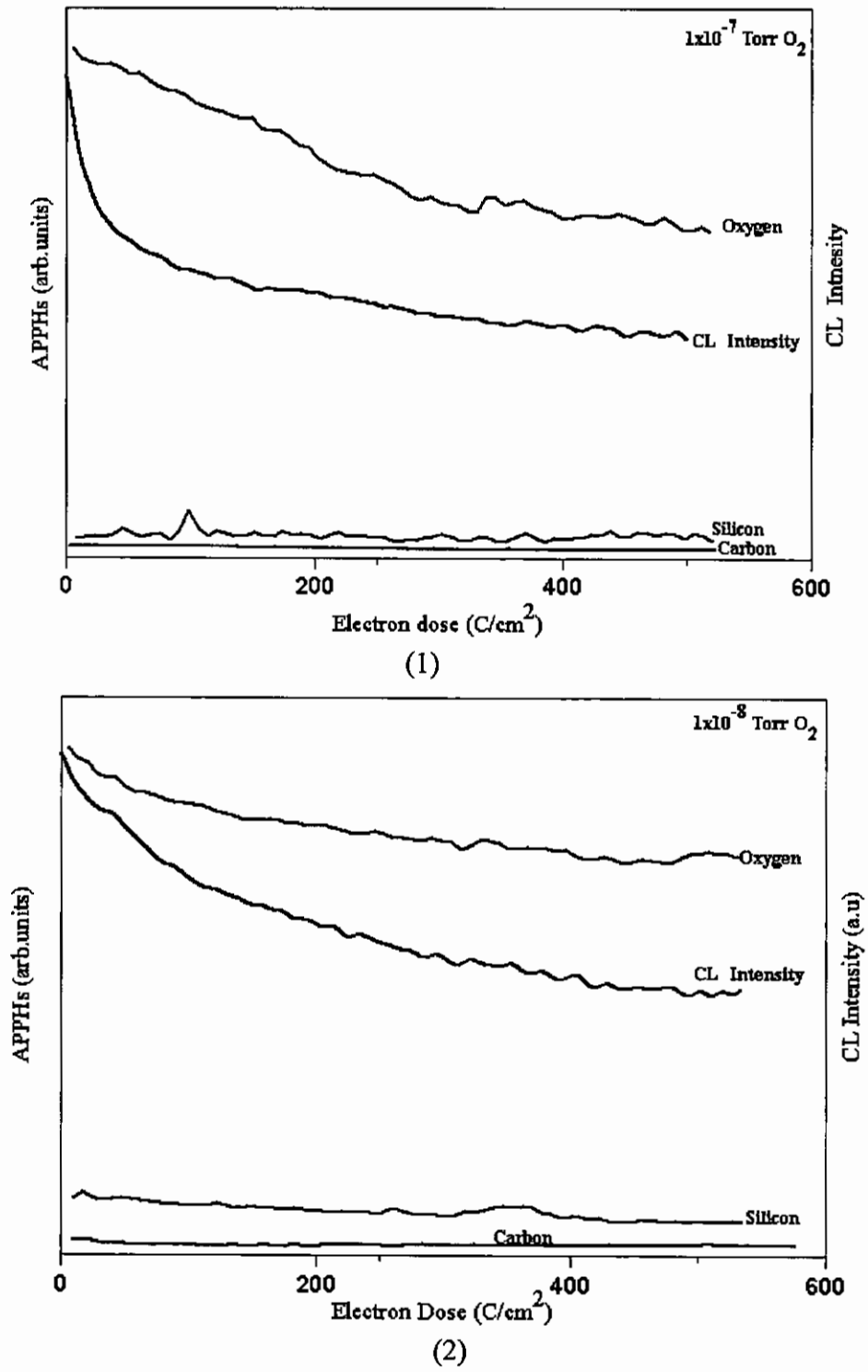

Figure 6.3. APPHs of O, Si and C as a function of 2 keV electron dose at (1) 1×1 0^{-7} and (2) 1×10^{-8} Torr O_2.

Figures 6.4 shows the normalized CL intensity at (1) 1×10^{-8} and (2) 1×10^{-7} Torr O_2 and Figure 6.5 show the normalized oxygen Auger peaks (1) 1×10^{-7} and (2) 1×10^{-8} Torr O_2 as a function of electron dose. It is clear that there is a correlation between degradation of the CL intensity and desorption of O. Consistent with the results of Swart *et al.*[5] and Pfahnl [6] the decrease of CL intensity was faster at high oxygen pressure, i.e. at 1×10^{-7} Torr O_2.

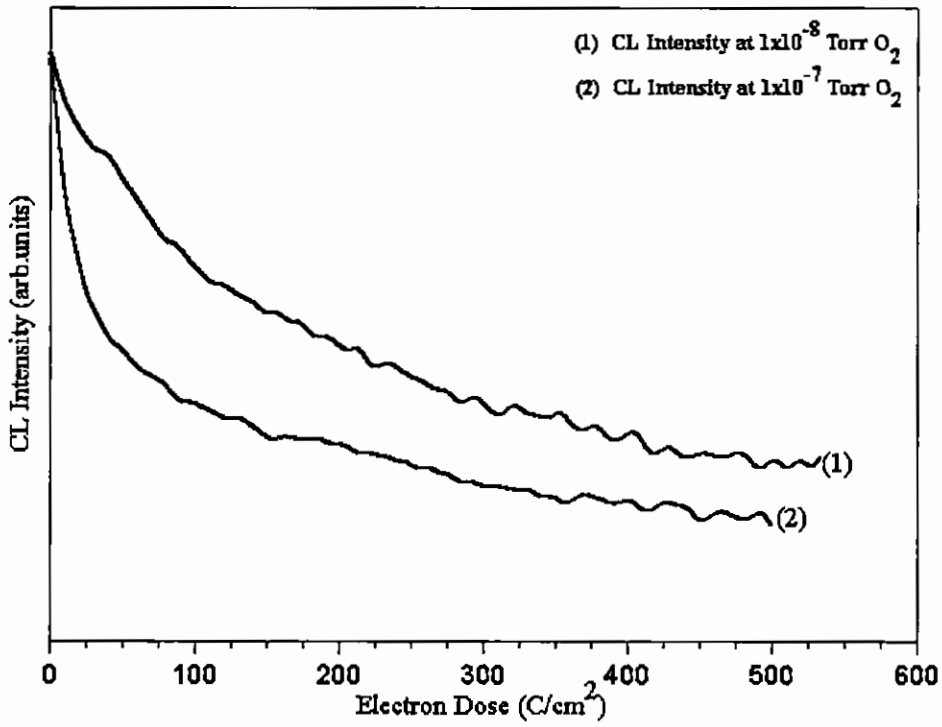

Figure 6.4. Normalised CL intensity as a function of dose of 2 keV electrons at (1) 1×10^{-8} Torr O_2 or (2)1×10^{-7} Torr O_2.

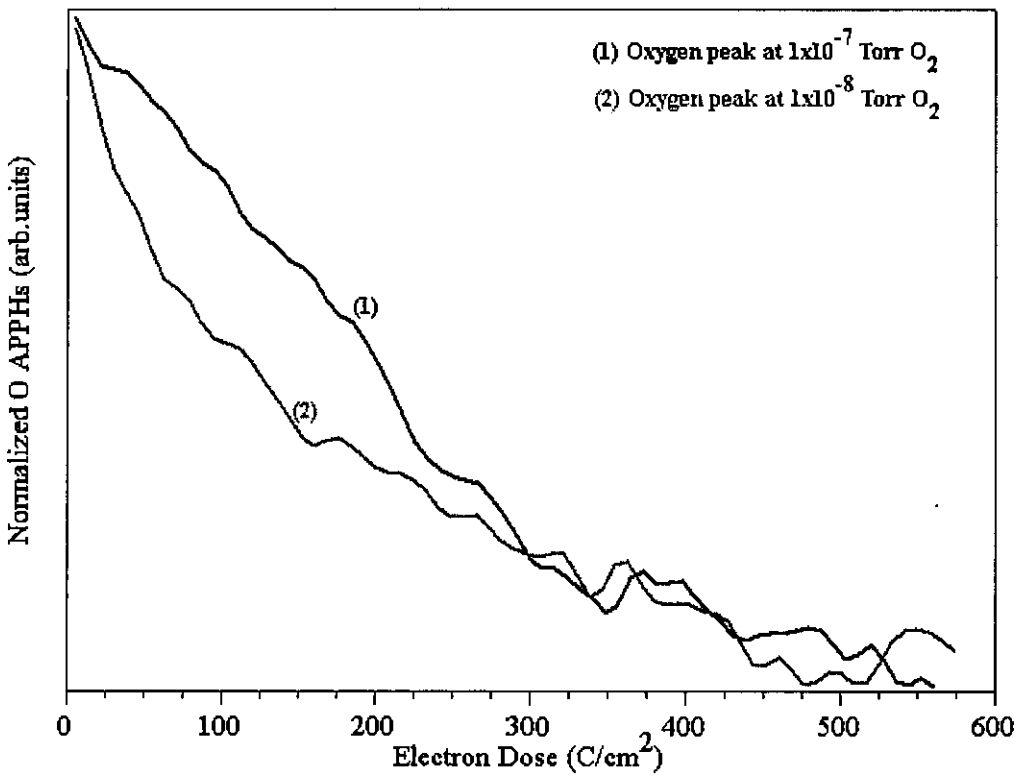

Figure 6.5 APPHs of O as a function of dose of 2 keV electrons at (1) 1×10^{-8} Torr O_2 or (2) 1×10^{-7} Torr O_2.

Figure 6.6 shows the XPS survey spectra of the degraded (spectrum 1) and undegraded (spectrum 2) SiO_2:Ce,Tb nanoparticle powders. Spectrum 1 shows peaks from elemental Si,O,Tb, Ce. The peak at 882 eV is associated with Ce in CeO_2 compound, suggesting that a non-luminescent oxide layer of CeO_2 was formed on the surface. The absence of Ce^{3+} and Tb^{3+} ions in spectrum (1) can tentatively be attributed to relatively low concentrations of these ions in the SiO_2 matrix.

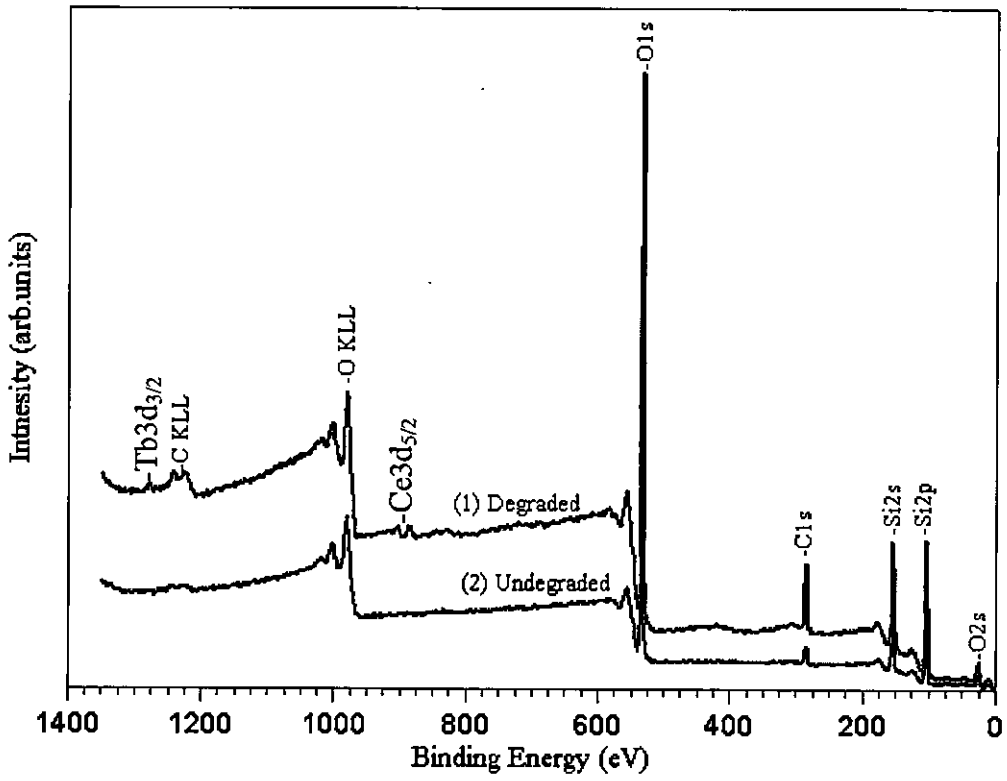

Figure 6.6. XPS survey spectra of (1) degraded and (2) undegraded SiO_2:Ce,Tb powder phosphors.

High resolution scans of SiO_2 peaks at ~103 eV from degraded (spectrum 1) and undegraded (spectrum 2) samples are shown in figure 6.7. Spectrum (1) is relatively narrow and has shifted by ~0.2 eV to the left. A relatively small peak associated with elemental Si appeared at ~98 eV in spectrum (1). The shifting of the spectrum and the appearance of Si peak at ~98 eV suggest that an oxygen-deficient SiO_x ($0<x<2$) layer was formed on the surface of the degraded sample.

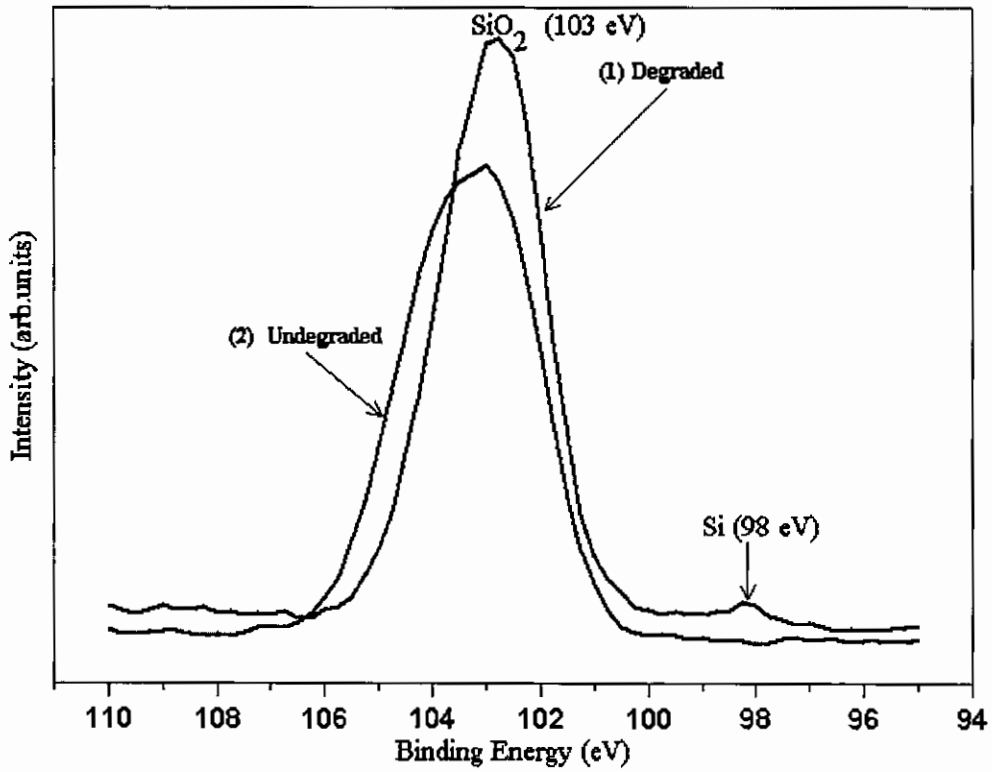

Figure 6.7. XPS high resolution peaks of SiO_2 from (1) degraded and (2) undegraded SiO_2:Ce,Tb powder phosphors.

Based on the XPS, AES and the CL data, a correlation between the decrease of CL intensity and of the Auger peak intensity from O could be established. Oxygen was desorbed from the surface following the electron-beam dissociation of SiO_2. An early mechanism for desorption of oxygen from soda glass proposed by Lineweaver [7] involves the production of a net negative charge in the glass when bombarded with high energy electrons. This net charge sets up an electric field in the glass. Under the influence of this field, the positive sodium ions present in the glass diffuse away from the surface and the oxygen ions move towards the surface and are eventually released into the vacuum. As documented by Thomas [2], the creation of an internal electric field is not a necessary condition for the dissociation of SiO_2 and the subsequent desorption of O. The mechanism of dissociation of SiO_2 is widely accepted to be electron stimulated desorption due to creation of an electron hole in the $L_{2,3}$ level of Si and Auger relaxation and emission from the valence band producing an O^+ species that desorbs according to

the Knotek-Feibelmann mechanism of electron stimulated desorption [8]. In this study, desorption of O is attributed to an ESSCR. Under electron beam bombardment, the Si-O bonds are broken and free oxygen is desorbed as ions [1,2] or as O_2 molecule following a reaction with dissociated species (H, O or C) from vacuum ambient gases (e.g H_2O, O_2 and CO_2). It is quite likely that desorption of oxygen resulted in the formation of a non-luminescent oxygen-deficient layer of silicon oxide (SiO_x), where $x<2$. Formation of a SiO_x rather than a Si layer could explain the absence of the 92 eV Auger peak associated with elemental Si in the AES spectra. Like the dead layer of ZnO on ZnS or the less luminescent layer of Y_2O_3:Eu on Y_2O_2S:Eu, the SiO_x dead layer could be the main cause of degradation of CL intensity of the SiO_2:Ce,Tb phosphor.

6.4. CONCLUSION

It was also shown that the intensity of CL emission from the SiO_2:Ce,Tb phosphor decreased simultaneously with desorption of oxygen from the surface. Possible mechanisms to explain the effect of oxygen desorption on the reduced CL emission from SiO_2:Ce,Tb powder phosphors were discussed. SiO_x ($x<2$) and possibly CeO_2 layers could be responsible for the degradation of CL intensity with increasing dose of 2 keV electrons.

REFERENCES

[1] Carrière B. and Lang B., *Surf. Sci.* **64** (1977) 209

[2] Thomas S., *J. Appl. Phys.* **45**(1) (1974) 161

[3] Joyce B.J. and Neave J.H., *Surf. Sci.* **27**(1971) 499

[4] Constantino F. and Devine R.A.B., *Phys. Rev. Lett.* **52**(23) (1984) 2081

[5] Swart H.C., Oosthuizen L., Holloway P.H. and Berning G.L.P., *Surf. Interface Anal.* **26** (1998) 339

[6] Pfahnl A., in *Advances in Electron Tube Techniques* (Pergamon, New York, 1961)

[7] Lineweaver J.L., *J. Appl. Phys.* **34** (1963) 1786

[8] Wang Y.X., Ohuchi F. and Holloway P.H., *J. Vac. Sci. Technol. A2* (1984) 732

CHAPTER 7: PREPARATION OF ZnO AND RARE-EARTHS-DOPED SiO_2 NANOPARTICLE PHOSPHORS BY A SOL-GEL PROCESS

7.1. INTRODUCTION

In recent years, significant progress has been made in an attempt to understand the fundamental concepts of synthesizing nanomaterials with different shapes and particle sizes for applications in a wide variety of technological areas such as electronic information displays, catalysis, ceramics, magnetic data storage, structural components etc. [1]. Various chemical processes including chemical vapour deposition (CVD), high temperature organometallic and sol-gel have been developed for the synthesis and commercial production of nanomaterials [1,2]. The sol-gel process has been used for many years to produce metal oxide and ceramic powders with high purity and homogeneity. The first silica and alumina gels were produced in the 1800s by Ebelman and Cossa respectively [1]. Over the past two decade, this process has been widely used to synthesise nanophosphors for possible application in low voltage FEDs. The most commonly synthesized nanophosphors are SiO_2 doped with rare-earth elements, and ZnO [3-6]. This chapter presents an overview of synthesis of nanophosphors of ZnO, SiO_2 doped with different concentrations of Ce^{3+}-Tb^{3+}, Ce^{3+}-Eu^{3+}, or Eu^{3+}-Tb^{3+} ion pairs, and SiO_2:Eu/Ce with embedded ZnO nanoparticles. The samples were characterized with XRD, FTIR, XPS and SEM.

7.2. SOL-GEL PROCESS

The sol-gel process involves the generation of a colloidal suspensions (sols) at relatively low temperature, which are subsequently converted into viscous gels [1]. The gels are usually dried at room temperature to form powders. In the sol-gel process, metal alkoxides are formed from hydrolysis (using water or alcohol) of reactive metal precursors, followed by condensation and polymerization reactions. Metal alkoxides are

compounds formed from direct or indirect reactions between a metal M and an alcohol ROH. During hydrolysis, the alkoxy groups (OR) are replaced by hydroxyl ligands (OH) according to the following reaction:

$$M(OR)_x + H_2O \rightarrow M(OH)(OR)_{x-1} + ROH, \quad (7.1)$$

where R is an alkyl group (C_nH_{2n+1}). The mechanism of this reaction involves the addition of a negatively charged $HO^{\delta-}$ group to the positively charged metal centre ($M^{\delta+}$) followed by the removal of ROH [1]. Condensation occurs only when at least one hydroxyl ligand (OH) is bonded to the cation M to form M-OH. Condensation can proceed via olation (reaction by which a hydroxo bridge is formed between two metal cations) or olation (formation of an oxo (O) bridge between two metal cations) according to the following reactions:

$$\text{olation: } M\text{-}OH + M\text{-}OH_2 \rightarrow M\text{-}OH\text{-}M + H_2O \quad (7.2)$$

$$\text{oxalation: } M\text{-}OH + H\text{-}OM(ROM) \rightarrow M\text{-}O\text{-}M + H_2O(ROH) \quad (7.3)$$

Removal of the solvents (water or alcohol) by condensation and unwanted impurities by using organic reagents, and drying under atmospheric conditions are important steps in the formation of organic, inorganic or composite organic-inorganic materials by the sol-gel process. Several factors which are known to affect the hydrolysis reaction are: (1) the nature of the alkyl group (2) the nature of the solvent (3) the concentration of each species in the solvent (4) temperature (5) solvent to alkoxide molar ratio and (6) the presence of an acid or a base catalyst [1].

7.3. EXPERIMENTAL

7.3.1 PREPARATION OF ZnO NANOPARTICLES

A detailed review of the preparation of ZnO nanoparticles by a sol-gel process can be found in the literature [3-5]. For this study, 0.459 g of $Zn(CH_3COO)_2$ (zinc acetate) was dissolved in 30 ml of ethanol (EtOH) using vigorous stirring at 80°C for 90 minutes. The

resulting transparent solution was cooled in ice water. Then 0.22 g of NaOH was dissolved in 10 ml of EtOH in a preheated ultrasonic bath and was also cooled in ice water. This solution was slowly added to the transparent solution using vigorous stirring in ice water. Oxides are formed during hydrolysis and condensation of dissolved species according to the following reactions [4]:

$$\text{Hydrolysis: } \text{ZnO-OAc} + \text{OH}^- \rightleftarrows \text{Zn-OH} + \text{OAc}^- \quad (7.4)$$

$$\text{Condensation: } \text{Zn-OH} + \text{Zn-OAc} \rightleftarrows \text{Zn-O-Zn} + \text{HOAc} \quad (7.5)$$

where Ac = acetate. A flow diagram for the preparation of ZnO nanoparticles is shown in figure 7.1.

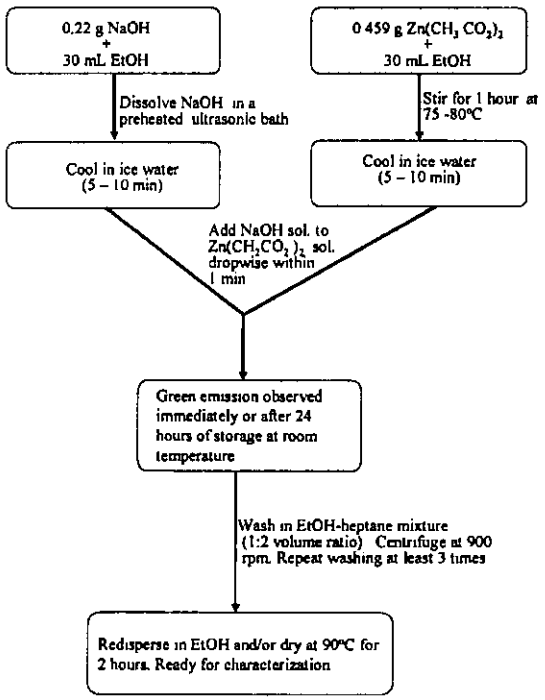

Figure 7.1. A flow diagram for the sol-gel preparation of ZnO nanoparticles.

The unwanted CH_3COO^- and Na^+ ions were removed by washing the gels repeatedly in a mixture of ethanol and heptane (volume ratio of 1:2). The ZnO nanoparticles were either precipitated by centrifuging and dried at 90°C for two hours or suspended in EtOH.

7.3.2. PREPARATION OF SiO_2:Eu (Eu^{3+} = 1 mol%) AND SiO_2:Ce(Ce^{3+}= 1 mol%) WTH ADSORBED ZnO NANOPARTICLES

A SiO_2:Eu gel was prepared by mixing 10.4 g of tetraethylorthosilicate (TEOS) solution with 4.6 g of EtOH and 4.5 g of 0.15 M HNO_3. The mixture was vigorously stirred at room temperature for 1 hour. Then 0.216 g of $Eu(NO_3).6H_2O$ was dissolved in 4.6 g of EtOH, then added to the TEOS solution, and stirred for 1 hour at room temperature. The resulting transparent solution was divided into two parts and one part was combined with the EtOH suspension of ZnO nanoparticles with a molar ratio of 20:1 (Si:Zn), and stirred for 1 more hour. A few drops (10-15 drops) of 0.15 M of NaOH were added to the mixture in order to balance the pH. The gels were dried at room temperature for 8 days, ground into powders and calcined at 600°C for 2 hours in laboratory air. Similar approach was used for preparation and embedding of ZnO in SiO_2:Ce. Figure 7.2 shows a flow diagram for the preparation of SiO_2:Eu with embedded ZnO nanoparticles.

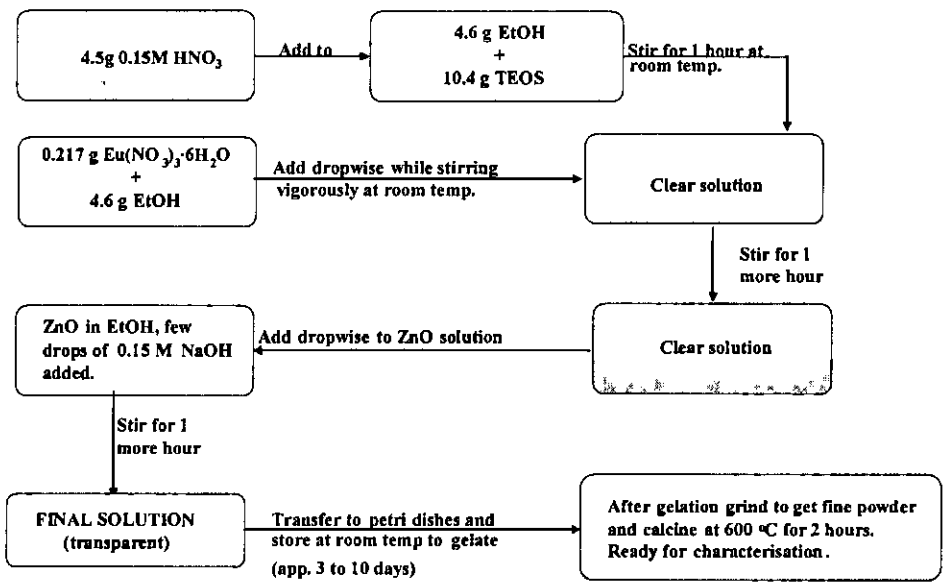

Figure 7.2. A flow diagram for the sol-gel preparation of SiO_2:Eu, with adsorbed ZnO nanoparticles.

7.3.3. PREPARATION OF SiO_2 NANOPHOSPHORS CO-DOPED WITH DIFFERENT CONCENTRATIONS OF Ce^{3+}-Tb^{3+}, Ce^{3+}-Eu^{3+} and Eu^{3+}-Tb^{3+} ION PAIRS

SiO_2:Ce,Tb gels were prepared by mixing 10.4 g of tetraethylorthosilicate (TEOS) solution, 4.6 g of EtOH, and 4.6 g of 0.15 M nitric acid (HNO_3) and stirred for 1 hour. The resulting transparent solution was mixed with a desired amount of $Ce(NO_3)\cdot 6H_2O$ dissolved in 4.6 g of EtOH and stirred for 30 minutes. A desired amount of $Tb(NO_3)\cdot 6H_2O$ dissolved in 4.6 g of EtOH was then added to the mixture and stirred for another 30 minutes. The gels were dried for 8 days at room temperature, ground into powders and annealed at 600°C for 2 hours in laboratory air. All steps were carried out at room temperature except the annealing part. A similar approach was used to prepare SiO_2:Ce,Eu and SiO_2:Eu,Tb. Samples of SiO_2:Ce,Tb, SiO_2:Ce,Eu and SiO_2:Eu,Tb with concentrations of activators varying between 0 and 5 mol% were prepared.

7.4. RESULTS AND DISCUSSIONS

XRD spectra from (a) ZnO-SiO_2 (b) ZnO nanoparticle powders (c) and standard ZnO micrometer-sized powders are shown in figure 7.3. Except for the broadening of ZnO peaks due to smaller particle sizes, the pattern of ZnO nanoparticles resembles that of ZnO micrometer particles. The ZnO-SiO_2 powders did not show any detectable diffraction peaks from ZnO either before or after calcining at 600°C (see Figure 7.2 (c)). The inability to detect diffraction from ZnO nanoparticles is associated with the size-broadened ZnO diffraction peaks and high amorphous scattering background from the SiO_2 matrix. The lack of diffraction both before and after calcining suggests that the ZnO particles remained small in the SiO_2 matrix. However, ZnO nanoparticles were present in the ZnO-SiO_2:Eu powders as detected by the XPS data.

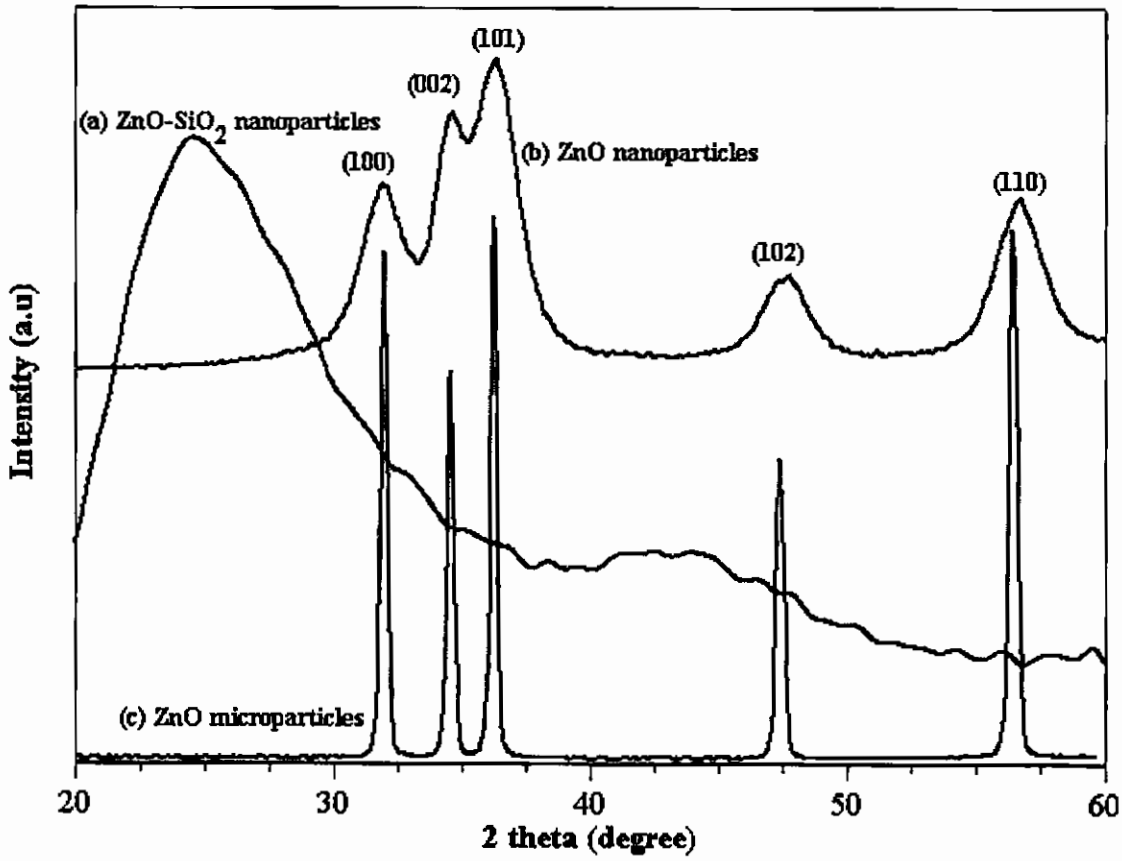

Figure 7.3. XRD patterns from (a) calcined ZnO-SiO_2 nanoparticle (b) dried ZnO nanoparticle and (c) standard ZnO microparticle powders.

Particle sizes of dried ZnO nanoparticle powders were estimated from the broadened XRD peaks using Scherrer's equation:

$$d = \frac{k\lambda}{\beta \cos\theta} \tag{7.4}$$

where d = diameter, k = Scherrer constant ~ 0.9, λ = wavelength of x-ray radiation, β = full width at half maximum of the diffraction peak, and θ is the angle of diffraction. The average ZnO nanoparticle diameter was 4 nm as calculated using (102) peak with 2θ = 0.83 rad, β = 0.04 rad and λ = 1.54 Å.

The SEM photographs of ZnO and calcined SiO_2:Eu nanoparticle powders are shown in figures 7.4 and 7.5 respectively. The photographs show that particles have different shapes and sizes. Most notably, the particles are agglomerated and overlap each other.

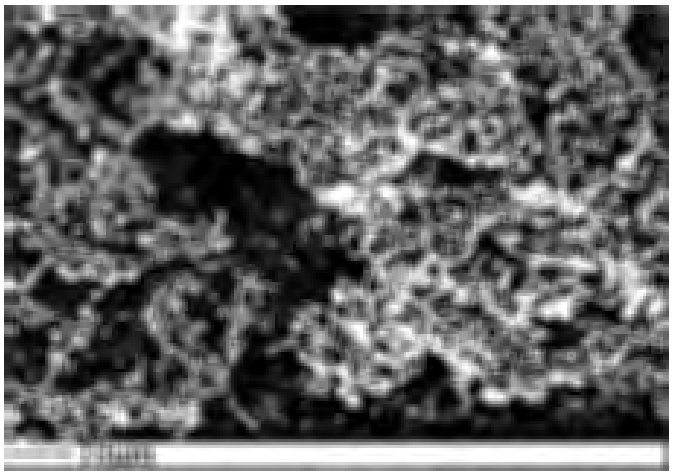

Figure 7.4. The SEM photograph of dried and powdered ZnO nanoparticles

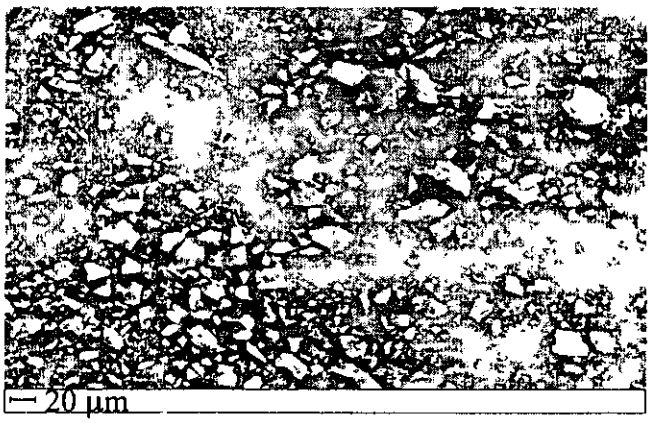

Figure 7.5. The SEM photograph of calcined SiO_2:Eu powder phosphor.

A particle may be a single unit (e.g. a single crystal) or it may consist of subunits [7]. The individual subunits are called primary particles and the agglomerated subunits are called secondary particles. Figure 7.6 shows the schematic diagram of the primary and secondary particles.

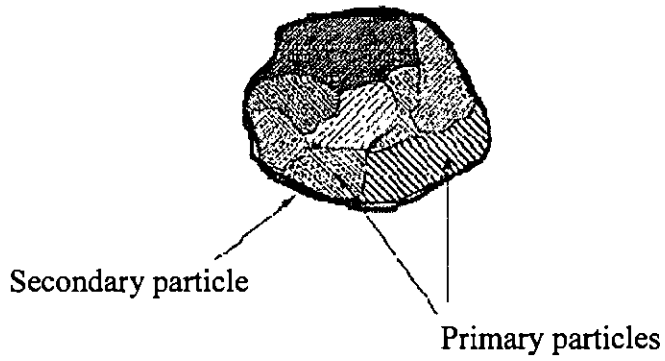

Figure 7.6. Schematic diagram showing the primary and secondary particles [7].

The SEM measurements often can only determine the particle size of secondary particles [7]. For crystalline materials (e.g. ZnO), the size of primary particles can best be estimated by the broadening of x-ray diffraction peaks, from dark-field imaging by transmission electron microscopy (TEM) or from lattice imaging by high resolution transmission electron microscopy (HRTEM) [7]. For amorphous materials (e.g. SiO_2), the size of primary particles can be estimated by bright-field imaging using TEM or HRTEM. It is therefore almost certain that the SEM photographs in figures 7.4 and 7.5 show only the secondary particles of ZnO and SiO:Eu respectively. In the case of ZnO, these secondary particles are assumed to consist of nanounits with the average diameter of 4 nm as estimated by Scherrer's equation. In the case of SiO_2:Eu, the secondary particle sizes estimated from the SEM photographs were in the range of 100 – 1000 nm. This means that the primary particles consisted of nanounits whose individual sizes were less than the individual sizes of the secondary particles.

FTIR spectra from dried ZnO nanoparticles, micrometer sized ZnO particles, SiO_2 and ZnO-SiO_2 gels are shown in Figure 7.7. The Zn-O stretching mode frequencies (460 cm^{-1} and 532 cm^{-1}) of ZnO nanoparticles overlap those from micrometer-sized ZnO particles, and they are consistent with those reported in the literature [8,9]. These stretching mode frequency peaks are indicative of the successful synthesis of ZnO nanoparticles. Small peaks were observed from ZnO nanoparticles at 1406 cm^{-1} and 1572 cm^{-1}, probably from the stretching mode frequencies of adsorbed CO. Similarly, a

2352 cm^{-1} band for ZnO and SiO_2 probably resulted from the absorption of CO_2 [8]. The well known stretching mode frequencies of SiO_2 at 465 cm^{-1}, 816 cm^{-1} and 1083 cm^{-1}[10] were present in the spectra from both ZnO-SiO_2: (1mol%)Eu mixtures (no. 3) and pure SiO_2 (no. 4). A peak at 938 cm^{-1} in spectrum no. 3 can tentatively be ascribed to the incorporation of ZnO nanoparticles. The broadening of the SiO_2 465 cm^{-1} peak in spectrum no. 3 can be attributed to overlap of the SiO_2 peak at 465 cm^{-1} and the 460 cm^{-1} peak from the 5 mol% of ZnO nanoparticles. Furthermore, there is more intensity at 531 cm^{-1} in spectrum no. 3, again consistent with the incorporation of 5 mol% ZnO into SiO_2. These spectra are consistent with those from ZnO-loaded silica molecular sieves (MCM-41) reported by Kwon *et al.* [8] and Gu *et al.* [10].

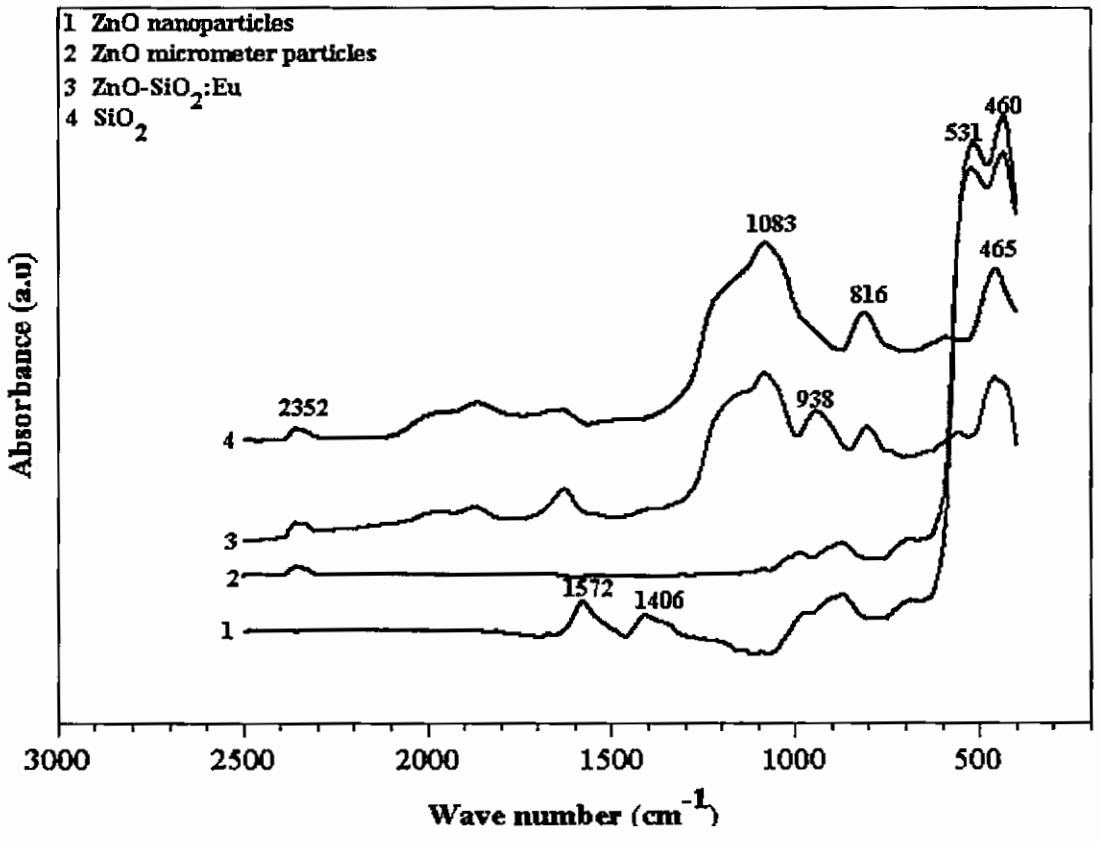

Figure 7.7. FTIR spectra from (1) ZnO nanoparticles, (2) ZnO micrometer particles (3) ZnO-SiO_2:Eu, and (4) SiO_2

The XPS spectrum of calcined ZnO-SiO_2:Eu in figure 7.8 shows that O, Si, Zn and an adventitious C were present on the surface. Eu^{3+} ions could not be detected by the XPS probably due to their relatively low concentration in the SiO_2 matrix. The data suggests that ZnO nanoparticles were incorporated in the SiO_2 matrix.

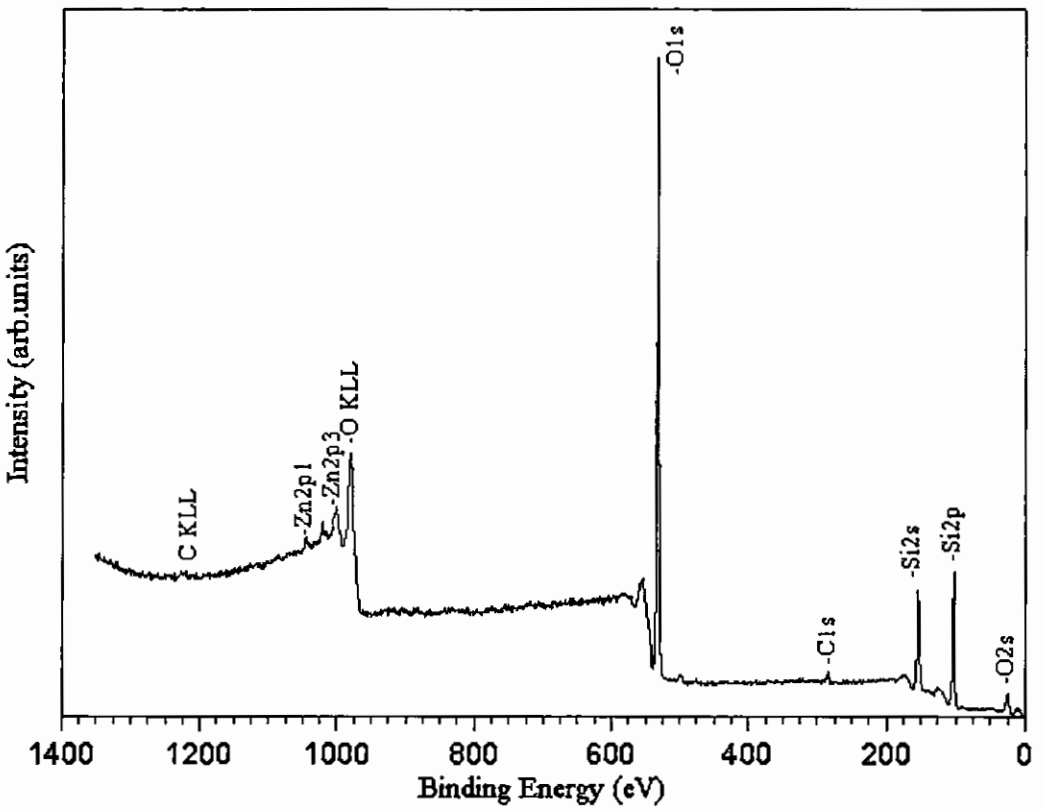

Figure 7.8. XPS survey spectrum of ZnO-SiO_2:Eu (ZnO = 5 mol% and Eu^{3+} = 1 mol%) powders calcined at 600°C.

7.5. CONCLUSION

Nanophosphors of ZnO, SiO_2 doped with different concentrations of Ce^{3+}-Tb^{3+}, Ce^{3+}-Eu^{3+} or Eu^{3+}-Tb^{3+} ion pairs, and SiO_2:Eu/Ce with adsorbed ZnO nanoparticles were successfully synthesized with a sol-gel process. The particles had different shapes and sizes. The average diameter of individual ZnO primary particles estimated using Scherrer's equation was 4 nm. The sizes of secondary particles of SiO_2:Eu estimated from the SEM photographs was in the range of 100 – 1000 nm.

REFERENCES

[1] Tjong S.C. and Chen H., *Mat. Sci. Eng. R.* **45** (1988) 1

[2] Reiss P., *Nano Lett.* **2** (7) (2002) 781

[3] Wong E.M., Bonevich J.E. and Searson P.C., *J. Phy Chem B* 102 (1998) 7770.

[4] Meulenkamp E.A., J. Phy Chem B 102 (1998) 7764

[5] Chakrabarti S., Ganguli D. and Chaudhuri S., *J. Phys. D* 36 (2003) 146.

[6] Bang J., Yang H. and Holloway P.H., *J. Chem. Phys.* **123** (084709) (2005) 1

[7] Chow G.M. and Gonsalves K.E., in Nanomaterials: synthesis, properties and applications, edited by Edelstein A.S. and Cammarata R.C., (Institute of Phyiscs, Bristol) (2001) 55

[8] Kwon Y.J., Kim K.H., Lim C.S. and Shim K.B., *J. Ceram. Proc. Research* **3** (3) (2002) 146

[9] Xiong Y., Zhang L.Z., Tang G., Zhang G. and Chen W., *J. Lumin.* **110** (2004) 17

[10] Gu G., Ong P.P. and Chu C., J. *Phys. and Chem. Sol.* **60** (1999) 943

CHAPTER 8: ENHANCED PHOTOLUMINESCENCE OF SiO_2:Eu AND SiO_2:Ce INDUCED BY AN ENERGY TRANSFER FROM EMBEDDED ZnO NANOPARTICLES

8.1. INTRODUCTION

This chapter deals with enhanced photoluminescence of Eu^{3+} and Ce^{3+} ions induced by ZnO nanoparticles embedded in SiO_2 matrices. Samples were prepared by a sol-gel process as discussed in chapter 7. Photoluminescence data were collected at room temperature using a 325 nm HeCd (25 mW) as the excitation source.

8.2. RESULTS AND DISCUSSIONS

Figure 8.1 shows the PL emission spectra of (1) dried ZnO nanoparticles, (2) ZnO nanoparticles suspended in EtOH and (3) standard ZnO micrometer-sized powders. A well known defect-related green emission from dried and suspended ZnO nanoparticles was observed around 560 nm (2.22 eV) and 581 nm (2.13 eV), respectively. This emission was sufficiently intense to be observed in ambient laboratory light. In the case of standard ZnO microparticles, the defect-related green emission was observed at 501 nm with very low intensity. A red-shift from the normal emission at ~ 500 -520 nm [1,2] in ZnO microparticles to 560 and 580 nm in dried and suspended ZnO nanoparticles, respectively, is associated with recombination of delocalised electrons at singly occupied oxygen vacancies with deep trapped holes and it is attributed to quantum confinement effects [3,4]. Direct bandgap (UV) emission attributed to the recombination of exciton centres in ZnO [2] was at: (1) 372 nm (3.34 eV) in suspended ZnO nanoparticles, (2) 376 nm (3.31 eV) in dried ZnO nanoparticles and (3) 386 nm (3.22 eV) in standard ZnO microparticles. These peaks are compared in figure 8.2. Due to quantum confinement effects [3,4], the peaks from ZnO nanoparticles are broader than the peak from ZnO

micropartilces, and have shifted to shorter wavelengths; and the bandgap energies of the nanoparticles are higher than that of the microparticles.

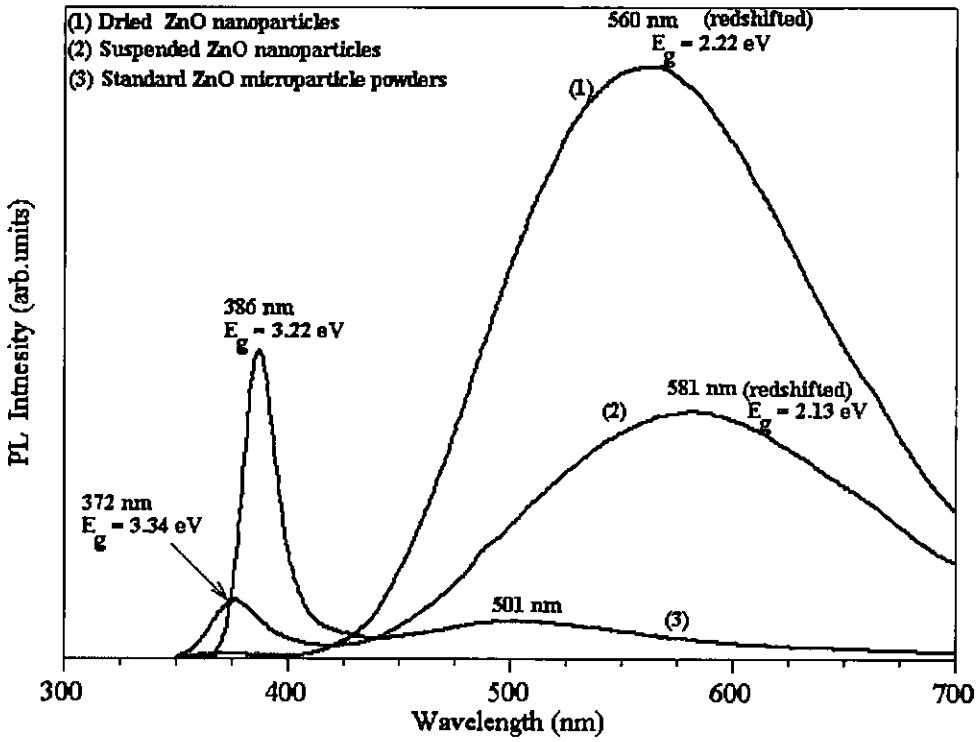

Figure 8.1. Photoluminescence emission spectra from (1) dried ZnO nanoparticles (2) ZnO nanoparticles suspended in EtOH and (3) standard ZnO microparticle powders.

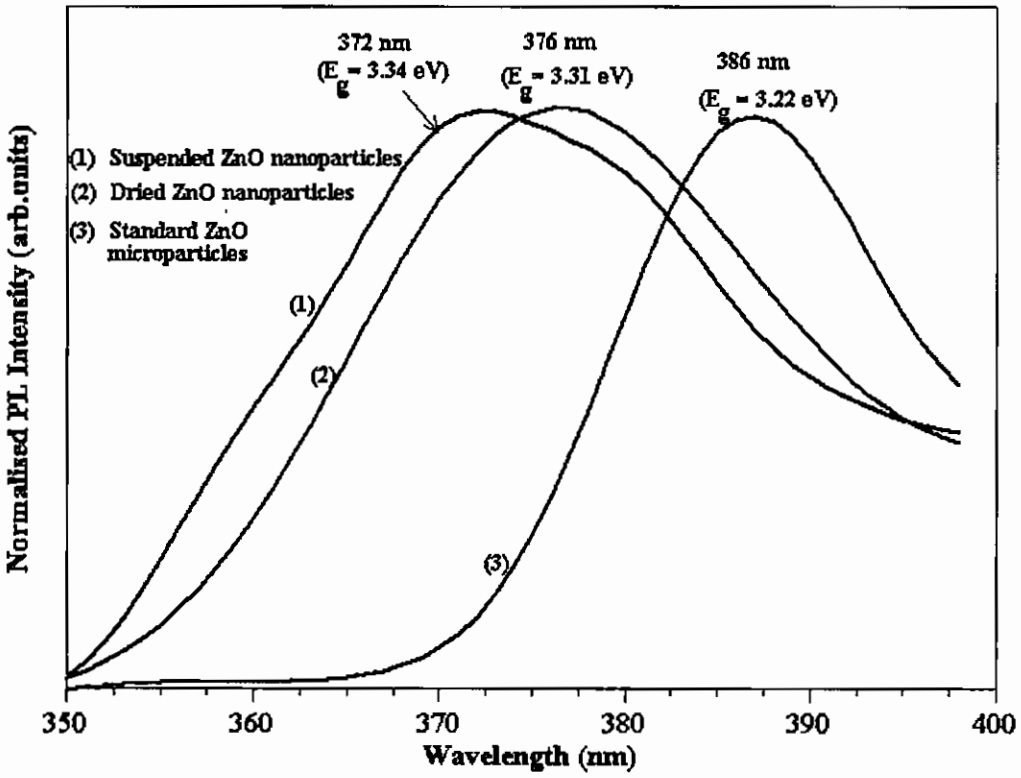

Figure 8.2. UV emission from (1) ZnO nanoparticles suspended in EtOH (2) dried ZnO nanoparticles and (3) standard ZnO microparticle powders.

Figures 8.3. compares the PL emission spectra of SiO_2:Eu and ZnO-SiO_2:Eu. The main peak of red emission from Eu^{3+} is at 613 nm in both spectra. The green emission of ZnO nanoparticles at 560 nm is completely suppressed. The intensity from ZnO-SiO_2:Eu is 3 times larger than that from SiO_2:Eu. The enhancement of the intensity of Eu^{3+} and the suppression of the green emission from ZnO nanoparticles suggests that energy from the excitation source (325 nm HeCd laser) was absorbed by ZnO nanoparticles and transferred non-radiatively to Eu^{3+} ions. Similarly, figure 8.4 shows intense blue emission of Ce^{3+} ions from ZnO-SiO_2:Ce at 417 nm, probably due to an energy transfer from the embedded ZnO nanoparticles. The intensity from ZnO-SiO_2:Ce is 4 times larger than the intensity from SiO_2:Ce.

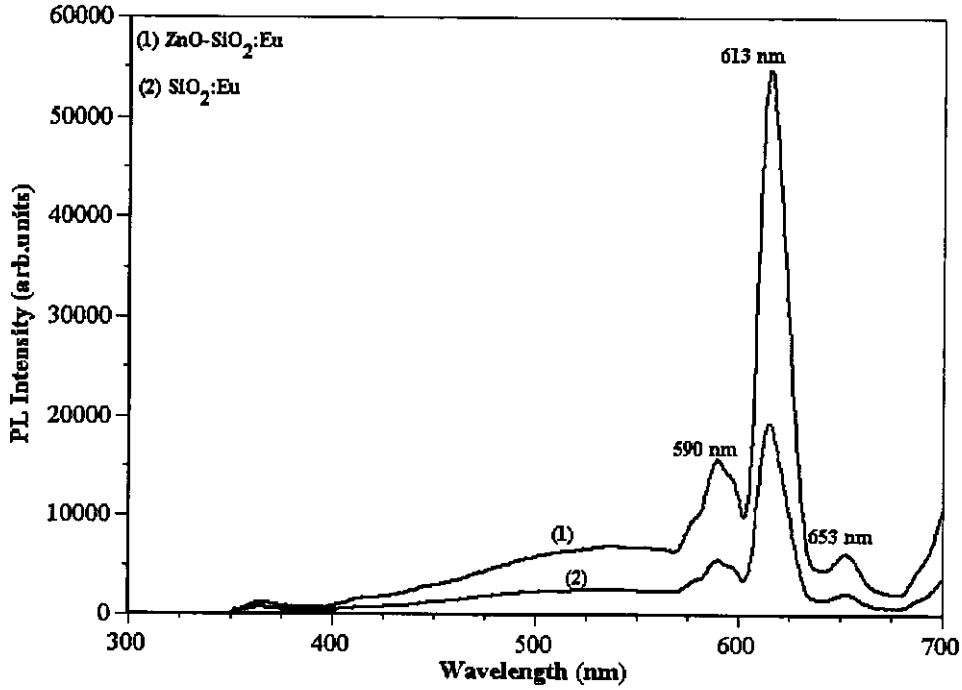

Figure 8.3. Photoluminescence emission spectra from (1) ZnO-SiO_2:Eu and (2) SiO_2:Eu.

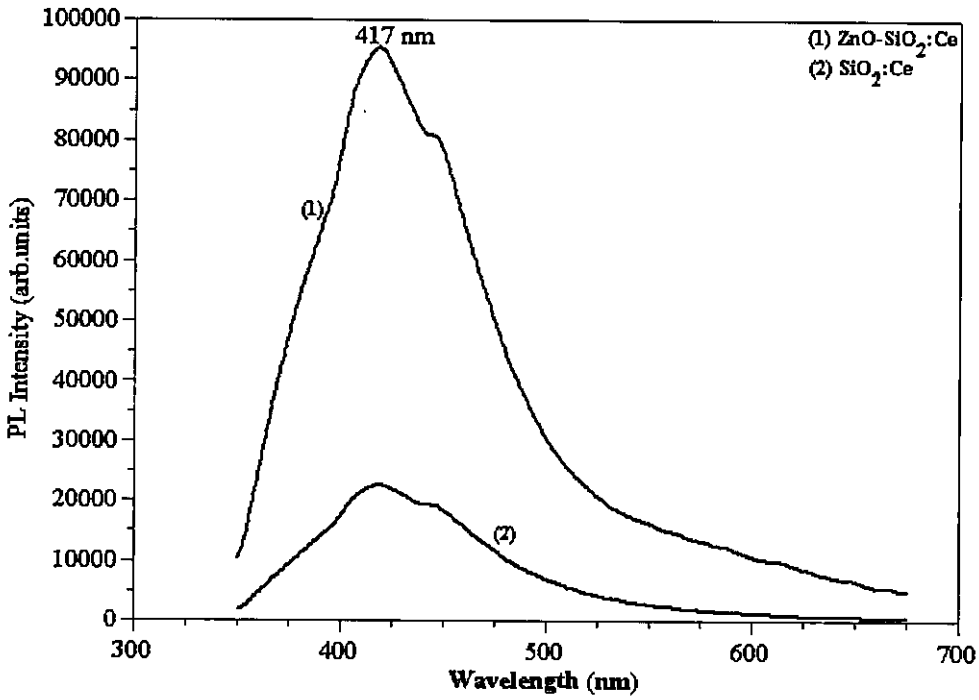

Figure 8.4. Photoluminescence emission spectra from (1) ZnO-SiO_2:Ce and (2) SiO_2:Ce.

The rate of energy transfer is known to depend on spectral overlap and other types of interaction between the energy donor and the energy acceptor [5]. The transfer rate from a broad-band donor (e.g. ZnO) to a broad-band acceptor (e.g. Ce^{3+}) must be faster than the transfer rate to narrow-line acceptor due to anticipated optimal spectral overlap of the broad bands. In addition, the strength of interaction is determined by the intensity of optical transition and this is larger for allowed (broad band) compared to forbidden (narrow line) transitions [5]. Energy transfer from an allowed broad-band donor (ZnO) to a forbidden narrow-line acceptor (Eu^{3+}) is only possible for nearest neighbours in the lattice [1]. The results in figures 8.3 and 8.4 show that the band-to-band energy transfer from ZnO to Ce^{3+} ions is more efficient (4 times larger) than the band-to-line energy transfer (3 times larger) from ZnO to Eu^{3+} ions.

ZnO-SiO_2:Eu was poorly excited (results not shown) by 325 nm photons suggesting that there a lack of spectral overlap between Eu^{3+} excitation band and ZnO emission band. Similar results were reported by Bang *et al.*[6]. They therefore attributed energy transfer from ZnO nanoparticles to Eu^{3+} to phonon-mediated processes. It is likely that this phonon-mediated energy transfer dominated over emission from ZnO nanoparticles when $R < R_c$ [6]. The excitation of ZnO nanoparticles and energy transfer to Eu^{3+} are illustrated schematically in figure 8.5. It is shown that emission from Eu^{3+} is sensitized by energy transfer from ZnO nanoparticles and partially by direct excitation of Eu^{3+}.

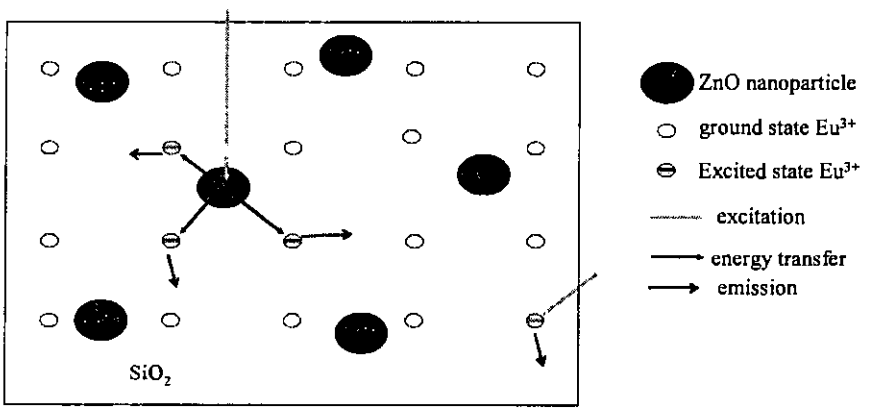

Figure 8.5. Excitation of ZnO nanoparticles and energy transfer to Eu^{3+} ions in SiO_2 [6].

Energy level diagrams of Eu^{3+} and ZnO, and an energy transfer process from ZnO nanoparticles that could lead to enhanced red emission from Eu^{3+} are shown in figure 8.6. Absorption of excitation energy is followed by relaxation to the defect states in the bandgap of ZnO nanoparticles. Subsenquently, the energy is transferred resonantly or by phonon-mediated processes to the ^5D_j (j = 0,1,2,3...) states of Eu^{3+}, resulting in enhanced photoluminescence during radiative relaxation to the ground state [6].

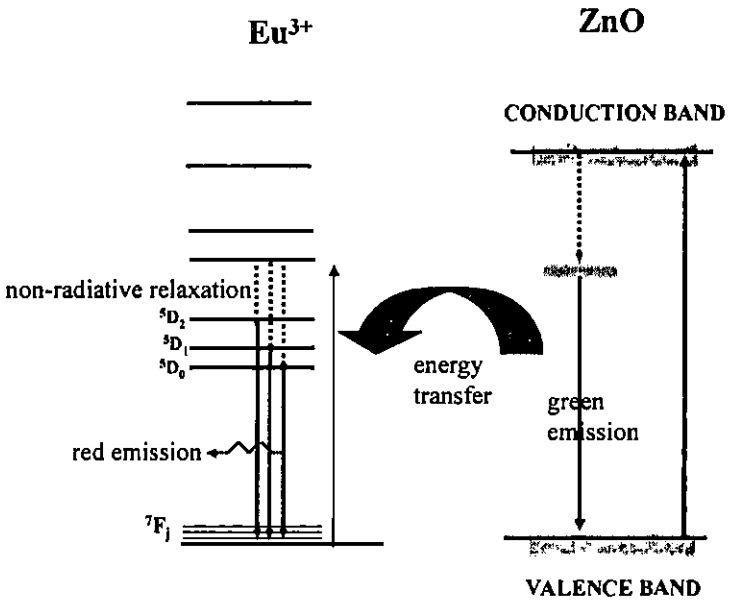

Figure 8.6. Possible transitions in ZnO and Eu^{3+} ions and mechanism of energy transfer from ZnO nanoparticles to Eu^{3+} ions [6].

Although the PL excitation data for SiO_2:Ce was not collected in this study, it is known that the excitation band of Ce^{3+} in silicate glass is at ~320 nm [7]. Based on this result and the PL emission spectra of ZnO nanoparticles in figure 8.1, the spectral overlap of Ce^{3+} absorption band and ZnO emission band is estimated to be at ~ 350 – 400 nm. This estimation is consistent with the interpretation that energy transfers from ZnO nanoparticles to Ce^{3+}. Energy level diagrams of Ce^{3+} and ZnO and postulated mechanism of energy transfer from ZnO nanoparticles to Ce^{3+} is illustrated in figure 8.7.

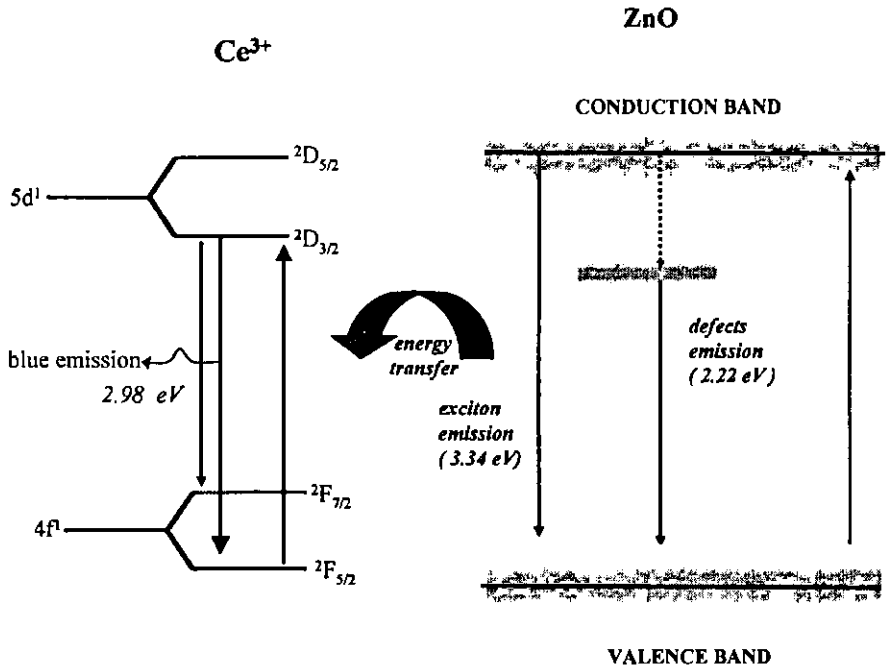

Figure 8.7. Possible transitions in ZnO and Ce^{3+} ions and proposed mechanism for energy transfer from ZnO nanoparticles to Ce^{3+} ions [5,6].

The $5d^1$ excited configuration in Ce^{3+} is split by the crystal field into two components ($^2D_{5/2}$ and $^2D_{3/2}$), and the $4f^1$ ground state configuration yields two components ($^2F_{5/2}$ and $^2F_{7/2}$) due to spin-orbit coupling [5]. Blue emission emanates from the lowest crystal field component of the $5d^1$ configuration to the two levels of the ground state. Since the green emission from ZnO results from states lying lower than the Ce^{3+} states, it seems reasonable to speculate that energy transfer results from bandgap excitation and recombination in the ZnO nanoparticles. In this model, energy transfer is faster than holes trapping and recombination with electrons, therefore the green emission from ZnO is quenched completely and blue emission from Ce^{3+} is enhanced considerably. This is shown in Figure 8.7, where the bandgap excitation of ZnO has resulted in creation of an exciton, and a subsequent non-radiative recombination results in excitation from the ground 4f states to the excited 5d states on the Ce^{3+} centre. Subsequent radiative relaxation on the Ce^{3+} would result in enhanced blue emission. This speculation is consistent with the Ce^{3+} emission being at a similar but lower energy (417 nm) than the bandgap emission from ZnO (372 nm). Finally, the relatively low Ce^{3+} emission intensity in SiO_2:Ce is consistent with its low excitation cross section at 325 nm [5],

however, the quenching of ZnO emission and significant enhancement of Ce^{3+} emission in ZnO-SiO_2:Ce demonstrates that energy transfer from ZnO nanoparticles to Ce^{3+} is occurring.

8.3. CONCLUSION

The incorporation of ZnO into SiO_2:Eu and SiO_2:Ce suppressed the normal green emission from ZnO nanoparticles resulting in an enhanced red and blue photoluminescence from the Eu^{3+} and Ce^{3+} activators, respectively. The enhancement of photoluminescence was attributed to an energy transfer from the ZnO nanoparticles. Possible mechanisms for energy transfer from ZnO nanoparticles to Eu^{3+} and Ce^{3+} were discussed.

REFERENCES

[1] van Dijken A., Meulenkamp E.A., Vanmaekelbergh D. and Meijerink A., *J. Lumin.* **90** (2000) 123

[2] Li Z, Xiong Y and Xie Y, *J. Inorg. Chem.* **42** (2003) 8105.

[3] Chakrabarti S., Ganguli D. and Chaudhuri S., J. Phys. D: Appl. Phys. 36 (2003) 146.

[4] Monticone S., Tufeu R. and Kanav A.V., *J. Phy Chem. B* **102** (16) (1998) 2854.

[5] Blasse G. and Grabmaier B.C., Luminescent Material, Springer-Verlag, Berlin, 1994.

[6] Bang J., Yang H., and Holloway P.H., *J. Chem. Phys.* **123** (084709) (2005) 1

[7] Stroud J.S., *J. Chem. Phys.* **35**(3) (1961) 844.

CHAPTER 9: ENERGY TRANSFER BETWEEN Ce^{3+}, Eu^{3+} and Tb^{3+} IN SiO_2 MATRICES

9.1. INTRODUCTION

This chapter deals with energy transfer between Ce^{3+}-Eu^{3+}, Ce^{3+}-Tb^{3+} and Eu^{3+}-Tb^{3+} ion pairs co-doped with different concentrations in SiO_2. Samples were prepared by a sol-gel process as discussed in chapter 7. The PL data were collected at room temperature using a 325 nm HeCd laser (8.8 mW) as the excitation source.

9.2. RESULTS AND DISCUSSIONS

Figure 9.1 shows the PL emission spectra of SiO_2:Ce,Eu nanoparticle powder phosphors with concentrations of Ce^{3+} and Eu^{3+} varied between 0 and 1 mol%. Spectra (1) and (5) show that the intensity of red emission from SiO_2:Eu (1 mol%Eu) was higher than that of blue emission from SiO_2:Ce (1mol%Ce). When Ce^{3+} and Eu^{3+} ions were co-doped with different concentrations (spectra 2-4), blue emission of Ce^{3+} ions was enhanced and red emission of Eu^{3+} ions was suppressed. The intensity was highest for 0.5 mol% Ce^{3+} and 0.5 mol% Eu^{3+}co-doping (spectrum 2). These results suggest that energy was transferred from Eu^{3+} ions to enhance blue emission of Ce^{3+} ions.

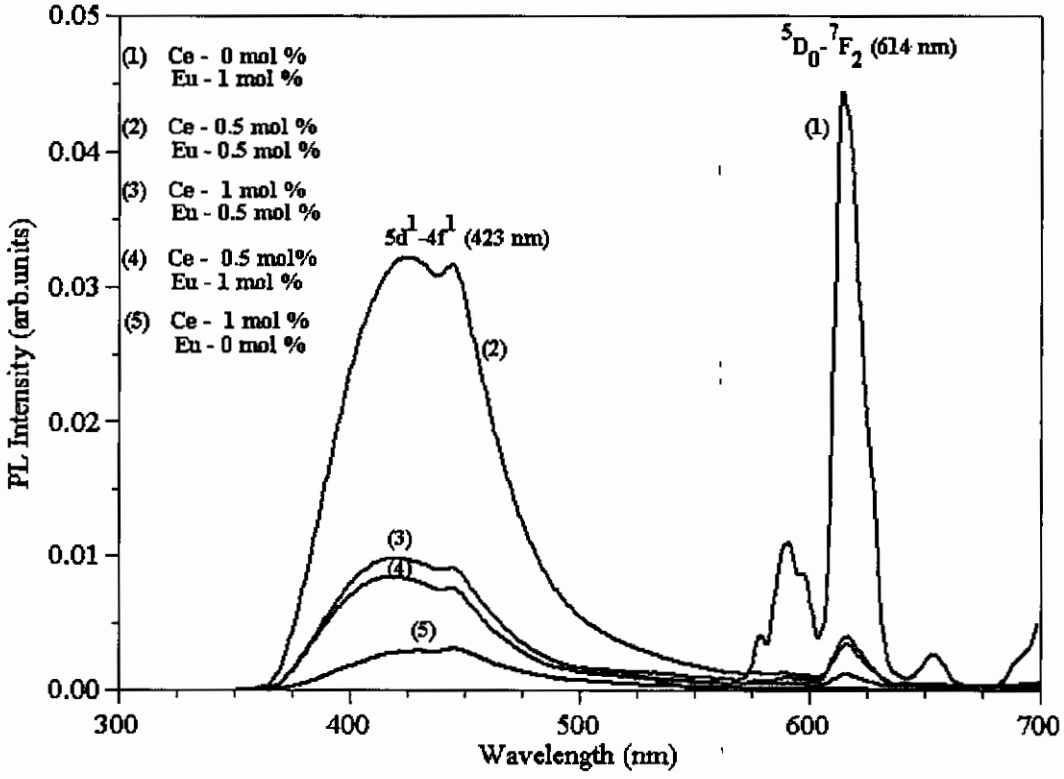

Figure 9.1. PL emission spectra of SiO_2:Ce,Eu nanoparticle powder phosphors with concentrations of Ce^{3+} and Eu^{3+} ions varied between 0 and 1 mol%.

An energy level model that explains an energy transfer from Eu^{3+} to Ce^{3+} is shown in figure 9.2. According to this model, the transfer of energy involves an interaction between two excited states, namely $^5D_3$ of Eu^{3+} and $^2D_{3/2}$ of Ce^{3+}. The $5d^1 \rightarrow 4f^1$ transition in Ce^{3+} is at ~24000 cm^{-1} (417 nm) [1] and the $^5D_3 \rightarrow {}^7F_J$ (J = 1,2,3,4...) transition in Eu^{3+} is at ~24500 cm^{-1}(408 nm) [2]. The $^5D_0 \rightarrow {}^7F_J$ transition in Eu^{3+} is at ~17000 cm^{-1} (588 nm), which is too low an energy to transfer to Ce^{3+}. Therefore the speculation that energy transfers from the $^5D_3$ state of Eu^{3+} to the $^2D_{3/2}$ state of Ce^{3+} is consistent with the law of conservation of energy.

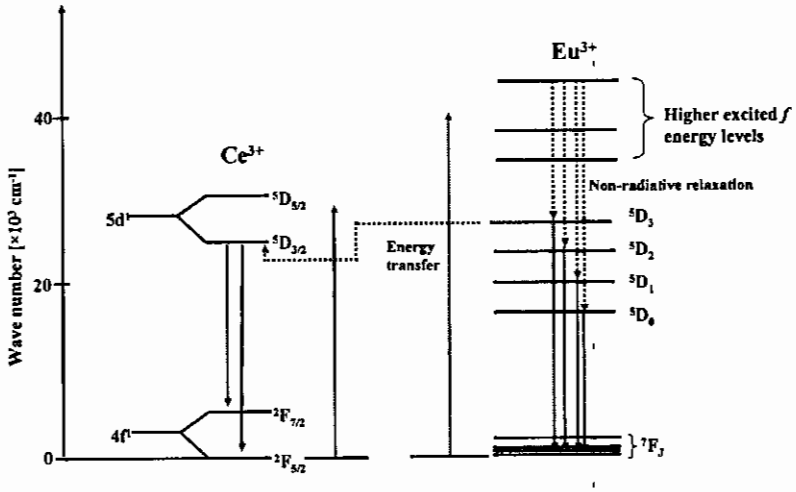

Figure 9.2. Possible transitions in Ce^{3+} and Eu^{3+} ions, and mechanism of energy transfer from Eu^{3+} ions to Ce^{3+} ions [1,4].

Energy transfer was also evaluated using higher concentrations (~2 -5 mol%) of Ce^{3+} and Eu^{3+}. Figure 9.3 shows that for concentration of 5 mol%, red photoluminescence of Eu^{3+} was still intense but blue photoluminescence of Ce^{3+} was quenched. This shows that Ce^{3+} ions are sensitive to concentration quenching. The quenching effect, probably due to higher concentrations, was also observed (results not shown) in samples co-doped with 2 mol% Ce^{3+}- 3 mol% Eu^{3+} and 3 mol% Ce^{3+} - 2 mol% Eu^{3+} ion pairs.

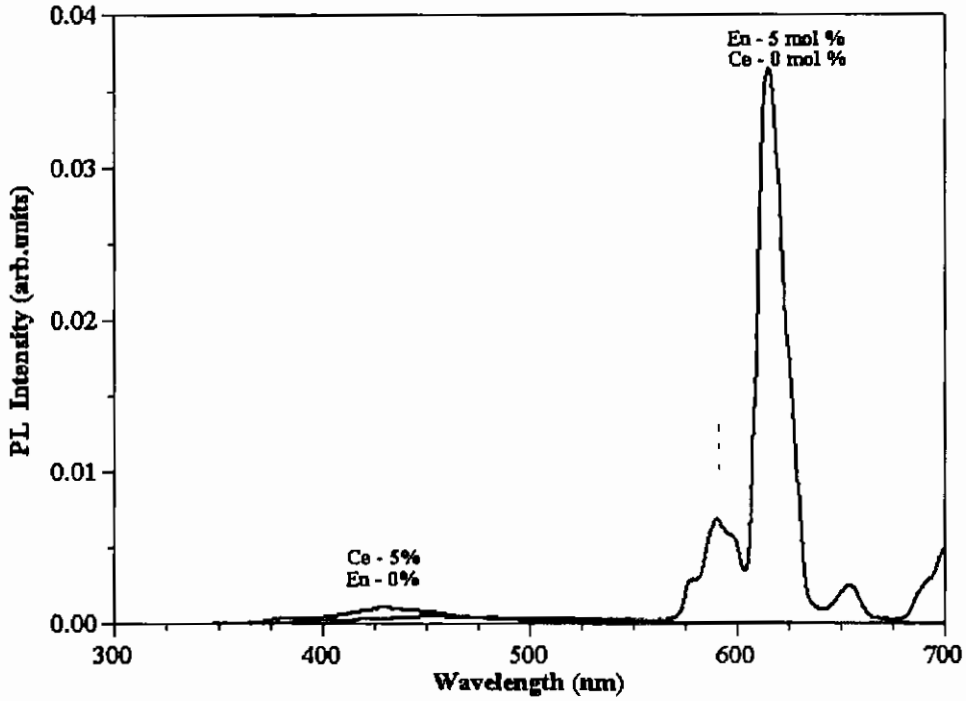

Figure 9.3. PL emission spectra of SiO_2:Ce (5 mol% Ce^{3+}) and SiO_2:Eu (5 mol% Eu^{3+}) nanoparticle powder phosphors.

Photoluminescence emission spectra of SiO_2:Ce,Tb powder phosphors with different concentrations of Ce^{3+} and Tb^{3+} are shown in figure 9.4. The PL emission spectrum of Tb^{3+} consists of four emission peaks located at 488 nm ($^5D_4 \rightarrow {}^7F_6$), 543 nm ($^5D_4 \rightarrow {}^7F_5$), 586 nm ($^5D_4 \rightarrow {}^7F_4$) and 622 nm ($^5D_4 \rightarrow {}^7F_3$). The strongest emission peak is located at 543 nm. The PL emission spectrum of Ce^{3+} consists of a broad band located at 430 nm ($5d^1 \rightarrow 4d^1$). The green emission of Tb^{3+} was enhanced considerably by Ce^{3+} co-doping. The enhancement was largest for addition of 0.5 mol% Ce^{3+} to 1 mol% Tb^{3+}. These results suggest that energy transfer from Ce^{3+} ions to Tb^{3+} ions took place, and this transfer was maximized with 0.5 mol% Ce^{3+} co-doping.

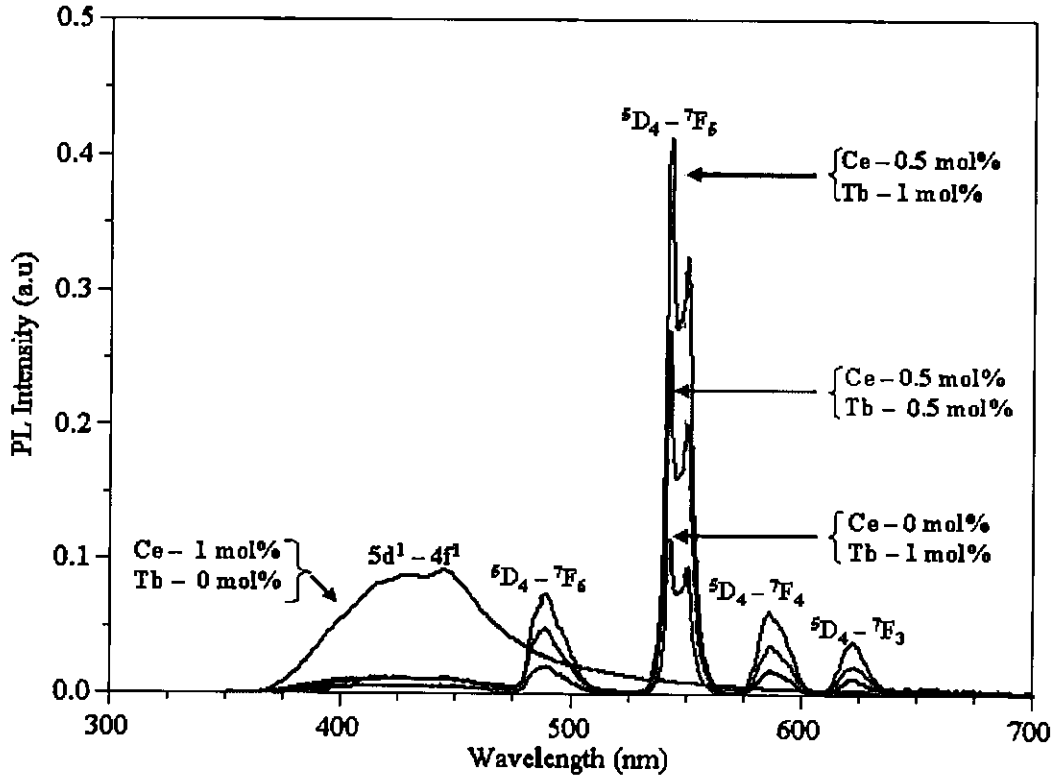

Figure 9.4. PL emission spectra of SiO_2:Ce,Tb with different concentrations of Ce^{3+} and Tb^{3+} ions.

An energy level model that explains an energy transfer from Ce^{3+} to Tb^{3+} is shown in figure 9.5. The transfer involves interaction between the $^5D_{3/2}$ state of Ce^{3+} and the $^5D_4$ state of Tb^{3+}. The $^5D_4 \rightarrow {}^7F_5$ (543 nm) transition in Tb^{3+}occurs at ~20600 cm^{-1} (485 nm) [3,4] and the blue emission in Ce^{3+} occurs at ~24000 cm^{-1} (417 nm) [1]. As a result, the transfer of energy from Ce^{3+} to Tb^{3+} is allowed by the law of conservation of energy.

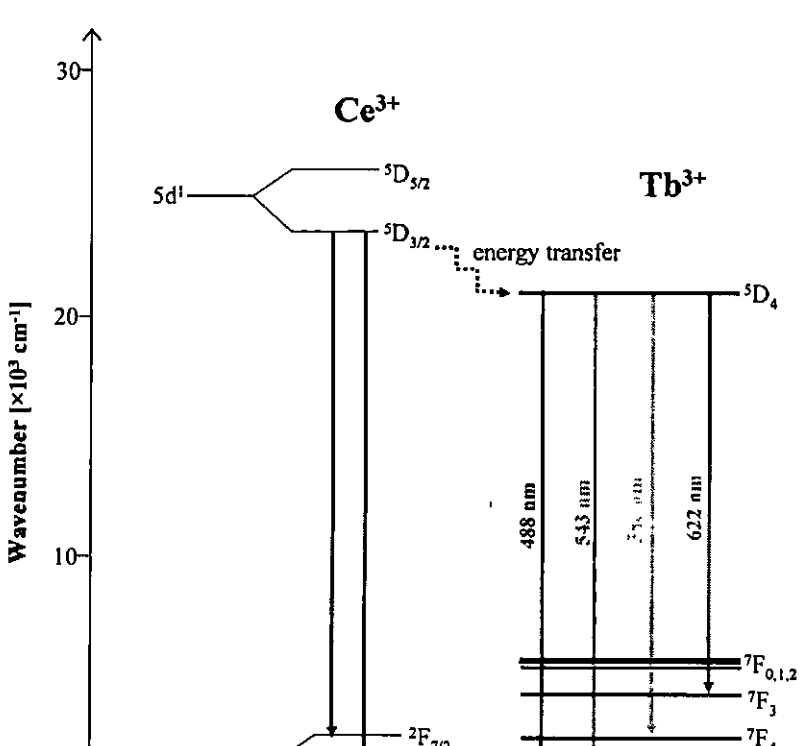

Figure 9.5. Possible transitions in Ce^{3+} and Tb^{3+} ions that result in an energy transfer from Ce^{3+} to Tb^{3+} ions [1,4].

The transfer of energy from Ce^{3+} to Tb^{3+} may be due to spectral overlap between the emission band of Ce^{3+} and the excitation band of Tb^{3+}. While PL excitation data were not collected in this study, Lin and Su [5] reported that spectral overlap between the Ce^{3+} emission band and Tb^{3+} excitation band in $Mg_2Y_8(SiO_4)_6O$:Ce,Tb occurred between 350 – 550 nm. The interpretation that energy transfers from Ce^{3+} to Tb^{3+} is consistent with this report of spectral overlap between Ce^{3+} emission and Tb^{3+} excitation. Moreover, energy transfer from an allowed broad-band energy donor (e.g. Ce^{3+}) to a forbidden narrow-line excitation energy absorber (e.g. Tb^{3+}) is possible for nearest neighbours in a host lattice [4]. Even though the critical distance, R_c, could not be

calculated from the present data, suppression of blue emission from Ce^{3+} ions suggests that the transfer rate (P_{DA}) from the energy donor (Ce^{3+}) to the energy acceptor (Tb^{3+}) was faster than the radiative rate (P_D) of the donor.

Extremely low photoluminescence was observed for Eu^{3+}-Tb^{3+} co-doping irrespective of the concentration of either Eu^{3+} or Tb^{3+} ions, suggesting that no energy transfer took place between these ions. Li and Su [5] attributed the lack of energy transfer between Ce^{3+} and Sm^{3+} to the formation of Ce^{4+} - Sm^{2+} ion pairs. Similarly, the lack of energy transfer between Eu^{3+} and Tb^{3+} could be due to charge transfer resulting in the formation of Eu^{2+}-Tb^{4+} ion pairs.

9.3. CONCLUSION

It was shown that the emission intensity of Ce^{3+} ions could be increased by Eu^{3+} co-doping. The increase was maximized for Ce^{3+} and Eu^{3+}concentrations equal to 0.5 mol%. Ce^{3+} and Eu^{3+} quenched each other when higher concentrations (~2-5 mol%) were used. This observation was attributed to the concentration quenching effect of Ce^{3+} ions. For Ce^{3+}-Tb^{3+} co-doping, energy was transferred from Ce^{3+} to enhance green emission of Tb^{3+}. The intensity of the green PL emission was highest for samples prepared with Ce^{3+} and Tb^{3+} concentrations equal to 0.5 mol% and 1 mol%, respectively. Possible mechanisms for energy transfer were discussed.

REFERENCES

[1] Blasse G. and B.C. Grabmaier., *Luminescent Materials* (Springer-Verlag, Berlin, 1994)

[2] Hayakawa T., Selvan T. and Nogami M, *J. Sol-Gel Sci. Technol.* **19** (2000) 779

[3] Joubert M.F. and Jacquier B, *Phys. Rev.(B)* **35**(16) (1987) 8322

[4] Labio L.D., *PhD Dissertation*, University of Bern, Switzerland, 2005

[5] Lin J. and Su Q, *J., Mat. Chem.* **5**(8) (1995) 1151

CHAPTER 10: SUMMARY AND CONCLUSION

The contents of this thesis could be divided into three categories, namely (1) cathodoluminescence degradation of Y_2O_3:Eu and SiO_2:Ce,Tb powder and pulsed laser deposited Y_2O_3:Eu thin film phosphors (2) enhanced photoluminescent intensity of red and blue emissions of SiO_2:Eu and SiO_2:Ce respectively induced by an energy transfer from embedded ZnO nanoparticles and (3) energy transfer was also evaluated between Ce^{3+}-Eu^{3+}, Ce^{3+}-Tb^{3+} and Eu^{3+}-Tb^{3+} ion pairs co-doped with different concentrations in SiO_2 matrices. Possible mechanisms for degradation and energy transfer were proposed.

In a first set of experiments, the AES and CL spectroscopy were used to study CL degradation of commercial Y_2O_3:Eu powder, pulsed laser deposited thin film phosphors and sol-gel SiO_2:Ce,Tb nanoparticle powder phosphors. Powder and thin film samples were irradiated with a 2 keV beam of electrons in a vacuum chamber maintained at 1×10^{-6}, 1×10^{-7} or 1×10^{-8} Torr O_2. The CL intensity of the samples was degraded considerably by prolonged electron beam irradiation. In the case of Y_2O_3:Eu thin films and SiO_2:Ce,Tb powders, CL degradation occurred simultaneously with desorption of O from the surface. Among other things, oxygen-deficient non-luminescent layers of Y_2O_{3-x} ($0< x <3$) and SiOx ($0< x <2$) could be responsible for the CL degradation of Y_2O_3:Eu thin films and SiO_2:Ce,Tb powders respectively. In the case of Y_2O_3:Eu powders, electron beam irradiation did not seem to induce desorption of atomic species from the surface. Instead, there was a relative increase in the concentration of O. An oxygen-rich non-luminescent layer of Y_2O_{3+x} ($x >0$) could be responsible for the CL degradation.

In a second set of experiments, enhanced photoluminescence of ZnO-SiO_2:Eu and ZnO-SiO_2:Ce phosphors prepared by a sol-gel process was demonstrated. Photoluminescence data were collected at room temperature using a 325 nm HeCd as an excitation source. Quenching of the normal green emission from ZnO nanoparticles and a subsequent increase of red and blue emissions of Eu^{3+} and Ce^{3+} ions respectively, point to the probability of an energy transfer from the ZnO nanoparticles to Eu^{3+} and Ce^{3+} ions. In the case of ZnO-SiO_2:Ce, energy transfer was attributed to spectral overlap between ZnO

emission band and Ce^{3+} absorption band. Because of lack of spectral overlap between ZnO emission band and Eu^{3+} absorption band, energy transfer in ZnO-SiO_2:Eu was attributed to phonon-mediated processes.

In a third set of experiments, energy transfer was investigated for different concentrations of Ce-Eu, Ce-Tb and Eu-Tb ion pairs co-doped in SiO_2. In the case of SiO_2:Ce,Eu, blue photoluminescence of Ce^{3+} was enhanced by an energy transfer from Eu^{3+} to Ce^{3+}. The PL intensity of the blue emission was maximized for 0.5 mol% Ce^{3+} versus 0.5 mol% Eu^{3+}. In the case of SiO_2:Ce,Tb, energy was transferred from Ce^{3+} to Tb^{3+} to enhance green emission of Tb^{3+} ions. The PL intensity of the green emission was maximized for 1 mol% Tb^{3+} vco-doped with 0.5 mol% Ce^{3+}. In both Ce-Eu and Ce-Tb ion pairs, energy transfer was attributed to spectral overlap between the emission and absorption bands of the energy donor and the energy acceptor, respectively. In the case of SiO_2:Eu,Tb, the PL emission of either Eu^{3+} or Tb^{3+} was very low irrespective of the concentration. This was attributed to quenching effect probably due to the formation of Eu^{2+}-Tb^{4+} ion pairs by charge transfer processes.

FUTURE PROSPECTS

The work presented in this thesis suggests many avenues for future research. To understand degradation phenomenon of oxide phosphors, it is important to do more experiments under different conditions. This include degrading in different gas mixtures (i.e. H_2, H_2O, CO_2), which are usually present in vacuum chambers and are known to influence degradation behaviour of FED phosphors. It is important to investigate further why degradation behaviour of Y_2O_3:Eu powders and thin film phosphors is different, i.e. why does oxygen desorb from the surface in the case of thin films but not in powders. Since mechanisms presented in this study about the correlation between desorption of oxygen from the surface and the decrease of CL intensity are based on speculations, it is imperative to do more experiments and monitor constantly the rate of desorption of oxygen and that of decrease of CL intensity during electron beam bombardment. This could help in developing a reasonable model to explain this correlation.

It is important to investigate tendency of activator ions to donate or absorb energy when co-doped with other activator ions in a matrix. It was found that in Ce^{3+}-Eu^{3+} co-doping, energy was transferred from Eu^{3+} to Ce^{3+}, but in the case of Ce^{3+}-Tb^{3+} co-doping it was transferred from Ce^{3+} to Tb^{3+}. It would therefore be interesting to investigate the cause for Ce^{3+} to behave like this. The quenching process between Eu^{3+} and Tb^{3+} in SiO_2 must also be investigated. There could be other factors than charge transfer such as the type of substrate that may be responsible for the quenching process. This can be done by co-doping in other substrates than SiO_2.

Transmission electron microscopy study must be conducted in order to determine particle sizes of amorphous SiO_2 nanounits that could not be determined by the SEM in this study. Samples with different particles sizes and shapes must be prepared in order to determine the effects of size and shape on cathodoluminescence degradation as well as cathodoluminescence and photoluminescence intensity.

PUBLICATIONS

- Coetsee E, Swart H.C., Terblans J.J., *Ntwaeaborwa O.M.* and Hillie K.T. Characterization of Y_2SiO_5:Ce thin films, *Optical materials*- accepted
- *Ntwaeaborwa O.M.*, Swart H.C., Kroon R.E., Holloway P.H. and Botha J.R, Enhanced luminescence and degradation of SiO_2:Ce,Tb powder phosphors prepared by a sol-gel process, *Physics and Chemistry of Solids*. **67** (2006) 1749
- *Ntwaeaborwa O.M.*, Swart H.C., Kroon R.E., Holloway P.H. and Botha J.R., Photoluminescence of Cerium-Europium co-doped SiO_2 phosphor prepared by a sol-gel process, *Surface and Interface Analysis*. **38** (2006) 458-461
- *Ntwaeaborwa O.M.* and Holloway P.H., Enhanced photoluminescence of Ce^{3+} induced by an energy transfer from ZnO nanoparticles encapsulated in SiO_2, *Nanotechnology* **16** (2005) 865 – 868
- Ntwaeaborwa O.M., Hillie K.T. and Swart H.C., Degradation of Y_2O_3:Eu powders, *Phys. Stat. Sol.* **C 1 (9)** (2004) 2366-2371
- Hillie K.T., Ntwaeaborwa O.M. and Swart H.C., Degradation of pulsed laser deposited Y_2O_3:Eu thin film phosphors, *Phys. Stat. Sol.* **C 1 (9)** (2004) 2360 – 2365
- Ntwaeaborwa O.M., Kgwadi N.D., Taole S.H., Strydom. R., Measurement of the Equilibrium Factor between Radon and its Progeny in the Underground Mining Environment, *Health Physics*, **86**(4) (2004) 374-377
- Ntwaeaborwa O.M., Kgwadi N.D., Taole S.H. and Strydom. R., Underground measurement of concentration of radon and that of its progeny. Proceedings of First Botswana International Conference on Mining, Gaborone, Botswana, 19–21 November 2002.

- Ntwaeaborwa O.M., Swart H.C., Kroon R.E., Holloway P.H., Cathodoluminescence degradation of SiO_2:Ce,Tb powder phosphors prepared by a sol-gel process, *American Vacuum Society*- in preparation.

INTERNATIONAL CONFERENCES

- 11th European Conference on Applications of Surface and Interface Analysis – Vienna (Austria) -September 2005
  Photoluminescence of Cerium-Europium co-doped SiO_2 phosphor prepared by a sol-gel process
  Ntwaeaborwa O.M., Swart H.C., Kroon R.E., Holloway P.H. and Botha J.R.

- 51st International Symposium and Exhibition of the American Vacuum Society – Anaheim (USA) -November 2004,
  In attendance

- Conference on Photo-responsive Materials: Kariega (RSA) -February 2004
  Degradation of Y_2O_3:Eu phosphors powder, and
  Electron-beam induced degradation of pulsed laser deposited Y_2O_3:Eu thin films
  Ntwaeaborwa O.M., Hillie K.T. and Swart H.C.

- Botswana's first international conference on mining: (Gaborone, Botswana) -November 2002
  Underground measurement of concentration of radon and that of its progeny
  Ntwaeaborwa O.M., Kgwadi N.D., Taole S.H. and Strydom R.

- Detecting Environmental Changes: Science and Society, London (UK) - July 2001
  Measurement of the equilibrium factor between radon and its progeny in the underground mining environment
  Ntwaeaborwa O.M., Kgwadi N.D., Taole S.H. and Strydom R.

NATIONAL CONFERENCES

- 51th Conference of the South African Institute of Physics- Western Cape (RSA)- July 2006

  (1) Enhanced luminescence and degradation of SiO_2:Ce,Tb powder phosphor prepared by a sol-gel process.

  Ntwaeaborwa O.M., Swart H.C., Kroon R.E., Botha J.R., and Holloway P.H.

  (2) Chemical vapour deposition growth of single wall carbon nanotubes

  Ntwaeaborwa O.M, Khamis S, Chen M, Johnston D.E., Swart H.C., and Johnson A.T.

  (3) Cathodoluminescence of Y_2SiO_5:Ce thin films.

  Coetsee E., Swart H.C, Terblans J.J., *Ntwaeaborwa O.M.,*. Hillie K.T. and Buttner U

  (4) Energy dispersive X-ray analysis (EDX), Scanning Electron (SEM) and Atomic force microscopy (AFM) of Y_2SiO_5:Ce thin films.

  Cotsee E., Swart H.C, Terblans J.J., *Ntwaeaborwa O.M.,*. Hillie K.T. and Buttner U

  (5) Luminescent properties of nanoparticle $SrAl_2$:Eu^{2+},Dy^{3+} phosphors

  S. Nieuwoudt, Swart H.C., Terblans J.J., *Ntwaeaborwa O.M.*, Coetsee E. and Hillie K.T.

- 50th Conference of the South African Institute of Physics- Pretoria (RSA)- July 2005

  (1) Enhanced Photoluminescence of Ce^{3+} and Eu^{3+} induced by an energy transfer from ZnO nanoparticles encapsulated in SiO_2.

  Ntwaeaborwa O.M., Swart H.C., Kroon R.E., Bang J-S., and Holloway P.H.

(2) Characterization of pulsed laser ablated cerium doped yttrium silicate (Y_2SiO_5:Ce) thin films on Si (100)

Cotsee E., Terblans J.J., *Ntwaeaborwa O.M.*, Buttner U. and Swart H.C.

- 47th Annual conference of the South African Institute of Physics-Potchefstroom (RSA) – September 2002

  All systems go at Kovsies

  Ntwaeaborwa O.M., Van Wyk G.N., Roos W.D., Terblans J.J., Greeff A.P. and Swart H.C.

- 45th Annual conference of the South African Institute of Physics- Johannesburg (RSA) – July 2000

  Measurement of the equilibrium factor between radon and its progeny in the underground mining environment

  Ntwaeaborwa O.M., Kgwadi N.D., Taole S.H. and Strydom R.

- 44th Annual conference of the South African Institute of Physics- Port Elizaberth (RSA) – July 1999

  Measurement of radon concentration in Mmabatho houses using Radon Gas Monitors

  Ntwaeaborwa O.M., Kgwadi N.D. and Strydom R.

BIOGRAPHY

Odireleng Martin Ntwaeaborwa was born and grew up at Taung Village in the North West Province, Republic of South Africa (RSA). He joined University of North West in 1993 as a student and obtained his MSc degree in Physics in 2000. He was appointed as a Physics Lecturer at University of the North (QwaQwa campus) in April 2000. He joined University of the Free State in 2002 as a Physics Lecturer and PhD student. He was a J1 research scholar at University of Florida (USA) in 2004 working with Prof. Paul H. Holloway on preparation and characterization of luminescent nanoparticle phosphors for low voltage field emission displays. In 2005, he visited University of Pennsylvania (USA) as a J1 research school to learn how to grow single wall carbon nanotubes by chemical vapour deposition in Prof. A.T. (Charlie) Johnson's research group.

Odireleng Martin Ntwaeaborwa has published six articles in internationally accredited journals. He is a referee of accredited journals including *Nanotechnology*, *Condensed Matter Physics*, *Physica Status Solidi E*, *Electrochemical Society and Materials Science Letters*. He was recommended by Prof. Paul Holloway to review research funding proposals for American Chemical Society–Petroleum Research Fund during his visit to University of Florida in 2004. He has been reviewing research funding proposals for the South Africa National Research Foundation (NRF) since 2003. He has given over 10 talks at national and international conferences including South African Institute of Physics, Photo-responsive Material Conference, Determining Environmental Changes Conference, Botswana's first international conference on mining, European Conference on Applications of Surface and Interface Analysis and American Vacuum Society.

He is an upcoming researcher working on luminescent nanoparticle materials for flat panel displays in collaboration with Prof. Holloway (Department of Materials Science and Engineering: University of Florida). The growth plan of his research is to explore biomedical applications, optical and luminescent properties of carbon nanotubes. This work will be done in collaboration with Prof. Johnson (Department of Physics and Astronomy: University of Pennsylvania).

Odireleng Martin Ntwaeaborwa received Research Excellence award from University of the Free State in 2004. He is the grant holder of Thuthuka Programme from NRF. He is listed in the 23rd edition of *Who's Who in the World.*